

**ISSN 2079-1372**

**DOI: 10.31891/2079-1372**

THE INTERNATIONAL SCIENTIFIC JOURNAL

***PROBLEMS  
OF  
TRIBOLOGY***

***Volume 30***

***No 2/116-2025***

---

---

МІЖНАРОДНИЙ НАУКОВИЙ ЖУРНАЛ

***ПРОБЛЕМИ ТРИБОЛОГІЇ***

# PROBLEMS OF TRIBOLOGY

INTERNATIONAL SCIENTIFIC JOURNAL

Published since 1996, four time a year

---

**Volume 30 No 2/116-2025**

---

**Establishers:**

**Khmelnytskyi National University (Ukraine)**  
**Lublin University of Technology (Poland)**

**Associated establisher:**

**Vytautas Magnus University (Lithuania)**

**Editors:**

**O. Dykha** (Ukraine, Khmelnytskyi), **M. Pashechko** (Poland, Lublin), **J. Padgurskas** (Lithuania, Kaunas)

**Editorial board:**

**V. Aulin** (Ukraine, Kropivnitskiy),  
**B. Bhushan** (USA, Ohio),  
**V. Voitov** (Ukraine, Kharkiv),  
**Hong Liang** (USA, Texas),  
**E. Ciulli** (Italy, Pisa),  
**V. Dvoruk** (Ukraine, Kiev),  
**M. Dzimko** (Slovakia, Zilina),  
**M. Dmitrichenko** (Ukraine, Kiev),  
**L. Dobzhansky** (Poland, Gliwice),  
**J. Zubrzycki** (Poland, Lublin),  
**G. Kalda** (Ukraine, Khmelnytskyi),  
**T. Kalaczynski** (Poland, Bydgoszcz),  
**M. Kindrachuk** (Ukraine, Kiev),  
**Jeng-Haur Horng** (Taiwan),  
**L. Klimenko** (Ukraine, Mykolaiv),  
**K. Lenik** (Poland, Lublin),

**O. Mikosianchyk** (Ukraine, Kiev),  
**R. Mnatsakanov** (Ukraine, Kiev),  
**J. Musial** (Poland, Bydgoszcz),  
**V. Oleksandrenko** (Ukraine, Khmelnytskyi),  
**M. Opielak** (Poland, Lublin),  
**G. Purcek** (Turkey, Karadeniz),  
**V. Popov** (Germany, Berlin),  
**V. Savulyak** (Ukraine, Vinnitsa),  
**A. Segall** (USA, Vancouver),  
**M. Stechyshyn** (Ukraine, Khmelnytskyi),  
**M. Chernets** (Poland, Lublin),  
**V. Shevelya** (Ukraine, Khmelnytskyi),  
**Zhang Hao** (China, Peking),  
**M. Śniadkowski** (Poland, Lublin),  
**D. Wójcicka-Migasiuk** (Poland, Lublin)

**Executive secretary: O. Dytyniuk**

**Editorial board address:**

International scientific journal "Problems of Tribology",  
Khmelnytskyi National University,  
Instytutska str. 11, Khmelnytskyi, 29016, Ukraine  
**phone** +380975546925

Indexed: CrossRef, DOAJ, Ulrichsweb, ASCI, Google Scholar, Index Copernicus

**E-mail:** tribology@khnmu.edu.ua

**Internet: <http://tribology.khnu.km.ua>**

# ПРОБЛЕМИ ТРИБОЛОГІЇ

МІЖНАРОДНИЙ НАУКОВИЙ ЖУРНАЛ

Видається з 1996 р.

Виходить 4 рази на рік

Том 30

№ 2/116-2025

## Співзасновники:

Хмельницький національний університет (Україна)  
Університет Люблінська Політехніка (Польща)

## Асоційований співзасновник:

Університет Вітовта Великого (Литва)

## Редактори:

О. Диха (Хмельницький, Україна), М. Пашечко (Люблін, Польща),  
Ю. Падгурскас (Каунас, Литва)

## Редакційна колегія:

В. Аулін (Україна, Кропивницький),  
Б. Бхушан (США, Огайо),  
В. Войтов (Україна, Харків),  
Хонг Лян (США, Техас),  
Е. Чуллі (Італія, Піза),  
В. Дворук (Україна, Київ),  
М. Дзимко (Словакія, Жиліна),  
М. Дмитриченко (Україна, Київ),  
Л. Добжанський (Польща, Глівіце),  
Я. Зубжицький (Польща, Люблін),  
Г. Калда (Україна, Хмельницький),  
Т. Калачинські (Польща, Бидгощ),  
М. Кіндрачук (Україна, Київ),  
Дженг-Хаур Хорнг (Тайвань),  
Л. Клименко (Україна, Миколаїв),  
К. Ленік (Польща, Люблін),

О. Микосянчик (Україна, Київ),  
Р. Мнацаканов (Україна, Київ),  
Я. Мушял (Польща, Бидгощ),  
В. Олександренко (Україна, Хмельницький),  
М. Опеляк (Польща, Люблін),  
Г. Парсек (Турція, Караденіз),  
В. Попов (Германія, Берлін),  
В. Савуляк (Україна, Вінниця),  
А. Сігал (США, Ванкувер),  
М. Стечишин (Україна, Хмельницький),  
М. Чернець (Польща, Люблін),  
В. Шевеля (Україна, Хмельницький),  
Чжан Хао (Китай, Пекин),  
М. Шнядковський (Польща, Люблін),  
Д. Войницька-Мігасюк (Польща, Люблін),

Відповідальний секретар: О.П. Дитинюк

## Адреса редакції:

Україна, 29016, м. Хмельницький, вул. Інститутська 11, к. 4-401  
Хмельницький національний університет, редакція журналу "Проблеми трибології"  
тел. +380975546925, E-mail: tribology@khmnu.edu.ua

Internet: <http://tribology.khnu.km.ua>

Зареєстровано Міністерством юстиції України  
Свідоцтво про держреєстрацію друкованого ЗМІ: Серія КВ № 1917 від 14.03. 1996 р.  
(перереєстрація № 24271-1411 ПП від 22.10.2019 року)

Входить до переліку наукових фахових видань України  
(Наказ Міністерства освіти і науки України № 612/07.05.19. Категорія Б.)

Індексується в МНБ: CrossRef, DOAJ, Ulrichsweb, ASCI, Google Scholar, Index Copernicus

Рекомендовано до друку рішенням вченої ради ХНУ, протокол № 16 від 12.06.2025 р.

© Редакція журналу "Проблеми трибології (Problems of Tribology)", 2025



ISSN 2079-1372 *Problems of Tribology*, V. 30, No 2/116-2025

## Problems of Tribology

Website: <http://tribology.khnu.km.ua/index.php/ProbTrib>

E-mail: [tribosenator@gmail.com](mailto:tribosenator@gmail.com)

### CONTENTS

<b>O. Milanenko, A. Bobro.</b> Multifactorial criterion evaluation of lubrication efficiency and wear resistance of friction units operating under extreme operating conditions.....	6
<b>O.I. Popil, A.-M.V. Tomina.</b> The influence of a binary alloy of the Al-Cr system on the tribological properties of ultra-high-molecular-weight polyethylene.....	14
<b>A. Goroshko, M. Zembytska.</b> Analysis of the influence of radial clearance in a bearing on its operating modes, taking into account mass and magnetic imbalance of the induction motor rotor.....	19
<b>M.O. Dykha, V.O. Dytyniuk, A.L. Staryi.</b> Probabilistic approach to assessing tribotechnical reliability indicators of friction units.....	27
<b>O.V. Bereziuk, Savulyak, V.O. Kharzhevskiy, A.Ye. Alekseiev.</b> Improved mathematical model of the hydraulic drive of the garbage truck's sealing plate mechanism taking into account the wear of its hydraulic cylinder.....	34
<b>K.E. Holenko, O.S. Kovtun, O.V. Dykha.</b> Modeling of contact interaction and wear of the trolleybus contact insert-wire tribopair.....	42
<b>A.-M.V. Tomina, D.V. Yakovenko, V.F. Bashev, S.I. Golovko.</b> Study of the influence of rapidly quenched aluminum alloy on the wear resistance of ultra-high-molecular-weight polyethylene.....	49
<b>F.F. Yusubov, V.K. Valiyev, U.B. Akbarova.</b> Morphological Analysis of Surface Degradation in Phenolic Friction Composites Using Image Processing Techniques.....	54
<b>Ie.V. Polunkin, S.M. Pleskun.</b> Study of the concentration effect and structure of multilayer spherical carbon nanoclusters on the carrying capacity of alternative fuels.....	62
<b>A. Lopata, V. Lopata, I. Kachynska, A. Solovykh.</b> Research into the possibility of improving the quality of electric arc coatings by nitriding.....	69
<b>V. Antonyuk, L. Lopata.</b> Optimization of discrete structure of electrospark coatings.....	77
<b>V.V. Shchepetov, S.S. Bys, M.R. Byalik, V.V. Medvedchuk, Ya.S. Bys.</b> The influence of hydrogen saturation on the wear mechanism of steel.....	84
<b>V.V. Aulin, Ye.V. Manko, V.M. Chumak, S.V. Lysenko, O.D. Derkach, D.O. Makarenko.</b> Texture of materials of elements of tribological systems of machines and mechanisms in non-equilibrium processing and functioning conditions.....	90
<b>Rules of the publication</b> .....	101

**ЗМІСТ**

<b>Міланенко О., Бобро А.</b> Багатофакторна критеріальна оцінка мастильної здатності та зносостійкості вузлів тертя, що працюють в екстремальних умовах роботи.....	6
<b>Попіль О.І., Томіна А.-М.В.</b> Вплив бінарного сплаву системи Al-Cr на трибологічні властивості надвисокомолекулярного поліетилену.....	14
<b>Горошко А.В., Зембицька М.В.</b> Аналіз впливу радіального зазору у підшипнику на режими його роботи з врахуванням масового і магнітного дисбалансу ротора асинхронного двигуна.....	19
<b>Диха М.О., Дитинюк В.О., Старий А.Л.</b> Ймовірнісний підхід до оцінки показників триботехнічної надійності вузлів тертя.....	27
<b>Березюк О.В., Савуляк В.І., Харжевський В.О., Алексеєв А.Є.</b> Удосконалена математична модель роботи гідроприводу механізму ущільнюючої плити сміттєвоза із урахуванням зносу його гідроциліндра.....	34
<b>Голенко К.Є., Ковтун О.С., Диха О.В.</b> Моделювання контактної взаємодії та зносу трибопари контактна вставка-провід тролейбусаю.....	42
<b>Томіна А.-М.В., Яковенко Д.В., Башев В.Ф., Головка С.І.</b> Дослідження впливу швидкозагартованого алюмінієвого сплаву на зносостійкість надвисокомолекулярного поліетилену.....	49
<b>Ф.Ф. Юсубов, В.К. Валієв, У.Б. Акбарова.</b> Морфологічний аналіз деградації поверхні фенольних фрикційних композицій з використанням методів обробки зображень....	54
<b>Полункін Є.В., Плєскун С.М.</b> Дослідження концентраційного впливу та структури багаточастикових сферичних карбонових нанокластерів на величину несучої здатності альтернативних палив.....	62
<b>Лопата О.В., Лопата В.М., Качинська І.Р., Солових А.Є.</b> Дослідження можливості підвищення якості електродугових покриттів шляхом обробки азотуванням.....	69
<b>Антонюк В.С., Лопата Л.А.</b> Оптимізація дискретної структури електроіскрових покриттів.....	77
<b>В.В. Щепетов, С.С. Бись, М.Р. Бялик, В.Ю. Медведчук, Я.С. Бись.</b> Вплив наводнювання на механізм зношування сталі.....	84
<b>Аулін В.В., Манько Є.В., Чумак В.М., Лисенко С.В., Деркач О.Д., Макаренко Д.О.</b> Текстурованість матеріалів елементів трибологічних систем машин і механізмів в нерівноважних умовах обробки та функціонування.....	90
<b>Вимоги до публікацій</b> .....	101



## Multifactorial criterion evaluation of lubrication efficiency and wear resistance of friction units operating under extreme operating conditions

O. Milanenko<sup>\*0000-0002-8197-5277</sup>, A. Bobro<sup>0009-0002-1193-117X</sup>

National Transport University, Kyiv, Ukraine

E-mail: [milanmasla@gmail.com](mailto:milanmasla@gmail.com)

Received: 01 March 2025; Revised 15 March 2025; Accept: 02 April 2025

### Abstract

A new multifactorial criterion approach to modifying lubricants by rheological properties and chemical composition is proposed in order to increase the lubricating ability of modified layers and wear resistance of friction units from the position of mixed lubrication conditions. Prevention of micro-EHD lubricating layer is achieved by a set of measures: implementation of stable micro-EHD lubrication by the criterion of lubrication mode; optimal viscosity class with an increase in the fraction of hydrodynamic pressure of modified layers relative to the contact pressure from micro-unevenness of rough surfaces by the pressure criterion; optimal type of lubricant by the rheological criterion; assessment of the appearance of a plastically deformed state by the criterion of plasticity; selection of the qualitative and quantitative chemical composition of active components in the lubricant to create durable modified layers with high structural adaptability and thermomechanical stability by the temperature criterion. A new concept for increasing lubricity and wear resistance for friction units operating in extreme operating conditions, using an appropriate criteria approach, takes into account: non-stationary friction conditions, the shape of local contact and friction kinematics, rheological properties of lubricating layers, contact temperature, and the composition of components in the lubricant.

**Key words:** elastohydrodynamic lubrication, micro-EHD friction contact, film thickness, rheological properties, chemically active ingredients, surface-active ingredients, chemically modified boundary layers

### Introduction. Analysis of recent research and publications

Most non-conformal assemblies with point or linear contact (friction bearing assemblies, gears, cams of the gas distribution mechanism, etc.) have limited areas of working surfaces. The contact load is applied to a relatively small area. These features of the contact form lead to contact fracture, which, unlike scoring, seizure, cavitation, and other types of damage, develops over time with the formation of crumbling (pitting) on the friction surfaces in the form of individual notches [1]. The initial size and shape of these pits depend on the material properties, nature and magnitude of stresses. During further operation of the assembly, their number increases, they merge and enlarge, and the fracture zone covers an increasingly large area of the surface. New stress concentrators appear, lubrication conditions and dynamic characteristics of the assembly deteriorate, the temperature rises, and a significant portion of the working surfaces lose their bearing capacity. Under conditions of a mixed lubrication regime in terms of speed and load and the material's tendency to wear, this process can slow down or even stop altogether. However, in heavily loaded bearing assemblies, high microhardness steels are used as indenter material - bearing balls made of the SHKH-15, which are poorly worked up, pitting becomes progressive, in most cases, the assembly fails prematurely [2]. Along with structural, technological, and operational factors, the root cause of such failure is the nature and level of stresses, which is influenced by the shape of the contact [3].

From the foregoing, it can be stated that the prediction of the durability of friction units operating under contact load conditions requires solving several important tasks, including

1. Depending on the calculated maximum normal and tangential loads, it is necessary to know the optimal form of contact with its equivalent mechanical properties, taking into account the position of the zones of frequent surface failure in depth and in the rolling direction, and to experimentally verify the obtained solution.
2. To take into account the influence of deformations of rolling surfaces when contact stresses change in the



process of friction.

3. Determine the necessary parameters of materials: reduced modulus of elasticity, microhardness, roughness of contact surfaces for specific friction units.

The theory of elastohydrodynamic (EHD) lubrication is used to explain the rheological and physicochemical effects of a lubricant [4, 5]. According to this theory, the thickness of the lubricating layer separating the surfaces of friction units is determined by the viscosity-pressure dependence of the lubricant. The contact of surface irregularities does not occur if it is possible to maintain a sufficient thickness of the lubricating layer - in this case, the EHD lubrication regime with long-term bearing life is ensured. If the thickness of the lubricating layer is reduced to the point where the micro-irregularities of the contact surfaces begin to touch, then as the frequency of contact increases, fatigue life will rapidly decrease. At present, there is no satisfactory explanation for how contact of surface micro-irregularities leads to fatigue damage.

The features of micro-EHD friction contact [6] are characterized by similar EHD conditions: the influence of elastic properties of the material and the characteristic dependence of viscosity on pressure and the influence of compressibility of the lubricant. However, for micro-EHD friction conditions, the influence of the mechanical properties of the surfaces (the magnitude and position of the localization of maximum tangential stresses at a certain depth) and the level of roughness of the contact surfaces is also important, since there are discrete areas of the contact pressure of the material that begin to reach the level of hydrodynamic pressure of the lubricating layers, which reduce the level of lifting force and viscous friction in the gap of the lubricating layer [7].

In [8], the rheological properties of fresh and used SAE 5W-30 diesel engine oils with a low content of sulfate ash, phosphorus, and sulfur (Low SAPS oils) were studied using an EHD tribometer and rotational viscometers of the HTHS (High Temperature High Shear) type, which provide low and high shear rates. Based on the thickness of the lubricating layer formed in the EHD contact in the range from 10 to 150 nm, two types of lubrication mechanisms were identified depending on the rolling speed. On the one hand, the classical behavior of the EHD lubrication with an optimal dynamic viscosity above a certain critical film thickness was observed. On the other hand, the authors recorded a sharp drop in film thickness, which is an indicator of the inability of polymeric viscosity modifiers to form a thin film within the contact, which was influenced by the particle size in the oil composition. The authors established a correlation between the critical film thickness and particle size and thus concluded that used oil has a more critical film thickness than fresh oil and that under certain conditions the friction properties of the oil were related to this critical film thickness. A characteristic feature of the studied oils was their non-Newtonian behavior, which was revealed in tribological experiments. These observations of the authors were related to rheological measurements made at shear rates up to  $10^7 \text{s}^{-1}$  at temperatures from 25 to 150°C.

Under extreme conditions of mixed friction, the chemical action of the lubricant and its additives (chemically active ingredients, CAS or surface-active ingredients, SAS) significantly affects fatigue life [9]. This is because under mixed lubrication conditions, contact surfaces are subjected to tangential stresses of much greater magnitude. The corresponding forces cause the appearance of maximum contact stresses on the contact surfaces, which stimulate fatigue of the surfaces themselves in the near-surface layers, as opposed to fatigue developing below the surface. In addition, chemical reactions of the lubricant with the material of the metal surfaces significantly reduce the resistance to crumbling. However, some additives, on the contrary, reduce surface forces and thus reduce tangential stresses, thereby increasing fatigue life.

Finally, it should be noted that according to the "unified" theory of boundary lubrication by A. Cameron [10], in the temperature range  $T_o > T > T_{cr}$ , the lubricating effect occurs due to the formation of "thick" polymer films and only after their destruction does the interaction of active components of the medium with friction surfaces begin with the formation of chemically modified boundary layers (CMBL). According to the relevant theory of boundary lubrication, the increase in the lubricating ability of modified layers and the wear resistance of friction units occurs due to the formation of optimal polymer films, and only after their destruction does the interaction of active components of the medium with friction surfaces begin with the formation of boundary layers, the strength of which depends on local temperatures in the contact zone.

Thus, the study of the influence of the qualitative and quantitative composition of chemical components, taking into account the temperature factor, using modern and automated equipment and adapted methods, opens up wide opportunities for modifying lubricants. Finally, this will make it possible to increase the wear resistance of contact surfaces and improve lubricity, taking into account the control of the critical temperature (thermomechanical stability) in the local contact zone in terms of contact-mechanical, rheological, and physicochemical aspects. From a practical point of view, an appropriate integrated approach will allow managing the process of approaching real operating conditions for specific friction units and ensuring uniformity in the creation of universal lubricants in hybrid vehicles, which should have the properties of, for example, motor, transmission and hydraulic oils at the same time.

### Statement of unresolved issues

Many problems of tribology associated with the operation of friction units require not only theoretical and experimental studies, but also bench and operational tests on real equipment, since many transient processes occurring in the micro-volume (micro-EHD) of the friction contact of real units make significant adjustments to the research results. The task of increasing the lubricating ability and wear resistance of friction pairs operating under extreme

conditions requires systematic studies of modifying lubricating layers with optimal chemically active components as one of the effective and modern technologies for improving rheological and tribotechnical parameters, including to provide versatility to lubricants in order to reduce material and financial costs for maintenance of friction units. Carrying out relevant research and testing is impossible without the use of modern automated equipment, both in laboratory and factory conditions and on original equipment in real-time operation to ensure the accuracy and reliability of the results. Otherwise, the results will remain at the level of a phenomenological fact, for which there is either no theoretical justification or it will be contradictory from the standpoint of different scientific schools dealing with these issues.

To date, there is no consensus on how to improve lubricity and wear resistance under mixed lubrication, an intermediate mode between liquid and boundary lubrication, in which most components are operated, where the structure of the lubricating layer, its rheological and tribotechnical characteristics change. It is also added that mixed lubrication is a predominantly unstable mode due to rapidly changing processes in the friction contact zone, for example, under conditions of lubrication starvation, in which there are breaks in the EHD of lubricating layers or modified boundary layers in discrete areas of the actual contact area under high loads. Therefore, a comprehensive solution to the above issues using the results of scientific and applied research on lubricants in laboratory and factory conditions and at enterprises-operators of equipment will allow developing modern methods and technologies for increasing the lubricating ability and wear resistance of friction pairs in the friction contact zone, taking into account contact-mechanical, rheological and physicochemical aspects. The corresponding integrated approach will form the basic basis for scientifically sound approaches to the development of modern lubricants and optimized designs of friction units operating under real-world conditions in vehicles.

Thus, the scientific and technical problem is the implementation of sustainable lubrication in mixed friction conditions and the creation of modified layers with optimal lubricity and structural adaptability to extreme operating conditions in the friction contact zone of non-conformal and conformal friction units, aimed at increasing the lubrication efficiency and wear resistance of friction pairs in terms of contact-mechanical, rheological, and physicochemical aspects.

### **Statement of the problem**

Most friction units in extreme operating conditions are operated in a mixed lubrication mode, which is characterized by micro-EHD lubrication (in foreign literature: partially elastic-hydrodynamic partial hydrodynamic lubrication), when the thicknesses of the lubricating layer become almost commensurate with the heights of micron irregularities of metal surfaces. Micro-EHD lubrication is characterized by the sensitivity of the influence of contact surface roughness, since contact pressures from discrete areas along the actual contact area arise, which begin to reach the total level of hydrodynamic pressure of the lubricating layers, which reduce the level of lifting force and viscous friction in the gap of the lubricating layer.

In the mixed lubrication regime, physical (viscous and rheological) aspects of lubrication have a significant impact, since the proportionality of the thickness of the lubricating layer with the height of the micron irregularities of the contact surfaces under extreme conditions at high stresses and shear rates can lead to the manifestation of pseudoplasticity and elasticity of the lubricating layers. Since very few works have been devoted to this issue, and they are mainly generalized by hypothetical calculations, the task is to conduct not only the necessary experimental studies, but also to make appropriate calculations to take into account the rheological properties in the micro-EHD contact zone.

Under conditions of boundary lubrication, the surfaces of conformal internal combustion engine assemblies have direct contact between sections of large length. At the boundary lubrication, the lubricating ability will be characterized by the physical and chemical aspects of the structural adaptability of the modified layers adsorbed on metal surfaces. The coefficient of friction in boundary lubrication is significantly higher than in liquid lubrication, but by modifying the surfaces with surfactants that form strong CMBL at high temperatures or surfactants that form polymerization chemisorption or physically adsorbed films at moderate temperatures, it is possible to prevent type 1 adhesion (cold seizure) and significantly reduce wear of contact surfaces.

It has been established that appropriate chemical reactions of the lubricant with the material of metal surfaces can reduce surface forces and thus reduce tangential stresses, thereby increasing fatigue life. Unfortunately, such studies under mixed lubrication conditions are fragmentary in nature, since, in general, the influence of the chemical component, as well as the relationship between the rheological properties of the boundary layers and the chemical properties of the components in the lubricant that create the corresponding modified layers, are considered only from the standpoint of boundary lubrication. Thus, it is necessary to ensure an integrated approach to conducting theoretical and experimental studies, taking into account the rheological and physicochemical aspects of lubricants for friction units.

One of the effective means of creating appropriate durable modified layers on friction surfaces is adsorption and surface shielding with certain CAS or SAS, which opens up wide opportunities for modifying lubricants to increase the lubricating ability of the corresponding modified layers and the wear resistance of friction pairs, and the corresponding means will be useful in implementing a unified approach to the use of universal lubricants in

modern hybrid machines.

For the friction units of internal combustion engines, the conditions of non-stationarity (start-stop) are important, which should be considered from the point of view of contact strength (contact-mechanical aspect), determination of thermomechanical stability in the friction contact zone and structural adaptability of modified layers under the conditions of the boundary lubrication regime, taking into account the mechanical component of the friction force and molecular interaction of contact surfaces. The contact-mechanical component of the friction force is ensured by taking into account the mechanical properties of materials, the level of maximum contact stresses and deformations occurring in the friction contact zone. The molecular component is provided by rheological and physicochemical aspects of the structural adaptability of the modified layers in the friction contact zone.

Taking into account the multifactorial nature of the task of increasing the lubricity and wear resistance of bearing units and ICE units, it is necessary to use an integrated approach to assessing contact-mechanical, rheological, and physicochemical aspects, and based on their results, to conduct bench and operational tests in real friction units in order to confirm the adequacy and accuracy of the multifactorial criterion approach to increasing the lubricity and wear resistance of friction units under extreme operating conditions.

### The purpose of the work

Liquid, plastic, solid, and gaseous lubricants are used to increase the lubricating ability and wear resistance of friction units, depending on the operating conditions. The most widely used are liquid lubricants (oils), which additionally provide heat dissipation and protection against corrosive environmental effects. In this regard, it is very important to optimally select and modify oils for specific operating conditions in order to minimize friction, prevent adhesion of the 1st kind of contact metal surfaces under extreme (heavily loaded and unsteady) friction conditions and create strong structured and modified lubricating layers on the surfaces, which facilitate the microplastic deformation in the subsurface friction contact zone in order to inhibit the propagation of fatigue processes in depth and along the direction of movement.

Fig. 1 shows a schematic diagram of the proposed new criterion-based approach for a comprehensive assessment of modifying the physical and chemical composition of lubricants to increase the lubricity and wear resistance of friction units operating under extreme operating conditions, in which there is a transition from liquid to boundary lubrication, which allows identifying the mixed lubrication mode.

At the first stage, in order to ensure the necessary conditions for the implementation of EHD lubrication, in which the wear of contact surfaces is observed in a steady state with a small supply of wear particles, and friction is minimal, it is necessary to observe the boundary of the transition zone from EHD to mixed lubrication mode with the corresponding input characteristics of the materials of friction surfaces and lubricant, the shape of the contact and the operating parameters of friction units.

The corresponding boundary is determined by the micro-EHD lubrication regime, which is influenced by the roughness of the micro-irregularities of the contact surfaces when forming the thickness of the lubricating layer, which is estimated by the lubrication regime criterion  $\lambda$  according to the expression in [11]:

$$\lambda = \frac{h}{\sqrt{R_{a1}^2 + R_{a2}^2}}, \quad (1)$$

where  $h$  – the thickness of the lubricating layer in the contact area (for steady-state operation, the value of the thickness of the lubricating layer in the central contact area is used  $h_0$ ; to establish a violation of the lubrication regime - the minimum value of the lubricating layer thickness at the contact outlet  $h_{min}$ ),  $\mu\text{m}$ ;

$R_{a1}$  – arithmetic mean deviation of the indenter surface profile,  $\mu\text{m}$ ;

$R_{a2}$  – arithmetic mean deviation of the counterbody surface profile,  $\mu\text{m}$ ;

$\sqrt{R_{a1}^2 + R_{a2}^2}$  – the arithmetic mean deviation of the tribopair profile under model tests,  $\mu\text{m}$ .

According to the criterion of lubrication regime  $\lambda$ , the regimes are divided: boundary, when  $\lambda < 1$ ; mixed, when  $\lambda = 1 \div 3$ ; the EHD, when  $\lambda = 3 \div 4$ ; hydrodynamic, when  $\lambda \geq 4$ . The micro-EHD regime characterizes the boundary of the transition from the mixed to the EHD lubrication regime or vice versa, when  $\lambda = 3$ .

At the second stage, the influence of the contact shape on mechanical properties (maximum contact normal and tangential stresses, deformations, position of localization of tangential stresses) in the friction contact zone is taken into account, especially for non-conformal friction units, since at the boundary of the transition from the mixed to the EHD lubrication mode from the position of mixed lubrication, only part of the load is perceived by the lubricating layer for units with a limited (concentrated) contact shape. The authors of [12], as a first approximation, proposed the following ratio:

$$\frac{P_h}{P_\Sigma} = \frac{1}{\lambda} \cdot \left( \frac{h_{min}}{h_0} \right)^{6,3}, \quad (2)$$

where  $P_h$  – hydrodynamic pressure perceived by the lubricating layer;

$P_{\Sigma}$  – total pressure in the contact;  
 $h_0$  – thickness of the lubricating layer in the central contact area;  
 $h_{min}$  – minimum thickness of the lubricating layer at the contact outlet.

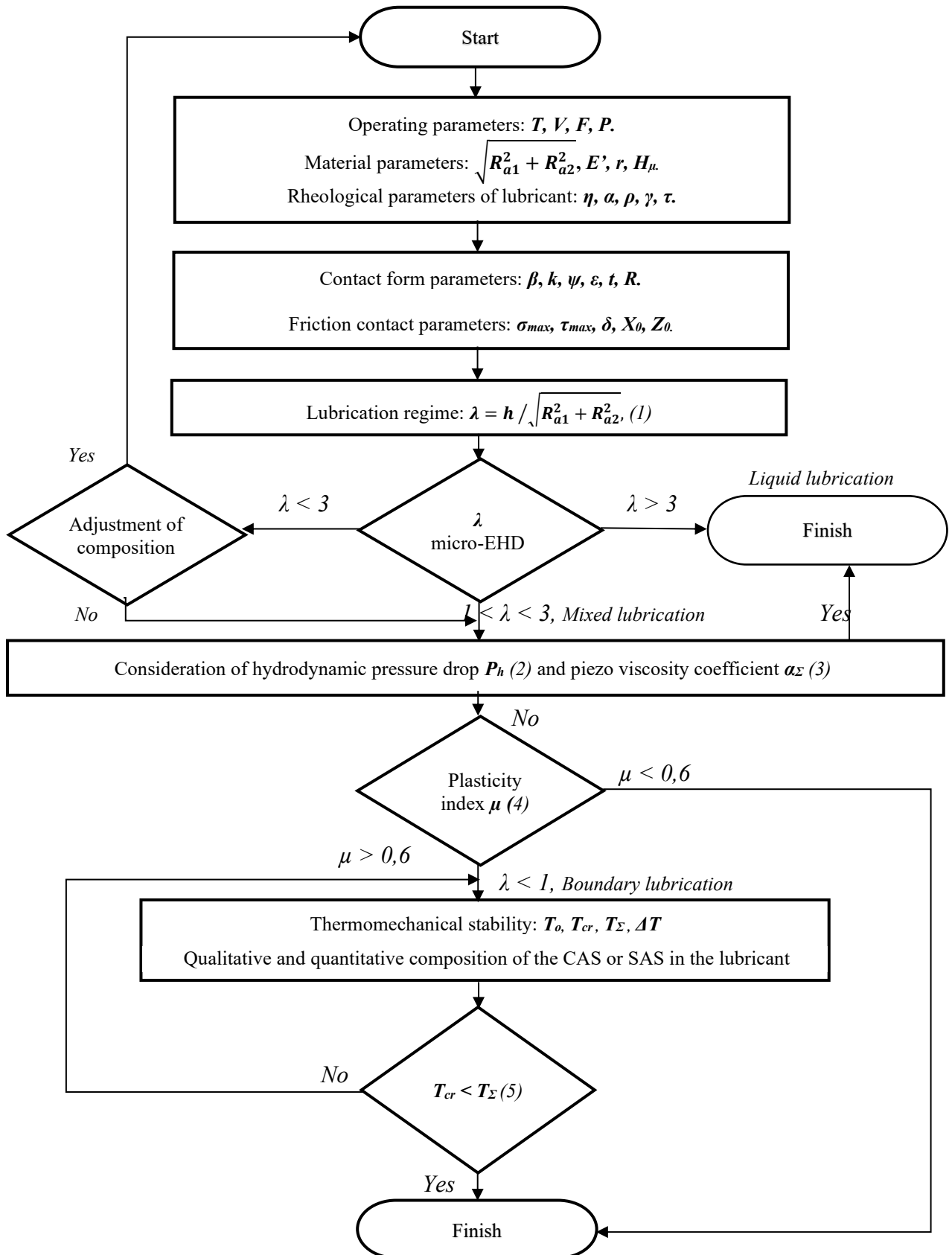


Fig. 1. Block diagram of the criterion approach to the integrated assessment of modification of the physical and chemical composition of lubricants.

At the second stage, the rheological properties of the lubricant are taken into account, i.e., ensuring optimal mechanical stability of the dynamic viscosity at high shear rate gradients of the lubricating layers in a wide range of low and high temperatures (bearing capacity). In other words, the lubricant must provide mechanical stability in terms of non-Newtonian properties at high shear rates under extreme operating conditions in a wide temperature range.

The main functionality that describes the influence of rheological properties is the calculation of dynamic viscosity with increasing load, but the corresponding definition is valid for Newtonian oils, which have a constant piezo viscosity coefficient  $\alpha$  at low shear rates. Although, most modern oils at high shear rates, reaching  $5 \cdot 10^6 \text{ s}^{-1}$ , can exhibit non-Newtonian properties and change the piezo viscosity coefficient  $\alpha$  at high shear rates. Therefore, the authors of [13] proposed the definition of the average value of  $\alpha_\Sigma$  that takes into account the change in this coefficient with pressure. The average value of the piezo viscosity coefficient  $\alpha_\Sigma$  as a criterion for assessing rheological properties is determined as follows:

$$\alpha_\Sigma = \frac{\ln(\eta_1/\eta_2)}{P_2 - P_1}, \quad (3)$$

in which the index 1 refers to the atmospheric pressure and temperature at  $T = 311\text{K}$ , the index 2 to the highest pressure relative to the viscosity at  $T = 311\text{K}$ .

At the same time, the piezo viscosity coefficient  $\alpha$  determines the tangent to the curve of  $\ln(\eta)$  versus  $P$  at atmospheric pressure, and  $\alpha_\Sigma$  will determine the tangent to the same curve in the region between atmospheric and increased pressure.

At the third stage, the appearance of a plastic-deformed contact is estimated by the value of the plasticity index  $\mu$  [12]:

$$\mu = \frac{E'}{H_\mu} \cdot \left( \frac{\sqrt{R_{a1}^2 + R_{a2}^2}}{r} \right)^{\frac{1}{2}}, \quad (4)$$

where  $E'$  – reduced elastic modulus, GPa;

$H_\mu$  - microhardness, determined experimentally by the method of artificial bases on the device PMT-3, Pa;

$\sqrt{R_{a1}^2 + R_{a2}^2}$  – the arithmetic mean deviation of the tribopair profile under model tests,  $\mu\text{m}$ ;

$r$  - average radius of microroughness vertices,  $\mu\text{m}$ .

At  $\mu > 0.6$ , a plastic-deformed contact;

at  $\mu < 0.6$ , elastically deformed contact under a slight thermal load.

At the fourth stage, first, the volumetric temperature of the lubricant  $T_o$ , measured by a thermocouple in the vicinity of the contact, is compared with the local temperature measured in the vicinity of the friction contact  $T_\Sigma$  by the thermal imaging method, which is the average of the specific points of local temperatures (thermomechanical resistance) under the same test conditions.

If the thermomechanical resistance of the studied modified layer  $T_\Sigma$  is higher than the thermomechanical resistance of the modified layer calculated for the nominal temperature resistance (critical temperature  $T_{cr}$ ), by the difference (flash) of temperature  $\Delta T$ , according to expression (5), with all initial parameters of friction and wear (tribotechnical and rheological parameters) being equal:

$$T_\Sigma = T_{cr} + \Delta T, \quad (5)$$

then the condition  $T_{cr} < T_\Sigma$  will be fulfilled, which will indicate the optimal qualitative and quantitative chemical composition of the active components in the lubricant.

If the condition  $T_{cr} < T_\Sigma$  is not fulfilled (see Fig. 1) with all friction and wear parameters being equal, then the corresponding physicochemical composition of the lubricant will have insufficient thermomechanical resistance of the modified layers to the corresponding operating conditions. In this case, the physicochemical composition of the lubricant is corrected by modifying the CAS or SAS with the determination of the optimal concentration. High surface activation due to changes in the physicochemical properties (modification) of the lubricant will increase the strength of the modified layers and improve the structural adaptability to specific operating conditions and hence increase the thermomechanical stability of the  $T_\Sigma$ . At the same time, the service life of friction units will be increased by reducing the wear rate of friction pairs.

Thus, if the condition  $T_{cr} < T_\Sigma$  is not fulfilled, the lubricant is introduced into the lubricant in the form of halogen-containing compounds or sulfides in order to create strong the CMBL on the friction surfaces, or organic nano modifiers in the form of fullerenes (SAS), that modify and polymerize the surface with self-generating organic films (SGFs) that minimize friction and reduce wear (sometimes, adhesive wear is replaced by softer corrosion-mechanical wear). In addition, the appropriate modification improves the structural adaptability of the modified layers in the friction contact zone of the friction units of the internal combustion engine or bearing units to extreme operating conditions at high temperatures.

## Conclusions.

The forward-looking multifactorial criterion approach to the modification of lubricants by their physical and chemical composition has been proposed to increase the lubricating ability of modified layers and the wear resistance of friction units from the standpoint of mixed lubrication conditions. Prevention of micro-EHD rupture of the lubricating layer is achieved by a set of measures: realization of stable micro-EHD lubrication according to the criterion of the lubrication mode ( $\lambda$ ); optimal viscosity class with an increase in the share of hydrodynamic pressure (lubricity) of the modified layers relative to the contact pressure from micro-irregularities of rough surfaces according to the pressure criterion ( $\frac{P_h}{P_\Sigma}$ ); optimal type of lubricant according to the rheological criterion ( $\alpha_\Sigma$ ); assessment of the appearance of a plastic-deformed state according to the plasticity criterion ( $\mu$ ); selection of the qualitative and quantitative chemical composition of active components in the lubricant to create durable modified layers with high structural adaptability and thermomechanical stability according to the temperature criterion ( $T_\Sigma$ ).

## References

1. Burstein, G. T., Liu, C., Souto, R. M., & Vines, S. P. (2004). Origins of pitting corrosion. *Corrosion Engineering, Science and Technology*, 39(1), 25–30. <https://doi.org/10.1179/147842204225016859>
2. Dmytrychenko M.F. Kinetics of the formation of operational stiffness of contact surfaces / M.F. Dmytrychenko, O.A. Milanenko // Scientific and technical collection of NTU. - Bulletin No. 15. - P. 15-18.
3. Hamrock B. Ball Bearing Elastohydrodynamic Lubrication of Point Contacts / B. Hamrock, D. Dowson. – New-York: Wiley Interscience Publication, 1981. — 386p.
4. Dmytrychenko N. Elastohydrodynamic Lubrication of Line Contacts / N. Dmytrychenko, A. Aksyonov, R. Gohar, G. Wan // *Wear*. – 1991. – Vol. 151. – P. 303-313.
5. Gohar R. Elastohydrodynamics / R. Gohar. – Chichester: Ellis Horwood Ltd., 1988. – 320p.
6. Christensen H. A theory of mixed lubrication / H. Christensen // *Proc. Inst. Mech. Engrs.* – 1972. - Vol. 186. - № 41. – P. 421–430.
7. Touche T. Friction of Textured Surfaces in EHL and Mixed Lubrication: Effect of the Groove Topography / T. Touche, J. Cayer-Barrioz, D. Mazuyer. - 2016. - Vol.63 (2). – № 25.
8. Meunier C. Correlation between the film forming ability and rheological properties of new and aged low sulfated ash, phosphorus and sulfur (Low SAPS) automotive lubricants / C. Meunier, D. Mazuyer, P. Vergne, M.E. Fassi, J. Obiols // *Tribology Transactions*. – 2009. – Vol.52. - № 4. – P. 501–510.
9. Chigareno G.G. Investigation of the influence of the chemical structure of complexing additives on the lubricating properties of oils / G.G. Chigareno, O.G. Ponomarenko // *Friction and wear*. - 1989. - № 6 (10). - C. 50-61.
10. Cameron A. Basic Lubrication Theory / A. Cameron / Pergamon Press. – London, 1971. – 295p.
11. Dmytrychenko M.F. Lubricating action of oils in conditions of elastohydrodynamic lubrication: monograph / M.F. Dmytrychenko, O.A. Milanenko. - K.: Ukravtodor, 2009 - 184 p.
12. Hebda M. Handbook of tribotechnics in three volumes / Edited by M. Hebda, O.V. Chichinadze // *Mechanical engineering*, 1990. - Vol. 2: Lubricants, lubrication techniques, sliding and rolling bearings. – 412p.
13. Sanborn D.M. Fluid Rheological Effects in Sliding Elastohydrodynamic Point Contacts with Transient Loading: 1 – Film Thickness / D.M. Sanborn, W.O. Winner // *ASME Trans.* – 1970. – P. 52 – 63.

**Міланенко О., Бобро А.** Багатофакторна критеріальна оцінка мастильної здатності та зносостійкості вузлів тертя, що працюють в екстремальних умовах роботи.

Запропоновано новий багатофакторний критеріальний підхід щодо модифікування мастильних матеріалів за реологічними властивостями та хімічним складом з метою підвищення мастильної здатності модифікованих шарів і зносостійкості вузлів тертя з позиції умов змішаного мащення. Запобігання розриву мікро-ЕГД мастильного шару досягається комплексом заходів: реалізації стійкого мікро-ЕГД мащення за критерієм режиму мащення ( $\lambda$ ); оптимального класу в'язкості при збільшенні долі гідродинамічного тиску (мастильної здатності) модифікованих шарів відносно контактного тиску від мікронерівностей шорстких поверхонь за критерієм тиску ( $P_h/P_\Sigma$ ); оптимального типу мастильного матеріалу за реологічним критерієм ( $\alpha_{сер}$ ); оцінки появи пластично-деформованого стану за критерієм пластичності ( $\mu$ ); підбором якісного і кількісного хімічного складу активних компонентів в мастильному матеріалі для створення міцних модифікованих шарів з високою структурною пристосовуваністю та термомеханічною стійкістю за температурним критерієм ( $T_{сер}$ ).

Нова концепція підвищення мастильної здатності та зносостійкості для вузлів тертя, що працюють в екстремальних умовах роботи, за відповідним критеріальним підходом, враховує: нестационарні умови тертя, форму локального контакту та кінематику тертя, реологічні властивості мастильних шарів, температуру контакту, склад компонентів в мастильному матеріалі.

**Ключові слова:** еластогідродинамічне змащення, фрикційний мікро-ЕГД контакт, товщина плівки, реологічні властивості, хімічно активні інгредієнти, поверхнево-активні інгредієнти, хімічно модифіковані граничні шари.



## The influence of a binary alloy of the Al-Cr system on the tribological properties of ultra-high-molecular-weight polyethylene

O.I. Popil<sup>0009-0004-8770-2351</sup>, A.-M.V. Tomina<sup>\*0000-0001-5354-0674</sup>

*Dniprovsk State Technical University, Kamyanske, Ukraine*

*E-mail: [an.mtomina@gmail.com](mailto:an.mtomina@gmail.com)*

*Received: 10 March 2025; Revised 25 March 2025; Accept: 15 April 2025*

### Abstract

The work studied the influence of a liquid-quenched binary alloy of the Al-Cr system with a chromium content of 5 wt.% on the tribological properties of ultra-high-molecular-weight polyethylene under friction without lubrication according to the “disk-pad” scheme and with rigidly fixed abrasive particles. We established that the introduction of 5-30 wt.% this alloy leads to a decrease in the intensity of linear wear and the abrasive wear rate of ultra-high-molecular-weight polyethylene by 2.8 and 2 times, respectively. The improvement of these indicators is due to several factors. A solid filler (HV $\approx$ 600 MPa) contributes to the strengthening of the surface layer of the material undergoing wear. On the other hand, this can be explained by the formation of a more strained Al-based solid solution lattice, since it is known that binary quenched from the liquid state aluminum-based alloys are characterized by a high degree of microstresses due to the significant difference in the sizes of Al-Cr atoms. A composite with a filler content of 20 wt.% has the best set of functional properties. We can recommend this material for the manufacture of tribotechnical (gears, sprockets, bushings, and plain bearings) and structural (rollers, gear wheels, and bearing housings) parts for agricultural machinery and the mining industry operating under conditions of impact-abrasive or fatigue wear.

**Keywords:** ultra-high-molecular-weight polyethylene, liquid-quenched binary Al-Cr alloy, dispersed filler, abrasive wear rate, linear wear intensity

### Introduction

Working bodies and friction units of agricultural machinery and the mining industry lose their performance due to impact-abrasive or fatigue wear [1] influenced by mechanical loads in almost 80% of cases. One of the promising directions for increasing their wear resistance is using polymer composite materials (PCMs). Using PCMs instead of serial parts allows us to increase mobility, work productivity, and the period of stable operation of units, as well as reduce maintenance and repair costs [2].

Therefore, the development, research, and implementation of wear-resistant materials that can effectively withstand intense mechanical loads [3] is the current task of many domestic and foreign researchers. Another important advantage of using PCMs instead of metals and semi-finished products based on them is the reduction of the labor intensity of manufacturing and the cost of products by up to 6 and 5 times, respectively, even for products of complex configuration. Using high-performance technologies that contribute to saving resources helps achieve this [4].

Analysis of modern domestic and foreign literature shows that PCMs based on ultra-high-molecular-weight polyethylene (UHMWPE), modified with various powder (dispersed) fillers (FLs), are of considerable interest for these purposes. It has been proven that the introduction of graphene nanoplatelets, diabase [5], natural and crucible graphite, graphene oxide [6], iron particles [7], silicon carbide, carbon nanotubes [8], high-entropy and binary alloys [9, 10] allows obtaining materials with high thermal conductivity, hardness, stiffness, resistance to corrosion and wear, low coefficient of friction and minimal water absorption.



## The purpose of the work

Considering the above, the work aims to study the influence of a powder filler, a binary alloy of the Al-Cr system, on the tribotechnical characteristics of polymer composite materials based on UHMWPE to increase their wear resistance under various friction conditions.

## Objects and methods of research

We used commercial UHMWPE from Jiujiang Zhongke Xinxing New Material Co., Ltd. (China) to create new wear-resistant PCM compositions. UHMWPE is a unique polymer with high functional properties, including chemical inertness, high self-lubricating ability, resistance to corrosion, cavitation erosion, wear (15 times higher than carbon steel), and impact (even at cryogenic temperatures), rigidity, and low static and dynamic coefficients of friction [11]. The high technical characteristics of UHMWPE are associated with its molecular structure. UHMWPE has extremely long molecular chains, with a high molecular weight (5-5.5 million g/mol), which ensure the effective transfer of applied loads along the polymer base.

A dispersed (40-100  $\mu\text{m}$ ) liquid-quenched single-phase binary state alloy of the Al-Cr system with a chromium content of 5 wt.% was chosen as a filler. FLs of this type are characterized by high indicators of functional properties because of the high ( $\Delta a/a \geq 2.5 \cdot 10^{-3}$ ) level of microstresses in the crystal lattice due to the significant difference in the atomic radii of aluminum ( $r_{\text{Al}}=0.142$  nm) and chromium ( $r_{\text{Cr}}=0.128$  nm) [12]. The formation of research samples from PCMs containing 5-30 wt.% FLs was performed by the compression pressing method [10]. We studied tribological properties of PCMs and UHMWPE under friction conditions without lubrication during rotational motion according to the "disk-pad" scheme in a pair with a steel cylindrical counterbody (steel 45,  $\phi 50$  mm, hardness was 45-48 HRC, and surface roughness was  $R_a=0.32$   $\mu\text{m}$ ) at a sliding speed of 1 m/s and a load of 1 MPa on the SMC-2 friction machine. We determined the abrasive wear ratio by rigidly fixed abrasive particles (dispersion was 100  $\mu\text{m}$ ) using a HECKERT experimental machine at a constant load of 10 N. The wear value of UHMWPE and PCMs based on it was determined by the gravimetric method using an analytical VLR-200 balance (accuracy was  $10^{-5}$  g). Then, the results were converted into wear intensity and abrasion ratio using known methods.

The roughness of the samples on the  $R_a$  scale was measured after friction using a 170621 probe profilometer. High-quality, detailed images of the friction surfaces of the studied samples, including their texture, structural features, and microroughnesses, were obtained in reflected incident light using a BIOLAM-M binocular microscope. We determined the hardness of UHMWPE and PCMs on the Rockwell HRR scale (preliminary and total load was 98.1 N and 588.4 N, respectively) using a 2074 TPR device. We measured the microhardness of the binary alloy using a PMT-3M microhardness tester with a load of 5 g. X-ray studies of the FL were performed on a DRON-2.0 diffractometer in monochromatized  $K_\alpha$  copper radiation along the lines (111) and (222) (Fig. 1).

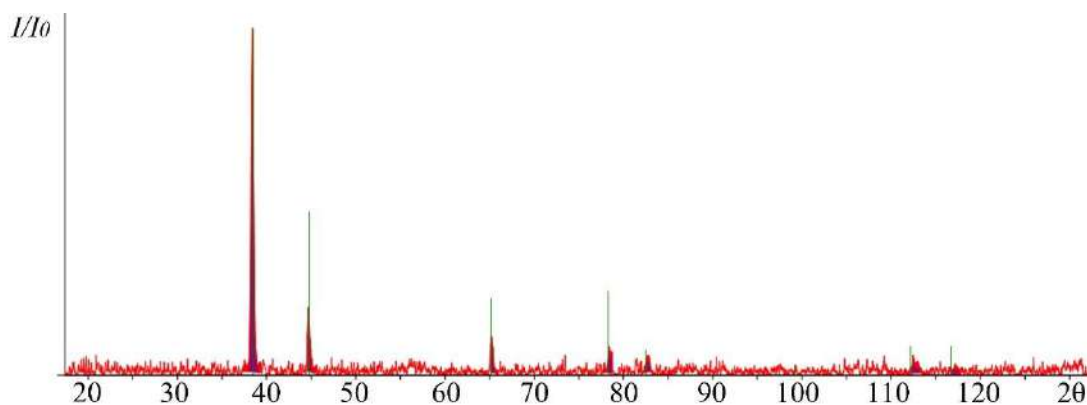


Fig. 1. Diffraction pattern of a liquid-quenched single-phase highly supersaturated fcc binary Al-5 wt.% Cr alloy

## Results

We can see from Table 1 that introducing the FL leads to a decrease in the intensity of linear wear and the abrasive wear ratio of UHMWPE by 2.8 and 2 times, respectively. The increase in wear resistance of UHMWPE in both friction conditions is because solid FL particles ( $HV \approx 600$  MPa) strengthen the surface layer, increasing its hardness by 1.5 times and resistance to mechanical stress. This, in turn, contributes to a uniform distribution of the applied load, a decrease in the depth of the ploughing furrows (roughness in both friction methods decreases by about 1.5 times), and local pressure concentration [13]. As a result, this contributes to a slowdown in the formation of microcracks (Fig. 2).

Table 1

Functional properties of UHMWPE and PCM based on it							
Indicator	Filler content, wt.%						
	0	5	10	15	20	25	30
linear wear intensity*, $I_h \cdot 10^{-7}$	15,8	11,2	8,7	6,9	5,7	6,8	8,1
abrasive wear rate*, $V_i, \text{mm}^3/\text{m}$	1,36	0,9	0,75	0,73	0,72	0,8	0,95
Hardness HRR, hardness units	32	38	41	45	48	46	44
Roughness of friction surfaces***, $R_a, \mu\text{m}$ :							
- under friction conditions without lubrication	2,14	1,90	1,72	1,51	1,45	1,63	1,85
- under the influence of rigidly fixed abrasive particles	2,57	2,11	1,97	1,92	1,87	1,97	2,24
Coefficient of friction, $f$	0,12	0,13	0,15	0,15	0,16	0,13	0,12

\* average value from 3 experiments

\*\*average value from 5 test cycles

\*\*\*average value of at least 12 measurements

In addition, a harder FL in the composition of UHMWPE leads to an improvement in the adhesive and cohesive properties of the polymer, the formation of an "antifriction coating" on the steel counterbody, which reduces the intensity of the formation of adhesion zones with the steel counterbody (Fig. 2), and the formation of fragmented wear particles in the process of friction without lubrication. These facts are confirmed by a comparison of the morphology of the friction surfaces of pure UHMWPE (Fig. 2, 1) and PCM based on it (Fig. 2, 2) [14].

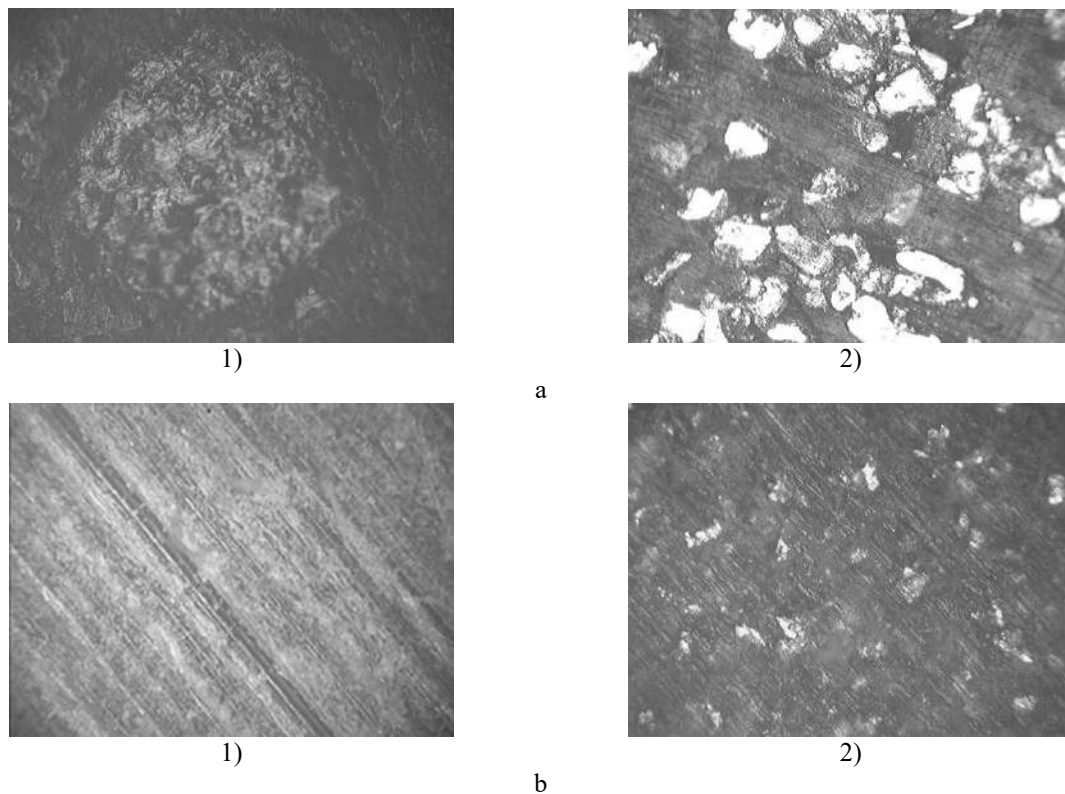


**Fig. 2. Friction surfaces ( $\times 200$ ) of pure UHMWPE (1) and polymer composite (2) based on it, containing 20 wt.% binary Al-Cr alloy according to the scheme under friction conditions without lubrication (a) and on rigidly attached abrasive particles (b)**

On the other hand, forming a more ordered supramolecular structure can explain the increase in the functional properties of UHMWPE.

Worth noting that the improvement of the functional properties of UHMWPE is observed at 5–20 wt.% filler content. Further increase to 25–30 wt.% in UHMWPE leads to a deterioration of all indicators due to the increase in structural defects, which in turn are caused by the agglomeration of binary alloy particles, their uneven distribution in the volume of UHMWPE, and a decrease in the adhesive interaction at the "FL-UHMWPE" interface. Consequently, this causes the formation of weak zones (pores and voids), which reduce the hardness and strength of the PCM and also cause the intensification of wear processes under the influence of the applied load.

The increase in friction coefficient for all PCMs containing metallic FL in the composition is observed (Table 1). The fact that the solid particles of the Al-Cr alloy contribute to the formation of additional mechanical bonds with the steel counterbody, which increases the sliding resistance, can explain this [15].

## Conclusions

Analysing the results of the study of the developed PCMs tribological properties showed that the introduction of 5-20 wt.% liquid-quenched binary Al-Cr alloy leads to an increase in wear resistance under conditions of friction without lubrication and the influence of abrasive particles by 2.8 and 2 times, respectively. The fact that harder FL particles strengthen the UHMWPE, as a result of which the friction surface more effectively counteracts destructive processes, can explain the improvement of these indicators. We can recommend PCMs with an effective FL content of 20 wt.% for the manufacture of working bodies (rollers, gears, and bearing housings) and friction units (gears, sprockets, bushings, and plain bearings) of agricultural machinery and the mining industry operating under conditions of impact-abrasive or fatigue wear.

## References

1. I.M. Rybalko, R.S. Ryzhkov Management of abrasive wear of machine parts "Youth and Industry 4.0 in the 21st Century" Materials of the 20th International Youth Forum (April 04-05, 2024, Kharkiv). Kharkiv: SBTU, 2024. P.142.
2. A.S. Kobets Application of polymer composites in the agricultural industry. Monograph. Dnipro: Zhurfond, 2022. 356 p.
3. O.O. Skvortsov, O.O. Mikosianchyk Research of the wear resistance of electro-spark coatings under abrasive conditions. Problems of friction and wear. 2023. Vol.100, №3. P. 64-72.
4. M.S. Khimko, A.M. Khimko, P.G. Mnatsakanov, V.V. Klipachenko, R.O. Makarenko Wear resistance of polymer composite materials for plane spherical bearings. Problems of friction and wear. 2024. Vol.103, No.2. P. 29-42.
5. M. Skakov, M. Bayandinova, Y. Kozhakhmetov, B. Tuyakbaev Microstructure and corrosion resistance of composite based on ultra-high molecular weight polyethylene in acidic media. Coatings 2025. Vol. 15, No.1. P. 89; <https://doi.org/10.3390/coatings15010089>
6. A.Y. Adesina, M.F. Khan, M.U. Azam, M. Abdul Samad, A.A. Sorour, Characterization and corrosion resistance of ultra-high molecular weight polyethylene composite coatings reinforced with tungsten carbide particles in hydrochloric acid medium. Journal of Polymer Engineering. 2019. Vol. 39. P. 861–873.
7. J.F. M. Borges, O.M. Cintho, A. Camilo Júnior, M.D. Michel Ultra-high molecular weight polyethylene filled with iron by mechanical alloying. Revista delos. 2024. 17(61). e2660. <https://doi.org/10.55905/rdelosv17.n61-098>
8. T. Deplancke, O. Lame, S. Barrau, K. Ravi, F. Dalmas Impact of carbon nanotube prelocalization on the ultra-low electrical percolation threshold and on the mechanical behavior of sintered UHMWPE-based nanocomposites. Polymer. 2017. Vol. 111. P. 204–213.
9. V.F. Bashev, A.-M.V. Tomina, K.A. Mykyta, T.V. Kalinina, S.I. Riabtsev, O.I. Kushnerov The influence of a rapidly-quenched filler on the wear resistance of ultrahigh molecular weight polyethylene. Functional Materials. 2024. Vol.31, No.3. P. 387-390.
10. V.F. Bashev, S.V. Tomin, T.V. Kalinina, O.I. Kushnerov, N.P. Bondar Effect of binary Al-Ni alloy on the rate of abrasive wear of ultra-high molecular weight polyethylene. Functional Materials. 2024. Vol.31, No.4. P. 557–560.
11. J. Baena, J. Wu, Z. Peng, Wear performance of UHMWPE and reinforced UHMWPE composites in arthroplasty applications. A Review. Lubricants. 2015. Vol. 3, No.2. P. 413–436.
12. S.I. Mudryi, Yu. O Kulik, A.S. Yakymovych. X-ray structural analysis in materials science. teaching-methodical manual. -Ivan Franko National University of Lviv. Lviv-2017. 226 p.
13. A.-M.V. Tomina, Y.A. Yeriomina Studying the influence of HB-4 amorphous alloy on tribological properties of phenylene aromatic polyamide. Functional Materials. 2022. Vol.29, No.3. P. 388–392.
14. Ye. Yeriomina, A. Burya, T. Rybak Investigating the influence of fine-dispersed aluminum, nickel and titanium on the properties of phenylene. Scientific Journal of TNTU. Tern.: TNTU, 2019. Vol. 94. No. 2. P. 58–63.
15. O. Burya, Ye. Yeriomina, O. Lysenko, A. Konchits, A. Morozov, Polymer composites based on thermoplastic binders, Dnipro: Srednyak T. K. Press. 2019. 239 p.

**Попіль О.І., Томіна А.-М.В.** Вплив бінарного сплаву системи Al-Cr на трибологічні властивості надвисокомолекулярного поліетилену

У роботі досліджено вплив загартованого з рідини бінарного сплаву системи Al-Cr з відсотковим вмістом хрому 5 мас.% на трибологічні властивості надвисокомолекулярного поліетилену в умовах тертя без змащення за схемою «диск-колодка» та за жорсткозакріпленими частками абразиву. Встановлено, що введення цього сплаву у кількості 5-30 мас.% призводить до зменшення інтенсивності лінійного зношування та показника абразивного стирання надвисокомолекулярного поліетилену в 2,8 та 2 рази відповідно. Покращення цих показників зумовлене декількома чинниками. Введення твердого наповнювача з мікротвердістю близько  $HV \approx 600$  МПа сприяє зміцненню поверхневого шару матеріалу, що, в свою чергу, збільшує його опір до механічного впливу та зменшує інтенсивність руйнування поліетилену в умовах тертя без змащення та за жорсткозакріпленими частками абразиву. З іншого боку, це можна пояснити формуванням більш напруженої решітки твердого розчину на основі Al, оскільки відомо, що загартовані з рідкого стану бінарні сплави на основі алюмінію характеризуються високим ступенем мікронапружень через значну різницю в розмірах атомів Al-Cr ( $r_{Al}=0,142$  нм та  $r_{Cr}=0,128$  нм). Що стосується коефіцієнту тертя, введення бінарного сплаву системи Al-Cr до надвисокомолекулярного поліетилену призводить до його збільшення. Це обумовлено появою додаткових механічних зчеплень твердих часток наповнювача з сталевим контртілом, що в свою чергу, сприяє зростанню опору ковзанню. Найкращим комплексом функціональних властивостей характеризується композит з вмістом наповнювача 20 мас.%. Даний матеріал можна рекомендувати для виготовлення деталей триботехнічного (шестерні, зірочки, втулки та підшипники ковзання) і конструкційного (ролики, зубчасті колеса та корпуси підшипників) призначення сільськогосподарської техніки і гірничодобувної промисловості, що працюють в умовах ударно-абразивного або втомного зношування.

**Ключові слова:** надвисокомолекулярний поліетилен, загартований з рідини бінарний сплав Al-Cr, дисперсний наповнювач, показник абразивного стирання, інтенсивність лінійного зношування



## **Analysis of the influence of radial clearance in a bearing on its operating modes, taking into account mass and magnetic imbalance of the induction motor rotor**

**A. Goroshko**<sup>\*0000-0002-1386-2326</sup>, **M. Zembytska**<sup>0000-0002-6671-9937</sup>

*Khmelnytskyi National University, Ukraine*

*\*E-mail: [iftomm@ukr.net](mailto:iftomm@ukr.net)*

*Received: 15 March 2025; Revised 30 March 2025; Accept: 25 April 2025*

### **Abstract**

The article studies the problem of the journal motion of a three-phase induction motor rotor in a bearing. A simplified model of the journal motion is studied at the moment of journal separation and transition from the pendulum mode of journal motion to the impact mode. In this case, the elastic-damping properties of the bearing and the final rigidity of the rotor are ignored. The model takes into account the eccentricity of the rotor mass and the radial internal clearance of the bearing. In addition, the forces of unbalanced magnetic pull (UMP) caused by the magnetic eccentricity of the induction motor rotor, which is caused by the radial clearance of the bearing, are taken into account. It is analytically shown that the forces of UMP cannot be ignored, since even the rated clearance of bearings of low- and medium-power motors causes an unbalanced force commensurate with the force caused by the eccentricity of the mass. Using numerical modeling and simulation for a three-phase induction motor with a squirrel-cage rotor with a power of 11 kW and a speed of 3000 rpm, the dependences of the critical frequency of the journal separation from the bearing for different values of the mass eccentricity and radial clearance are presented. It is shown that without taking into account the UMP, an increase in the radial clearance leads to a decrease in the critical separation speed. In this case, a bearing with a passport radial clearance is able to switch to the mode of periodic impacts of the journal at a speed lower than the nominal speed of rotation of the rotor with an acceptable eccentricity. Taking into account the UMP, on the contrary, it significantly increases the value of the critical separation speed. At the same time, it is necessary to take into account that with an increase in UMP, the radial load on the bearing also increases, which in turn leads to increased wear of the bearing.

**Keywords:** Bearing internal clearance, Induction motor, Unbalanced magnetic pull, Mass eccentricity, Bearing vibration

### **Introduction and review of publications**

When the rotor of an induction motor rotates, dynamic forces caused by rotor imbalance act on its pins. In general, unbalance can be caused by mass eccentricity, rotor deflection, and magnetic eccentricity. Unbalanced dynamic forces act on the bearings, causing increased bearing wear [1, 2].

According to researchers, more than 40% of induction motor failures are related to bearings [1]. During operation of rotor machines, radial clearances in rolling bearings increase, which leads to reduction of design values of critical shaft speeds [2, 3]. Excessive clearance can cause vibration at the fundamental train frequency (FTF) as the rolling elements accelerate and decelerate through the load zone which can result in large impact forces between the rolling elements and cage pockets. Also outer race defects and roller defects can be modulated with the FTF fundamental frequency [4]. Several researchers have studied the increase of bearing loads due to Unbalanced Magnetic Pull (UMP) [5-7]. It has been shown that the additional bearing loads are affected by curved eccentricity and the axial variation of eccentricity, and this can shorten the lifetime of the bearing.

It is known that, depending on the dynamics, bearings can operate in three modes: the mode of pendulum oscillations, the mode of periodic journal impacts on the bearing, and the mode of journal movement around the bearing circumference, in which the journal rolls with slippage [8-10]. The most dangerous is the second mode, the impact mode of bearing operation, which occurs as a result of the journal separation from the bearing. This



causes rapid bearing failure. The journal separation from the bearing occurs at a certain frequency, the value of which depends on the geometric and mass parameters of the bearing and rotor. Therefore, the criterion for smooth, reliable operation of the rotor of an induction motor is a rotor speed that is less than the critical speed that occurs when the journal separates from the bearing.

The issue of the stability of operating modes of bearings with radial clearance is well studied [11, 12, 13]. Researchers use the Hertz theory, models with elastic and elastic-plastic contact [14, 15]. The issue of modeling the dynamics of bearings with defects has also been well studied [16-19]. However, most studies on bearing failures do not take into account the peculiarities of electric motors, such as unbalanced magnetic pull (UMP) on the rotor of a three-phase induction motor.

### Aims of the paper

This paper analyzes the effect of internal radial clearance in a bearing of a three-phase induction motor on the occurrence of unbalanced forces and the conditions for the emergence of an undesirable shock mode of bearing operation.

### Problem analysis and model justification

Let's estimate the actual radial internal clearance of a radial single row bearing of an 11 kW induction motor with a rated speed of 3000 rpm. According to ISO 5753, the internal clearance of a 6208 ZZ-C3 deep groove ball bearing is 15...33  $\mu\text{m}$ . It is known that average bearing wear can lead to a 100% increase in the nameplate clearance. The actual clearance consists of the nameplate clearance and the clearance caused by elastic deformation. For stiffness  $5,52 \cdot 10^7$  N/m, under the influence of rotor gravity and imbalance from the permissible mass eccentricity of 20  $\mu\text{m}$  at the nominal speed  $\omega=304$  rad/s, the gap will additionally increase by 26,4  $\mu\text{m}$  [20]. Thus, the total gap of the worn bearing during operation of the motor under consideration is about  $2\Delta=56...92$   $\mu\text{m}$  and can lead to a significant unevenness of the air gap  $\delta$  between the rotor and stator of the induction motor (Fig. 1). In particular, for the engine under study, the average air gap is  $\delta_0=450$   $\mu\text{m}$ . The variable unevenness of the air gap, called dynamic eccentricity, causes a change in the bearing's restoring force, which leads to wear. The permissible magnetic eccentricity of the rotor in question is 10%. In the event of improper motor assembly, thermal deformation of the rotor, severe wear of the bearing during operation, and an increase in its clearance, the magnetic eccentricity may increase, increasing dynamic unbalanced forces that further accelerate bearing failure.

### Research methodology

#### Mathematical modeling of the problem of journal movement in a bearing

To create a simplified mathematical model of the journal dynamics in a bearing with an internal radial clearance  $2\Delta$  we neglect the elastic-damping properties of the bearing and rotor. We assume that the rigid rotor rotates in rigid supports, and the centrifugal forces acting on it are caused only by mass and magnetic eccentricity. This assumption is valid for a significant number of low- and medium-power induction motors. Let's also assume that the unbalanced magnetic pulling forces are applied in the geometric center of the rotor and result from a reduction of the air gap between the stator and rotor by the value  $\Delta/2$ , which is equal to half the radial displacement of the journal in the bearing of the gap in the bearing  $\Delta$ . Then the minimum air gap formed is equal to  $\delta_{\min} = \delta_0 - \Delta/2$ , the maximum is equal to  $\delta_{\max} = \delta_0 + \Delta/2$ . In the following, we will assume that the angular position of the minimum air gap between the stator and rotor  $\delta_{\min}$  and the angular position of the journal are the same and equal to the angle  $\psi$ . The resulting magnetic eccentricity of the rotor is equal to  $(\delta_{\max} - \delta_{\min})/2 = \Delta/2$ .

Let a rotor with mass eccentricity  $e$  rotate with angular speed  $\omega$ . At a certain moment of the pendulum mode, the journal occupies the position in the bearing shown in Fig. 2. Due to the clearance  $\Delta$  the movement of the journal relative to the bearing consists of a rotational movement with a speed  $\omega$  and angular oscillations determined by the angle  $\psi$ . The speed of the journal movement along the bearing is equal to  $\Omega = \frac{d\psi}{dt}$ .

Forces act on the journal: gravity  $mg$ , centrifugal force of the trunnion movement  $m\Omega^2\Delta$ , tangential force of inertia  $m\dot{\Omega}\Delta$ , centrifugal force due to rotor unbalance  $m\omega^2e\cos(\omega t - \psi)$ , friction force  $F$ , interaction force between the journal and bearing  $R$ , projections of the unbalanced magnetic pull force  $F_{UMP}$ .

The equilibrium condition implies that

$$mg \cos \psi + m\Omega^2\Delta + m\omega^2e \cos(\omega t - \psi) + F_{UMPx} - R = 0, \quad (1)$$

$$-m\dot{\Omega}\Delta - mg \sin \psi + m\omega^2e \sin(\omega t - \psi) + F + F_{UMPy} = 0, \quad (2)$$

where  $g$  is the acceleration of free gravity;  $m$  is the reduced mass of the rotor;  $\psi$  is the angular displacement of the journal from the vertical equilibrium position;  $\Omega$  is the journal movement speed along the bearing;  $\Delta$  is half the bearing clearance;  $F$  is the friction force;  $R$  is the bearing reaction force;  $F_{UMPx}$ ,  $F_{UMPy}$  are projections of the unbalanced magnetic pulling forces on the axes Ox, Oy, respectively.

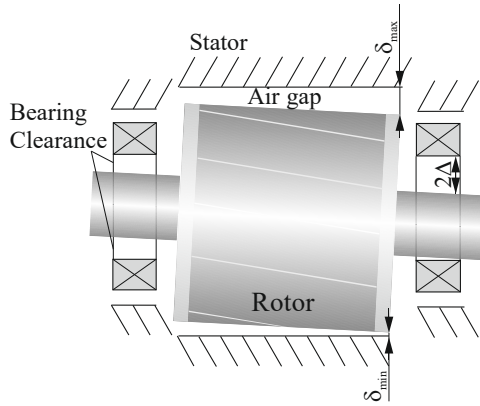


**Fig. 1. Formation of an uneven air gap between the stator and rotor**

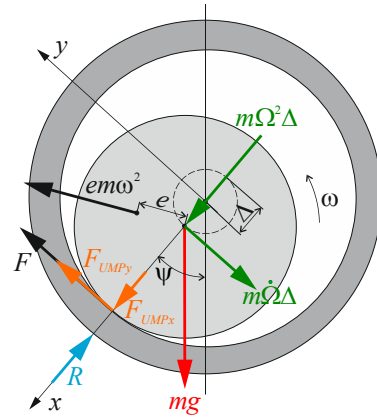


**Fig. 2. Diagram of the forces acting on the journal in the bearing**

Assuming a constant rotational speed  $\omega = \text{const}$  we use the theoretical expressions proposed in [21, 22] to estimate the UMP force (Fig. 4). UMP is highly nonlinear. Without loss of generality, let us consider the UMP of a bipolar motor. The projections of the unbalanced magnetic pulling forces on the given coordinate axes for the number of pole pairs  $p=1$  are approximately defined as

$$\begin{aligned} F_{UMPx} &= f_1 + f_2 \cos 2\omega_e t, & f_1 &= 0.25 R l \pi \mu_0^{-1} F_j^2 (2\Lambda_0 \Lambda_1 + \Lambda_1 \Lambda_2 + \Lambda_2 \Lambda_3), \\ F_{UMPy} &= f_2 \sin 2\omega_e t, & f_2 &= 0.125 R l \pi \mu_0^{-1} F_j^2 (2\Lambda_0 \Lambda_1 + \Lambda_1 \Lambda_2 + \Lambda_2 \Lambda_3), \end{aligned} \quad (3)$$

where  $\omega_e$  is the angular frequency of the power supply of the motor stator windings,  $\omega_e = \omega(1-s)^{-1}$ ,  $s$  is the slip of the motor;  $f_1, f_2$  are the amplitudes of the UMP components,  $R$  is the rotor radius;  $l$  is the rotor length;  $F_j$  is the amplitude of the fundamental harmonic of the rotor magnetomotive force (MMF) excitation;  $\mu_0$  is the absolute magnetic permeability of air;  $\Lambda_i$  Fourier coefficients in the record of the magnetic permeability of the air gap, which can be calculated as

$$\Lambda_i = \frac{\mu_0}{\delta_0} \frac{1 + (1 - \delta_{i0})}{\sqrt{1 - \varepsilon^2}} \left( \frac{1}{1 + \sqrt{1 - \varepsilon^2}} \right)^i, \quad i \geq 0. \quad (4)$$

where  $\varepsilon = \Delta/2\delta_0$  is the relative eccentricity,  $\delta_0$  is the average value of the air gap when the rotor is centered;  $\delta_{i0}$  is Kronecker symbol.

The condition for journal separation from the bearing is  $R=0$ . Having differentiated (2) according to  $\psi$  and adding the result from (1), we have

$$\frac{d}{d\psi} (m\dot{\Omega}\Delta) = m\Omega^2\Delta + F_{UMPx}. \quad (5)$$

Multiplying both parts of equation (5) by  $\frac{d\Omega}{dt}$  and taking into account (3) and  $\Omega = \frac{d\psi}{dt}$  after simplifications we have

$$d \left( \frac{d\Omega}{dt} \right)^2 = \frac{1}{2} d(\Omega^4) + \frac{f_1 + f_2 \cos 2\omega_e t}{m\Delta} \cdot d(\Omega^2), \quad (6)$$

After integrating both parts, we have

$$\left( \frac{d\Omega}{dt} \right)^2 = \frac{1}{2} (\Omega^4) + \frac{f_1 + f_2 \cos 2\omega_e t}{m\Delta} \cdot \Omega^2 + \frac{f_2}{m\Delta} \int \Omega^2 d(\cos 2\omega_e t) + C. \quad (7)$$

Let us find the integration constant  $C$  from the initial conditions. Suppose that at the initial moment  $t=0$  the journal has an angular displacement from the vertical position  $\psi_0$ . This can only be accomplished when the journal speed is very high. Hence, we have the initial condition: at  $t=0$   $\psi=\infty$ . Analyzing (10), it is clear that the term on the right-hand side  $\frac{1}{2}(\Omega)^4$  is asymptotically increasing much faster than the other terms and the latter can be neglected. With sufficient accuracy, equation (7) can be simplified to the form

$$\left(\frac{d\Omega}{dt}\right)^2 = \frac{1}{2}(\Omega)^4. \quad (8)$$

By integrating, we have

$$\Omega = \frac{\sqrt{2}}{t}. \quad (9)$$

Since  $\psi(t)$  has a break at  $t=0$ , integrating expression (11) using the Dirac delta function, we obtain the value of the journal separation angle from the bearing [8]

$$\psi_{cr} = \sqrt{2} \int_0^{t_{cr}} \delta t dt = \sqrt{2}. \quad (10)$$

According to (10) the trunnion separation angle is equal to  $\cong 81^\circ$  and does not depend on the unbalance forces caused by the mass and magnetic eccentricity.

Analysis of (1) shows that the condition for journal separation is  $R=0$ , which is possible only when the condition

$$m\omega^2 e \cos(\omega t - \psi) + F_{UMPx} < 0. \quad (11)$$

Considering what  $f_1 \geq 0$  is an integral part of the zero frequency, we have

$$\cos(\omega t - \psi) + \frac{f_2}{m\omega^2 e} \cos\left(\frac{2}{1-s}\omega t\right) < 0. \quad (12)$$

Special cases of dependence (12).

1. The component force of the UMP of a double electric frequency is small compared to the unbalanced force from the mass imbalance  $f_2 \ll m\omega^2 e$ :

$$\cos(\omega t - \psi) < 0 \Rightarrow \frac{\pi}{2} < \omega t - \psi \leq \frac{3\pi}{2}. \quad (13)$$

The smallest value of the unbalanced force corresponds to the condition  $\omega t - \psi = \pi$ , hence the critical rotor speed is equal to

$$\omega_{cr} = \frac{\pi + \sqrt{2}}{t_{cr}}. \quad (14)$$

After substituting expression (14) into (1), we have the value of the separation time  $t_{cr}$ . Using  $t_{cr}$ , the critical rotor speed can be found from the expression:

$$\omega_{cr} = \frac{\left(\frac{\pi}{\sqrt{2}} + 1\right) \sqrt{\cos \sqrt{2} + \frac{f_1}{mg}}}{\sqrt{\frac{(\pi + \sqrt{2})^2 e}{2\Delta} - 1}} \cdot \omega_p, \quad (15)$$

where  $\omega_p = \sqrt{\frac{g}{\Delta}}$  is frequency of pendulum oscillations of the journal.

Under this condition  $\Delta = 0.5(\pi + \sqrt{2})^2 e$  we have  $\omega_{cr} \rightarrow \infty$  and the pendulum mode is ensured at any speed without journal separation.

Consequently, the component of the unbalanced magnetic pulling force of the zero electric frequency increases the value of the critical frequency of rotor journal separation from the bearing.

The analysis of the magnitude of the UMP forces for the considered induction motor shows that the condition is fulfilled only for very small values of  $\Delta < 1 \mu\text{m}$ , which are not encountered in practice, so dependence

(15) has no practical significance. This confirms the need to take into account the UMP when analyzing the dynamics of induction motor bearing supports.

2. The UMP force component of the double electric frequency is significantly higher than the unbalanced force from the mass imbalance, we have  $f_2 \gg m\omega^2 e$ :

$$\cos \frac{2}{1-s} \omega t < 0 \Rightarrow \frac{\pi}{2} < \frac{2}{1-s} \omega t \leq \frac{3\pi}{2}. \quad (16)$$

Assuming that the separation occurs at the lowest value of  $f_2$ , we have  $2(1-s)^{-1} \omega t = \pi$ , hence the critical rotor speed is equal to

$$\omega_{cr} = \frac{\pi}{2t_{cr}}(1-s). \quad (17)$$

Substituting the value of (17) into (1), we have the value of the separation time  $t_{cr}$ . Using  $t_{cr}$ , the critical rotor speed can be found from the expression:

$$\omega_{cr} = \frac{\pi(1-s)}{2\sqrt{2}} \sqrt{\frac{f_2 - f_1}{mg} - \cos\sqrt{2}} \cdot \omega_p. \quad (18)$$

The analysis of the components of the UMP force in (3) in the case of the condition  $f_2 \gg m\omega^2 e$  shows that it is always  $f_2 - f_1 \leq 0$ , and therefore dependence (18) cannot be fulfilled, i.e., the pendulum mode of bearing operation never goes into the shock mode.

We analyze the general case of dependence (12) using numerical methods.

### Numerical experiment and simulation results

To change from the pendulum mode to the impact mode, the eccentricity  $e$  of the rotor mass must be sufficient to make the unbalanced force  $m\omega^2 e$  caused by it exceed the vector sum of the forces  $F_{UMP}$  and  $mg$ . This condition can be investigated using the example of a specific induction motor. An 11 kW motor was chosen for modeling. The main characteristics of the motor are shown in Table 1. The simulation was carried out in the *Simulink* environment of the *MATLAB* mathematical package.

Table 1

Parameters of the three-phase motor		
Notation	Description	Value
Motor data		
$n$	Synchronous speed (rpm)	3000
$s$	Rated slip	0,033
$R$	Radius of the rotor (mm)	63,5
$l$	Length of the rotor (mm)	130
$m_r$	Mass of the rotor (kg)	14,22
$\delta_0$	Mean air-gap length (mm)	0,45
$\mu_0$	Air permeance (H/m)	$4\pi \cdot 10^{-7}$
$F_j$	Fundamental MMF amplitude of the rotor excitation current (A)	358
$p$	Number of pole pairs	1
$e$	Permissible eccentricity ( $\mu\text{m}$ )	20

The radial force of pressing the journal against the bearing is found from (1):

$$R = mg \cos \psi + m\Omega^2 \Delta + m\omega^2 e \cos(\omega t - \psi) + F_{UMPx}. \quad (19)$$

At the moment of journal separation from the bearing, we have:  $R=0$ ,  $\psi = \sqrt{2}$ ,  $\Omega = \sqrt{2}t^{-1}$  and the following relationship is fulfilled

$$g \cos \sqrt{2} + \Delta \frac{2}{t^2} + \omega^2 e \cos(\omega t - \psi) + \frac{f_1}{m} + \frac{f_2}{m} \cos\left(\frac{2}{1-s} \omega t\right) = 0. \quad (20)$$

Comparative dependences of the critical separation velocity on the mass eccentricity at different values of the radial air clearance in the bearing without and with consideration of UMP forces are shown in Figs. 3, 4.

An increase in the radial clearance in the bearing leads to an increase in the critical journal separation rate. But at the same time, the radial force increases significantly.

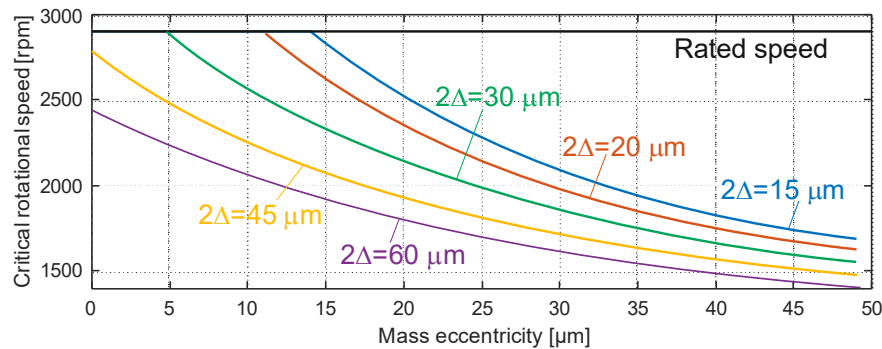


Fig. 3. Dependence of the critical separation speed on the mass eccentricity at different values of the radial air gap in the bearing without taking into account the UMP forces

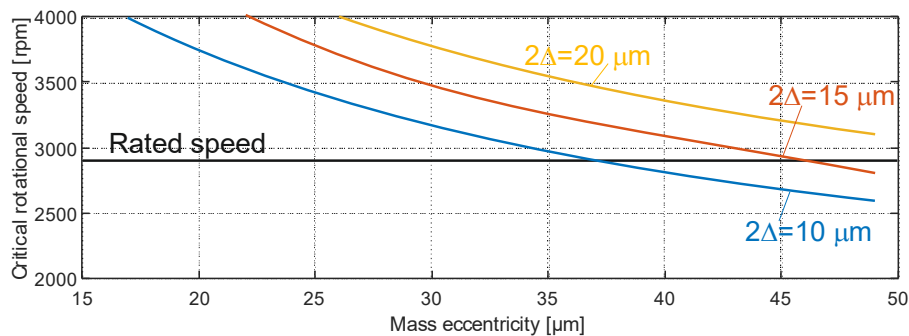


Fig. 4. Dependence of the critical separation speed on the mass eccentricity at different values of the radial air gap in the bearing, taking into account the UMP forces

### Research conclusions and recommendations for further research in this area

In addition to mechanical forces, electromagnetic forces, in particular, UMP forces, affect the magnitude of the rotor journal pressing force against the bearing in a three-phase induction motor. Since the UMP are applied at the point of the smallest air gap between the stator and rotor and increase with the magnetic eccentricity, they have a significant impact on the critical rotor speed at which the journal separation from the bearing occurs.

Neglecting the UMP phenomenon, it can be concluded that an increase in the radial clearance in the bearing leads to a decrease in the critical journal separation speed and a faster transition from the pendulum to the dangerous shock mode of bearing operation. This shock mode is more dangerous because it leads to faster wear.

The presence of radial bearing clearances indicates that it is unlawful to neglect the UMP phenomenon when analyzing a three-phase induction motor. The UMP phenomenon creates additional forces of double electrical frequency that press the journal against the bearing. An increase in the radial clearance in the bearing leads to an increase in the critical journal separation speed. But at the same time, the radial force acting on the bearing increases significantly. The pendulum mode of operation is preserved, but the load on the bearing increases significantly, which in turn leads to accelerated one-sided wear.

Despite the fact that the developed model is approximate and does not take into account the elastic-damping properties of the bearing and the flexibility of the rotor, important results have been obtained. The analysis of the bearing assembly in accordance with the Hertzian contact stress theory will make it possible to refine the results obtained here.

### References

1. Report of Large Motor Reliability Survey of Industrial and Commercial Installations: Part 3. IEEE Trans. Ind. Appl. 1987, IA-23, 153–158. <https://doi.org/10.1109/TIA.1987.4504880>
2. Huang, L., Shen, G., Hu, N., Chen, L., & Yang, Y. (2022). Coupled Electromagnetic-Dynamic Modeling and Bearing Fault Characteristics of Induction Motors considering Unbalanced Magnetic Pull. *Entropy*, 24(10), 1386. <https://doi.org/10.3390/e24101386>
3. Petryna, J., Duda, A., & Sułowicz, M. (2021). Eccentricity in induction machines—A useful tool for assessing its level. *Energies*, 14(7). <https://doi.org/10.3390/en14071976>
4. Lacey, S. J. (2008). An overview of bearing vibration analysis. *Maintenance & asset management*, 23(6), 32-42

5. Dorrell, D. G. (2011). Sources and characteristics of unbalanced magnetic pull in three-phase cage induction motors with axial-varying rotor eccentricity, *IEEE Trans. Ind. Appl.*, vol. 47, no. 1, pp. 12–24. <https://doi.org/10.1109/ECCE.2009.5316545>
6. Di, C., Bao, X., Wang, H., Lv, Q. and He, Y. (2015). Modeling and Analysis of Unbalanced Magnetic Pull in Cage Induction Motors With Curved Dynamic Eccentricity, *IEEE Trans. Magn.*, vol. 51(8), p. 8106507. <https://doi.org/10.1109/TMAG.2015.2412911>
7. Ruf, A., Schröder, M., Putri, A. K., Konrad, R., Franck, D., and Hameyer K. (2016). Analysis and determination of mechanical bearing load caused by unbalanced magnetic pull, *Int. J. Comput. Math. Electr. Electron. Eng.*, vol. 35, no. 2, pp. 728–743. <https://doi.org/10.1108/COMPEL-03-2015-0111>
8. Theory and practice of balancing technology. Edited by V. A. Shchepetilnikov. M. Mashinostroenie. 1973. 467 p. In Russian.
9. Xu, M., Shao, Y., Han, Y., Gu, F., & Ball, A. (2020). A Numerical Analysis of Internal Radial Clearances on Affecting Vibration of Rolling Element Bearings with Local Defects. In *International Conference on Maintenance Engineering* (pp. 1-13). Cham: Springer International Publishing. [https://doi.org/10.1007/978-3-030-75793-9\\_1](https://doi.org/10.1007/978-3-030-75793-9_1)
10. Kurvinen, E., Viitala, R., Choudhury, T., Heikkinen, J., & Sopanen, J. (2020). Simulation of Subcritical Vibrations of a Large Flexible Rotor with Varying Spherical Roller Bearing Clearance and Roundness Profiles. *Machines*, 8(2), 28. <https://doi.org/10.3390/machines8020028>
11. Tian, Q., Flores, P., & Lankarani, H. M. (2018). A comprehensive survey of the analytical, numerical and experimental methodologies for dynamics of multibody mechanical systems with clearance or imperfect joints. *Mechanism and Machine Theory*, 122, 1-57. <https://doi.org/10.1016/j.mechmachtheory.2017.12.002>
12. Liu, C. S., Zhang, K., & Yang, R. (2007). The FEM analysis and approximate model for cylindrical joints with clearances. *Mechanism and machine theory*, 42(2), 183-197. <https://doi.org/10.1016/j.mechmachtheory.2006.02.006>
13. Dykha, O., Makovkin, O., & Posonsky, S. (2021). Influence of lubrication on the friction and wear of car rolling bearings. *Problems of Tribology*, 26(3/101), 81–88. <https://doi.org/10.31891/2079-1372-2021-101-3-81-88>
14. Ambrożkiewicz, B., Syta, A., Georgiadis, A., Gassner, A., & Meier, N. (2022). Experimental Verification of the Impact of Radial Internal Clearance on a Bearing's Dynamics. *Sensors*, 22(17), 6366. <https://doi.org/10.3390/s22176366>
15. Changqing, B., & Qingyu, X. (2006). Dynamic model of ball bearings with internal clearance and waviness. *Journal of Sound and Vibration*, 294(1-2), 23-48. <https://doi.org/10.1016/j.jsv.2005.10.005>
16. Luo, W., Yan, C., Liu, Y., Wang, Z., Tian, Y., & Wu, L. (2024). Dynamic response of rolling element bearing with compound fault considering defect-rolling-element interaction. *Proceedings of the Institution of Mechanical Engineers, Part C: Journal of Mechanical Engineering Science*, 238(4), 879-894. <https://doi.org/10.1177/09544062231179076>
17. Liu, J., Xue, L., Wang, L., Shi, Z., & Xia, M. (2023). A new impact model for vibration features of a defective ball bearing. *ISA transactions*, 142, 465-477. <https://doi.org/10.1016/j.isatra.2023.08.014>
18. Nirwan, N. W., & Ramani, H. B. (2022). Condition monitoring and fault detection in roller bearing used in rolling mill by acoustic emission and vibration analysis. *Materials Today: Proceedings*, 51, 344-354. <https://doi.org/10.1016/j.matpr.2021.05.447>
19. Guo, B., Wu, W., Zheng, J., He, Y., & Zhang, J. (2023). Dynamics modeling and analysis of rolling bearings variable stiffness system with local faults. *Machines*, 11(6), 609. <https://doi.org/10.3390/machines11060609>
20. Goroshko A. V., Zembytska M. V., Paiuk V. P. (2024). Induction motor vibrations caused by mechanical and magnetic rotor eccentricity. *Journal of Engineering Sciences (Ukraine)*, Vol. 11(1), pp. D66–D77. [https://doi.org/10.21272/jes.2024.11\(1\).d8](https://doi.org/10.21272/jes.2024.11(1).d8)
21. Liu, Y, Chen, Z, Hua, X, Zhai, W. (2022) Effect of rotor eccentricity on the dynamic performance of a traction motor and its support bearings in a locomotive. *Proceedings of the Institution of Mechanical Engineers, Part F: Journal of Rail and Rapid Transit*. 236(9):1080-1090. <https://doi.org/10.1177/09544097211072335>
22. Dorrell, D. G., Hsieh, M., & Guo, Y. (2009). Unbalanced Magnet Pull in Large Brushless Rare-Earth Permanent Magnet Motors With Rotor Eccentricity. *IEEE Transactions on Magnetics*, 45, 4586-4589. <https://doi.org/10.1109/TMAG.2009.2022338>

**Горошко А.В., Зембицька М.В.** Аналіз впливу радіального зазору у підшипнику на режими його роботи з врахуванням масового і магнітного дисбалансу ротора асинхронного двигуна

У статті досліджується проблема руху цапфи ротора трифазного асинхронного двигуна в підшипнику. Досліджується спрощена модель руху цапфи в момент відриву цапфи та переходу від маятникового режиму руху цапфи до ударного режиму. Модель враховує ексцентриситет маси ротора та радіальний внутрішній зазор підшипника. У моделі не враховуються пружно-демпфувальні властивості підшипника та кінцева жорсткість ротора. Крім того, враховуються сили незбалансованого магнітного тяжіння, викликані магнітним ексцентриситетом ротора асинхронного двигуна, який зумовлений радіальним зазором підшипника. Аналітично показано, що силами незбалансованого магнітного тяжіння не можна нехтувати, оскільки навіть номінальний зазор підшипників двигунів малої та середньої потужності викликає незбалансовану магнітну силу, порівнювану з силою, викликану ексцентриситетом маси. За допомогою чисельного моделювання та симуляції для трифазного асинхронного двигуна з короткозамкненим ротором потужністю 11 кВт та синхронною швидкістю 3000 об/хв отримано залежності критичної частоти відриву шийки від підшипника для різних значень ексцентриситету маси та радіального зазору. Показано, що без урахування магнітного ексцентриситету ротора збільшення радіального зазору призводить до зменшення критичної швидкості відриву. У цьому випадку підшипник з паспортним радіальним зазором здатний переходити в режим періодичних ударів шийки на швидкості, нижчій за номінальну швидкість обертання ротора з допустимим ексцентриситетом. З урахуванням магнітного дисбалансу, навпаки, зростання радіального зазору викликає підвищення критичної швидкості відриву. Водночас необхідно враховувати, що зі збільшенням радіальної магнітної сили збільшується і радіальне навантаження на підшипник, що, в свою чергу, призводить до збільшення зносу підшипника.

**Ключові слова:** радіальний зазор підшипника, асинхронний двигун, незбалансоване магнітне тяжіння, ексцентриситет маси, вібрація підшипників



## Probabilistic approach to assessing tribotechnical reliability indicators of friction units

M.O. Dykha\*<sup>0000-0002-6075-1549</sup>, V.O. Dytyniuk<sup>0000-0001-6377-524X</sup>, A.L. Staryi<sup>0000-0001-7668-606X</sup>

*Khmelnytskyi national University, Ukraine*

\*E-mail: [tribosensor@gmail.com](mailto:tribosensor@gmail.com)

Received: 15 March 2025; Revised 10 April 2025; Accept: 28 April 2025

### Abstract

The article presents a theoretical and analytical review of the probabilistic approach to assessing the tribotechnical reliability of mechanical systems, in particular friction units. The influence of the random nature of loads and wear on the reliability of machine elements is considered. The feasibility of using distribution functions and probability density functions to describe the wear process is substantiated. Mathematical models are described in detail that allow determining the probability of element failure for given statistical characteristics of the load and permissible wear. Both constant and block load conditions are taken into account. The results of the study can be used in the design and operation of highly reliable tribotechnical systems, as well as for predicting their resource under conditions of operational uncertainty.

**Keywords:** tribotechnics, wear, probabilistic approach, reliability, failure function, coefficient of variation, block load.

### Introduction

Ensuring the reliability of technical systems is one of the main tasks of modern mechanical engineering, in particular in conditions of intensive operation and high loads. Friction units are one of the most vulnerable parts of mechanisms, and their premature failure can cause significant economic losses or even accidents. The traditional approach to reliability assessment often ignores the stochastic features of the operation of tribotechnical elements, which leads to an underestimation of the accuracy of predictions.

Given that the wear process is complex, non-uniform and largely random, there is a need to switch to probabilistic analysis methods. This approach allows us to take into account not only the average values of loads and wear, but also their variations, dispersions and other statistical characteristics. In particular, the use of probability density distribution functions allows us to estimate the probability of failure, construct reliability functions and optimize design parameters.

This article highlights the basic concepts and mathematical tools underlying the probabilistic approach to tribotechnical reliability. This research has practical implications for designers of mechanisms operating under conditions of significant and variable loads.

### Purpose and objectives of the study

The aim of the work is to develop a probabilistic model for assessing the reliability of friction units taking into account the random nature of wear and load. To achieve the set goal of the research, the following tasks were solved: to build mathematical models of wear and load distribution; to determine distribution and density functions for key parameters; to propose a methodology for assessing reliability under constant and block loading; to calculate reliability based on statistical characteristics.

### Research methods

The work uses methods of mathematical statistics, probability theory, as well as approximate analytical



methods (linearization of functions) to estimate the distribution characteristics. Both normal and arbitrary probability density distributions were used to model wear. The analysis was carried out by constructing reliability functions and failure functions for different load modes.

### Literature review

Tribological reliability issues in engineering have been widely discussed in the scientific literature. In [1], the main focus is on identifying failure modes and mechanisms. This is especially true for the emerging technology of microelectromechanical systems (MEMS). The focus here is on the mechanism of wear failure and how the methodology was used to create a predictive model. The MEMS device that was emphasized in these studies was a Sandia-developed micromotor with orthogonal electrostatic linear actuators connected to a gear on a hub. The dominant failure mechanism was wear in the sliding/contact zones. A sliding beam-on-post test structure was also used to measure friction coefficients and wear morphology for different surface coatings and environments. The results show that a predictive model of failure time as a function of drive frequency based on wear fits the functional form of the reliability data quite well and demonstrates the benefits of a fundamental understanding of wear. In [2], it is stated that tribological experimental studies have improved significantly in recent years, leading to a significant number of results and, as a result, an increasing number of papers are appearing. The scatter found in the data is often explained by many variables involved in the experiments, namely: the environment (especially humidity), layers of contaminants, differences in test conditions, uncertainty in the evaluation of the results and rarely - the response of the experimental equipment. This work aims to discuss several sources of inaccuracies that lead to the scatter of experimental tribology results. A reliability method is proposed to characterize friction and wear data. Experimental results obtained by unidirectional sliding and microabrasion will be used to support the discussion. In [3], it is stated that system reliability is an extremely important issue, especially in multi-core systems, which tend to have high power density and, consequently, temperature. Existing reliability-based methods are either slow and non-adaptive, or do not use task assignment and scheduling to compensate for the uneven wear state of the core. This paper presents a dynamically activated task assignment and scheduling algorithm based on theoretical results, which clearly optimizes the system lifetime. In the study [4], the effects of the coupling between linear guide wear and vibration of a machine table system are studied based on the infinitesimal method. A nonlinear dynamic model is developed to analyze the wear and vibration failure mechanisms under parameter uncertainty. To assess the dynamic reliability of a machine table system under multiple failure modes, a time-dependent and conditional reliability approach based on the Kriging model with active learning and Monte Carlo simulation is proposed. The approach eliminates the need to recalculate the real values of the limit state function, and the calculation efficiency is significantly increased. The document [5] describes methods for formulating and assessing the reliability of the system in conditions where failure is the result of wear of system parts reaching a critical threshold. A model is proposed related to the stochastic behavior of wear, in which a continuous, right-hand non-decreasing wear process consists of a “continuous” and a “jump” part. Several properties of the model we have proposed are presented. Also, a number of applied problems on wear and reliability are highlighted in the works [6-9]. At the same time, it should be noted a small proportion of works that analyze numerical dependencies for calculating tribotechnical reliability parameters.

### Main material.

#### Wear and tear as a random variable.

The dependence of wear on the friction path even under constant load is random (Fig. 1). At each given friction path, wear at pressure  $\sigma$  is a random variable. Like any random variable, wear is characterized by a probability distribution  $p(u_w)$  the appearance of this wear.

$p(u_w)$  is the density of the wear probability distribution or wear probability  $uw$ ;

$Q(u_w)$  is the probability distribution function of wear  $uw$ , or the probability of wear occurring from zero to the value  $uw$ ; this function is called the failure function:

$$Q(u_w) = \int_{-\infty}^{\infty} p(u_w) du_w, \quad (1)$$

$P(u_w)$  is a reliability function or probability of failure-free operation, i.e. the probability that wear  $u_w$  will not be achieved:

$$P(u_w) = 1 - Q(u_w). \quad (2)$$

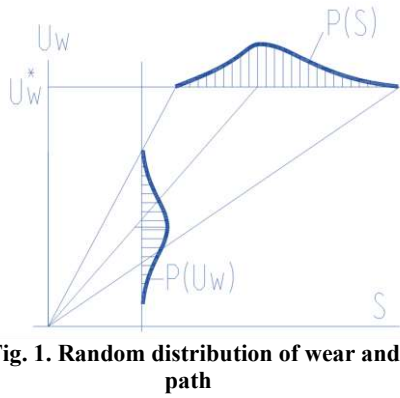


**Fig. 1. Random distribution of wear and friction path**

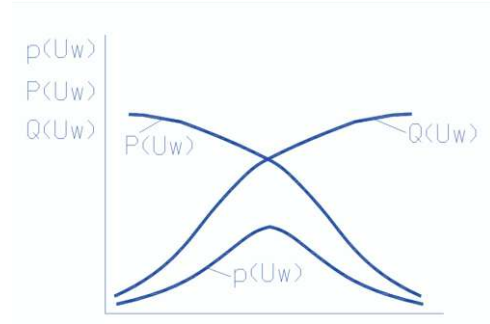


**Fig. 2. Reliability functions**

The probability distribution density is characterized by:

1) the mean or mathematical expectation

$$\bar{u}_w = m_{u_w} = \frac{1}{N} \sum_{i=1}^N u_{wi}; \quad (3)$$

2) dispersion

$$D_{u_w} = \frac{1}{N} \sum (u_{wi} - u_w)^2; \quad (4)$$

3) standard deviation

$$S_{u_w} = \sqrt{D_{u_w}}, \quad (5)$$

4) coefficient of variation

$$V_{u_w} = \frac{S_{u_w}}{\bar{u}_w}. \quad (6)$$

According to the above formulas, the characteristics of the distributions are determined from experimental data  $u_w$  and  $S_i$ .

Depending on the wear pressure and the friction path, the random nature of the wear is reflected in the value of the wear coefficient  $k_w$ :

$$u_w = k_w \sum_{i=1}^N \sigma_i^m \Delta s_i$$

Or in integral form:

$$u_w = k_w \sigma^m s. \quad (7)$$

In this dependence (7), in addition to the random variable  $k_w$ , there is, as a rule, the value of the acting pressures  $\sigma$ . Let the system be subjected to a random pressure  $\sigma$ . Random variable  $\sigma$ , as well as  $k_w$ , is described by the density distribution  $P(\sigma)$  with characteristics: average value  $\bar{\sigma}$ , pressure dispersion  $D_\sigma$ , the standard deviation  $S_\sigma$  and the coefficient of variation of pressures  $v_\sigma$ .

It should be emphasized that the random nature of a constantly acting load applies only to the set (set) of friction pairs operating under all other equal conditions, except for the load, the random nature of which is manifested in the random selection of the load at the beginning of the operation of the unit.

The task of constructing the density of the wear distribution for given wear coefficient distributions  $k_w$  and pressure  $\sigma$  in formula (7) can practically only be solved approximately. The average wear value  $\bar{u}_w$  is calculated by the formula for the average values of the arguments of random  $\bar{k}_w$  and  $\bar{\sigma}$ :

$$\bar{u}_w = \bar{k}_w \bar{\sigma}^m s. \quad (8)$$

To calculate the variance  $D_{u_w}$  we will use the approximate method of linearization of functions, according to which for the independent variables  $k_w$  and  $\sigma$ :

$$D_{u_w} = \left( \frac{\partial \bar{u}_w}{\partial \bar{k}_w} \right)^2 D_{k_w} + \left( \frac{\partial \bar{u}_w}{\partial \bar{\sigma}} \right)^2 D_{\sigma} \quad (9)$$

or taking into account (7):

$$D_{u_w} = (\bar{\sigma}^m s)^2 D_{k_w} + (\bar{k}_w m \bar{\sigma}^{m-1} s)^2 D_{\sigma}. \quad (10)$$

It is obvious that the constant value  $s$  can be placed outside the brackets:

$$D_{u_w} = s^2 \left[ (\bar{\sigma}^m)^2 D_{k_w} + (\bar{k}_w m \bar{\sigma}^{m-1})^2 D_{\sigma} \right]. \quad (11)$$

### Reliability assessment from wear under constant load.

The problem is posed as follows: there is a random variable of current wear  $u_w(s)$ , for example, (7) and the random variable of permissible wear  $u_w^*$ , it is necessary to find the probability that the current wear does not exceed the permissible one, that is:

$$P = P(u_w < u_w^*)$$

or

$$P = P[(u_w - u_w^*) > 0]. \quad (12)$$

From probability theory it is known that if the density of the distribution of quantities is given  $f_1(u_w)$  and  $f_2(u_w^*)$ , then the distribution density  $P(z = u_w - u_w^*)$  is calculated using the integral:

$$P(z) = \int_{-\infty}^{\infty} f_1(u_w) \left[ \int_{u_w}^{\infty} f_2(u_w^*) du_w^* \right] du_w. \quad (13)$$

This integral is taken only for certain types of density distributions  $f_1(u_w)$  and  $f_2(u_w^*)$ .

In the case where the distribution of effective and limit stresses obeys the normal law for determining  $P(s)$ , taking the integral (13) is not required in this case.

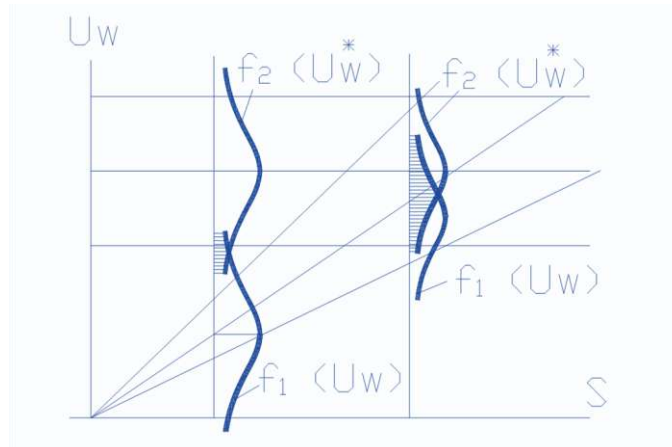


Fig. 3. Normal law of wear distribution

The function  $P(s)$  also obeys the normal law:

$$P(s) = \frac{1}{s_z \sqrt{2\pi}} e^{-\frac{(z-\bar{z})^2}{2D_z}}, \quad (14)$$

where:

$$z = u_w - u_w^*, D_z = D_{u_w} + D_{u_w^*}, s_z = \sqrt{D_z}, \bar{z} = \bar{u}_w - \bar{u}_w^*.$$

The value of the random variable  $z$  corresponding to a certain probability  $P(s)$  is determined from the expression:

$$z_p = \bar{z} + u_p s_z. \quad (15)$$

where  $u_p$  is the quantile corresponding to the probability  $P$ .

Value  $z = u_w - u_w^* = 0$  delimits the regions of negative and positive values of  $z$  so that the probability of destruction is determined by the condition:

$$z_p = \bar{z} + u_p s_z = 0,$$

from which the expression for the desired quantile follows:

$$u_p = -\frac{\bar{z}}{s_z} = -\frac{\bar{u}_w - \bar{u}_w^*}{\sqrt{D_{u_w} + D_{u_w^*}}}. \quad (16)$$

Entering the depreciation reserve factor:

$$u_p = -\frac{n_w - 1}{\sqrt{n_w^2 v_{u_w^*}^2 + v_{u_w}^2}}; \quad n_w = \frac{u_w^*}{u_w}, \quad (17)$$

expression (16) is reduced to the form:

$$u_p = -\frac{n_w - 1}{\sqrt{n_w^2 v_{u_w^*}^2 + v_{u_w}^2}}, \quad (18)$$

where  $v_{u_w^*}$  and  $v_{u_w}$  are the coefficients of variation:

$$v_{u_w^*} = s_{u_w^*} / \bar{u}_w^*, \quad v_{u_w} = s_{u_w} / \bar{u}_w.$$

According to formula (18), the probability quantile  $P$  is determined, and then any of the quantities  $p(s)$ ,  $P(s)$  and  $Q(s)$ .

### Calculation of wear reliability under random block loading.

Randomness in block loading can manifest itself in:

1) in the random choice of pressure in the stage; 2) in the random choice of interval in the stage; 3) in the random alternation of stages; 4) in the given probability of stages.

Let us consider for example the case where the choice of pressure in a stage is random. Let us assume that in each  $i$ th stage:

$$\sigma_i = \bar{\sigma}_i (1 + u_p v_\sigma) = \bar{\sigma}_i \varepsilon. \quad (19)$$

The size  $\varepsilon$ , which reflects the random nature of the load, we will assume the same for all stages. Substituting expression (19) into the equation for wear (7), we obtain the statistical expression for wear:

$$u_w = k_w \varepsilon^m \sum \sigma_i^m \Delta s_{i\tau} \quad (20)$$

Similarly, substituting expression (19) for the number of blocks before reaching the limit of wear, we obtain:

$$\lambda = \frac{u_w^*}{k_w \varepsilon^m \sum_1^N \bar{\sigma}_i^m \Delta s_{i\ddagger}}. \quad (21)$$

Average number of blocks before reaching wear limit:

$$\bar{\lambda} = \frac{\bar{u}_w^*}{\bar{k}_w \sum_1^N \bar{\sigma}_i^m \Delta s_{i\ddagger}}. \quad (21 \text{ a})$$

Average resource of the friction unit:

$$\bar{s} = \lambda s_{\ddagger}. \quad (22)$$

It is necessary to find the probability density function of exceeding the wear limit above the current one. Solving this problem in the case of a normal distribution for  $u_w^*$  and  $u_w$ , is given by expression (18), which can be used to construct the reliability function  $P(s)$ . In this case, it is necessary to know the wear dispersion  $D_{u_w}$ , which we find taking into account (20):

$$D_{u_w} = \left( \frac{\partial u_w}{\partial k_w} \right)^2 D_{k_w} + \left( \frac{\partial u_w}{\partial \varepsilon} \right)^2 D_{\varepsilon}, \quad (23)$$

$$D_{u_w} = \left( \sum \bar{\sigma}_i^m \Delta s_{i\ddagger} \right)^2 D_{k_w} + \left( \bar{k}_w \sum \bar{\sigma}_i^m \Delta s_{i\ddagger} \right)^2 D_{\varepsilon}. \quad (23 \text{ a})$$

Resource distribution taking into account the average value (22):

$$s = \bar{s} (1 + u_p v_{\lambda}), \quad (24)$$

where  $v_{\lambda} = s_{\lambda} / \bar{s}$ .

Taking into account (21):

$$s_{\lambda}^2 = D_{\lambda}, \quad D_{\lambda} = D_{u_w} + D_{u_w^*}, \quad v_{\lambda} = \sqrt{v_{u_w}^2 + v_{u_w^*}^2}, \quad v_{u_w} = \sqrt{D_{u_w}} / \bar{u}_w. \quad (25)$$

The most common is the random load, given in the form of the probability  $P_i$  of the load action at each stage. In the case of a continuous load application, this is the pressure distribution density problem  $P(\sigma)$ . With a discrete load assignment, this is  $P_i(\sigma_i)$ , so  $\sum P_i = 1$ .

## Conclusions

The probabilistic approach allows for more accurate modeling of the behavior of friction units in real-world conditions. The constructed models take into account the variability of loads and wear, which is crucial for predicting reliability. In particular, when applying the models to block loading, significant differences in reliability functions were found compared to constant loading. The proposed methods can be used to design more reliable machines and mechanisms.

## References

1. Tanner, DM, & Dugger, MT (2003). Wear mechanisms in a reliability methodology. Reliability, testing, and characterization of MEMS/MOEMS II, 4980, 22-40.
2. Ramalho, A. (2010). A reliability model for friction and wear experimental data. Wear, 269(3-4), 213-223.
3. Chantem, T., Xiang, Y., Hu, XS, & Dick, RP (2013, March). Enhancing multicore reliability through wear compensation in online assignment and scheduling. In 2013 Design, Automation & Test in Europe Conference & Exhibition (DATE) (pp. 1373-1378). IEEE.
4. Wang, W., Shen, G., Zhang, Y., Zhu, Z., Li, C., & Lu, H. (2021). Dynamic reliability analysis of

mechanical systems with wear and vibration failure modes. *Mechanism and Machine Theory*, 163, 104385.

5. Ebrahimi, N. (2006). System reliability based on system wear. *Stochastic models*, 22(1), 21-36.

6. Pfeifer, T., & Wiegers, L. (2000). Reliable tool wear monitoring by optimized image and illumination control in machine vision. *Measurement*, 28(3), 209-218.

7. Yang, MC, Chang, YH, Tsao, CW, & Huang, PC (2013, May). New ERA: New efficient reliability-aware wear leveling for endurance enhancement of flash storage devices. In *Proceedings of the 50th Annual Design Automation Conference* (pp. 1-6).

8. Rao, RN, & Das, S. (2010). Wear coefficient and reliability of sliding wear test procedure for high strength aluminum alloy and composite. *Materials & Design*, 31(7), 3227-3233.

9. Chen, X., He, X., Tang, L., Li, Y., Zhou, M., Jin, W., & Gao, Z. (2020). A heat transfer tube wear reliability analysis method based on the first-order reliability method. *Journal of Computational Design and Engineering*, 7(6), 803-815.

**Диха М.О., Дитинюк В.О., Старий А.Л.** Ймовірнісний підхід до оцінки показників триботехнічної надійності вузлів тертя

У статті представлено теоретико-аналітичний огляд ймовірнісного підходу до оцінки триботехнічної надійності механічних систем, зокрема вузлів тертя. Розглядається вплив випадкового характеру навантажень і зношування на надійність елементів машин. Обґрунтовано доцільність використання функцій розподілу та щільності ймовірностей для опису процесу зносу. Детально описано математичні моделі, що дозволяють визначити ймовірність відмови елемента при заданих статистичних характеристиках навантаження й допустимого зносу. Враховано як умови постійного, так і блочного навантаження. Результати дослідження можуть бути використані при конструюванні та експлуатації високонадійних триботехнічних систем, а також для прогнозування їх ресурсу в умовах експлуатаційної невизначеності.

**Ключові слова:** триботехніка, знос, ймовірнісний підхід, надійність, функція відмов, коефіцієнт варіації, блочне навантаження.



## Improved mathematical model of the hydraulic drive of the garbage truck's sealing plate mechanism taking into account the wear of its hydraulic cylinder

O.V. Bereziuk<sup>1</sup>[1000-0002-2747-2978](https://orcid.org/1000-0002-2747-2978), V.I. Savulyak<sup>1</sup>[0000-0002-4278-5155](https://orcid.org/0000-0002-4278-5155), V.O. Kharzhevskiy<sup>2</sup>[0000-0003-4816-2781](https://orcid.org/0000-0003-4816-2781),  
A.Ye. Alekseiev<sup>2</sup>[0009-0009-0485-9414](https://orcid.org/0009-0009-0485-9414)

<sup>1</sup>Vinnitsia National Technical University, Ukraine

<sup>2</sup>Khmelnitskyi National University, Ukraine

E-mail: [berezyukoleg@i.ua](mailto:berezyukoleg@i.ua)

Received: 20 March 2025; Revised 10 April 2025; Accept: 05 May 2025

### Abstract

This article is dedicated to the improvement of the mathematical model of the hydraulic drive of the mechanism of the garbage truck's sealing plate, taking into account the wear of the hydraulic cylinder. An improved nonlinear mathematical model of the operation of the hydraulic drive of the garbage truck's sealing plate mechanism is proposed, which takes into account the wear of the hydraulic cylinder and allows to numerically study the dynamics of the drive and determine that taking into account the wear of the hydraulic cylinder significantly affects the main parameters of the hydraulic drive of the garbage truck's sealing plate mechanism. This study of the mathematical model was carried out using the fourth-order numerical Runge-Kutta-Felberg method with an adaptive integration step. Graphical dependencies were plotted to compare changes in the main parameters of the hydraulic drive of the garbage truck's sealing plate mechanism without taking into account the wear of the hydraulic cylinder and with taking into account the wear. It has been established that the creation of a linearized mathematical model of the hydraulic drive of the garbage truck's sealing plate mechanism, taking into account the wear of the hydraulic cylinder, and its analytical solution in order to obtain dependencies for an improved methodology for engineering calculations require further research.

**Keywords:** wear, wear rate, hydraulic cylinder, mechanism, sealing plate, garbage truck, pressing force, municipal solid waste, mathematical model.

### Introduction

One of the key tasks of mechanical engineering is to increase the wear resistance and reliability of machine actuators [1, 2], in particular utility machines, which is mostly equipped with hydraulic actuators of working bodies [3]. One of the leading technologies for the primary processing of municipal solid waste (MSW), aimed at reducing the cost of its transportation and minimizing the negative impact on the environment, is waste compaction directly during loading into a garbage truck. Solid waste is compacted in the garbage truck using a sealing plate driven by a hydraulic cylinder. This hydraulic cylinder is subject to intense wear due to the large number of operating cycles and high compression forces caused by the nonlinear compression characteristics of MSW. Hydraulic cylinders are usually made of alloy steel, and it is advisable to use wear-resistant coatings to increase their operational durability. Improving the mathematical model of the hydraulic drive of the garbage truck's sealing plate mechanism, taking into account the wear of the hydraulic cylinder, contributes to more efficient planning of upgrading, renewal, maintenance, and repair of municipal utility machines.

### Analysis of recent research and publications

In the paper [3], the pressure losses were determined on the basis of computer modeling of hydrodynamic processes of the working fluid flow through the water seal. To reduce them, structural changes to the water seal



were proposed that did not affect its functionality. This made it possible to reduce the pressure loss in the working part of the hydraulic distributor, which, in turn, reduces the overall energy losses in the hydraulic drive system.

The scientific article [4] discusses the peculiarities of the wood chip pressing process in screw machines and analyzes the processes occurring in different parts of the screw. The established dependencies make it possible to calculate the loads on the screw turns and determine the required power for pressing. In addition, the degree of raw material heating and specific energy consumption during the pressing process were determined.

In the article [5], the exponential dependence of changes in the rate of wear of the working hydraulic cylinder of the mechanism of the garbage truck's sealing plate was established, depending on the pressing force. Taking this dependence into account allows to improve maintenance and repair planning and to increase the efficiency of garbage trucks in general. For better understanding of the process, a graphical dependence of the change in the wear rate of the working hydraulic cylinder of the garbage truck's sealing plate mechanism on the pressing force was plotted, which confirmed the sufficient convergence of the obtained dependence. It was determined that for a Ukrainian-made garbage truck of the serial model KO-436, the wear rate of the working hydraulic cylinder of the mechanism of the garbage truck's sealing plate, according to the obtained dependence, will be  $0.257 \mu\text{m/h}$ , and an increase in the pressing force from 30 MN to 150 MN leads to a decrease in the wear rate of the working hydraulic cylinder of the hydraulic press mechanism by 3.6 times. This effect is explained by the peculiarities of contact processes between the working surfaces and the operating conditions of the mechanism at different load levels.

According to the study [6], among the main components of garbage trucks with side loading of MSW, the hydraulic system has the lowest working resource before failure, which is the main factor in the increased wear and tear of these vehicles. According to the results of research [7], the structure and most common causes of failures of the hydraulic equipment of garbage trucks were determined: hydraulic cylinders – 34.92 % (wear of cuffs, seals, rod; rupture of the piston mounting nut; rod bending; mechanical damage), hydraulic pumps – 16.40 % (casing wear, gear wear, squeezing of seals, casing cracks), pipelines and hoses – 15.34 % (hose breaks, pipeline wear), hydraulic distributors – 13.23 % (wear of seals and spools, casing cracks).

The analysis of the causes of typical technical failures of garbage trucks presented in [8] showed that a significant number of failures (about 45 %) are related to hydraulic drive failures. The main factors of these failures are manufacturing defects related to the usage of low-quality components, as well as significant fluctuations in the loads on the actuators. The study of the causes of actuators' failures showed that the main failures are caused by heat treatment defects and deviations from the design dimensions during manufacturing (35%), errors during assembling, adjustment and tightening of threaded connections (30%), as well as poor welding (30%). It was found that most failures (80-90 %) are related to the wear and corrosion of the working surfaces of parts, and failure occurs when a critical level of degradation is reached, i.e. when a machine or its component reaches the limit of its technical condition. In particular, up to 28% of all hydraulic drive component failures are related to hydraulic cylinders, caused by wear of mating surfaces, deformation of the rod and cylinder during operation. The durability analysis showed that the average time between failures of hydraulic drive elements, including hydraulic cylinders, is only about one-third of their maximum service life. In many cases, the manufacturer's service life is reached not more than 45-55%. The highest percentage of hydraulic cylinder failures at the initial stage of operation or after repair relates to rods (31%) and sealing cuffs (42%). In addition, the analysis of failures of hydraulic system elements showed that the main manifestation of failures is the loss of external and internal tightness caused by contamination of the working fluid, which leads to malfunctioning of the units.

The above data are consistent with the results published in [9], where the main causes of garbage truck's hydraulic system failures caused by wear are identified: for a hydraulic pump – wear of gears; for hydraulic cylinders – wear of cuffs, seals, and rod; for a hydraulic distributor – wear of seals and spools; for hoses – wear of pipelines. In addition, the paper establishes adequate dependencies of wear of garbage truck tires on the front and rear axles, depending on the transported mass of solid waste and the vehicle mileage, according to the Fisher criterion. According to the Student's criterion, it was determined that the weight of the transported solid waste has the greatest impact on the wear of tires on both the front and rear axles, while the mileage of the garbage truck has the least impact. The dependences of the number of garbage truck trips before reaching the maximum permissible tire wear on the front and rear axles were also obtained.

Paper [10] provides a detailed review of the main causes of garbage truck failures, which shows that the leading factors in the occurrence of failures are external and internal leaks in hydraulic systems. In particular, the percentage of the external leaks is about 48% of all reported failures and are caused mainly by damage to hoses and pipelines, as well as leaks in the seals of hydraulic cylinders and other units. These damages lead to leaks of working fluid, which negatively affects the operation of the entire hydraulic system, causing a decrease in its efficiency and increasing the risk of serious breakdowns. In addition, an important and common cause of failure is internal leakage, which is approximately 36% of the total number of failures. Internal leakage occurs due to a leak between the working cavities of hydraulic components, which leads to the flow of working fluid into non-working areas and a decrease in system pressure. Such problems are often observed in important elements of the hydraulic system: spool valves, safety and check valves, hydraulic cylinders, and hydraulic pumps. These units are important to the normal functioning of garbage trucks, so their malfunctions due to internal leaks significantly affect the overall performance and reliability of the equipment.

In the paper [11], it was found out that the “conical” wear of the hydraulic cylinder rod in the range of 0.2 to 0.4 mm in length before the first overhaul causes a decrease in system pressure by 7.2 %, an increase in specific fuel consumption by 11.4 %, and an increase in the content of carbon monoxide in exhaust gases by 26 %. Increasing of the rod wear at the working area to 0.6-0.7 mm leads to a 13.4% drop in hydraulic system pressure, a 21.3% increase in specific fuel consumption, and an increase in exhaust gas toxicity from 25% to 59%, which exceeds the permissible limits. The maximum permissible wear of the geometric parameters of the hydraulic cylinder rod of the hydraulic drive of construction and road machines is proposed to be less than 0.4 mm. In addition, it was found that rod wear negatively affects the physical and chemical properties of the working fluid, increasing the content of iron and impurities in it by two times, which leads to the need for more frequent replacement and increase in cost. This significantly reduces the efficiency and durability of the hydraulic actuator, shortening its service life in construction and road machines.

In the paper [12], it is stated that the wear of sealing elements in hydraulic systems leads to the gradual penetration of hydraulic fluid into non-working cavities of hydraulic machines. Although this process is not always noticeable externally, it causes unproductive power losses of the hydraulic drive, which, in turn, leads to excessive fuel and lubricant consumption and reduced power of the working bodies. Power losses due to seal wear can cause non-optimal hydraulic motor operation, which negatively affects the overall efficiency of the hydraulic drive. The study considers the mechanical system "hydraulic cylinder – sealed piston – compressed hydraulic fluid", where the dependence of the efficiency of the hydraulic cylinder on the value of the leakage is established. The results of piston deflection when using VMGZ working fluid are also determined and the mechanism of fluid flow through the hydraulic cylinder seal is analyzed.

The authors of the article [13], while analyzing observations of garbage trucks, found that the largest number of failures relate to the wear and corrosion of the working surfaces of the parts of working equipment. Failures of hydraulic cylinders caused by wear of the working surfaces of the mating surfaces, deformations of the rod and cylinder during operation are found to be 32 % of all breakdowns of hydraulic drive parts. This is due to uneven loading of the body and abrasive wear in the difficult operating conditions of the garbage truck. Studies of the causes of failures have shown that the main cause is wear on the working surfaces of key hydraulic drive parts, including spools and hydraulic distributor housings, hydraulic cylinder rods, etc. The main factor of wear is water-abrasive damage, which occurs due to untimely replacement of the hydraulic fluid and the use of low-quality or worn sealing elements, such as hydraulic cylinder seals. This leads to dust and wear products entering the sliding zone, which accelerates the wear of working surfaces. One of the most promising methods for restoring worn parts in the paper is chrome plating in a cold self-regulating electrolyte, which produces high quality chrome coatings with high performance.

In the article [14], a nonlinear mathematical model described by a system of differential equations with appropriate boundary conditions was proposed and studied in detail, which characterizes the operation of the hydraulic drive of the mechanism of the garbage truck’s sealing plate, in particular for the static method of solid waste compression – an important stage of primary waste processing. However, despite the high accuracy and detail of the model, it does not take into account the impact of wear on the power hydraulic cylinder, which is one of the key elements of the hydraulic drive. Ignoring this factor may limit the application of the model for long-term forecasting of the mechanism's effectiveness in real operating conditions, where hydraulic cylinder wear significantly affects the performance and reliability of the system.

However, as a result of the analysis of known publications, the authors did not find a specific mathematical model describing the operation of the hydraulic drive of the garbage truck’s sealing plate mechanism taking into account the wear of the hydraulic cylinder.

### Aims of the article

Improvement of the mathematical model of the hydraulic drive of the mechanism of the garbage truck’s sealing plate taking into account the wear of the hydraulic cylinder.

### Methods

Fig. 1 shows a calculation scheme of the garbage truck’s operation at the technological operation of static compaction of MSW [14], with the following structural elements and values: PP – pressing plate; HC – hydraulic cylinder; HD – hydraulic distributor; P – hydraulic pump; SV – safety valve; F – filter; T – working fluid tank. The diagram also shows the following basic geometric, kinematic, and power parameters:  $p_1, p_2, p_3, p_4$  – pressures at the pump outlet, hydraulic cylinder inlet, hydraulic cylinder outlet, and filter inlet, respectively;  $W_1, W_2, W_3, W_4$  – volumes of pipelines between the pump and hydraulic distributor, hydraulic distributor and hydraulic cylinder inlet, hydraulic cylinder outlet and hydraulic distributor, hydraulic distributor and filter;  $Q_P$  – actual pump flow rate;  $S_P$  – cross-sectional area of the distributor opening;  $S_f$  – surface area of the filter element;  $k_f$  – specific filter capacity (not shown in the diagram);  $\mu_d$  – dynamic viscosity coefficient (not shown in the diagram);  $D, d$  – diameters of the piston and rod;  $G_P$  – weight of the pressing plate;  $G_C$  – weight of the hydraulic cylinder;  $G_{W1}$  – weight of the waste above the pressing plate;  $G_{W2}$  – weight of the waste outside the pressing plate;  $F_{FR}$  – friction force between the pressing plate and the guides;  $F_{TW}$  – the friction force between the MSW and the body;  $F_C$  – the



$$\sigma = \frac{\pi D \delta^3}{12 \nu \rho_{WF} l} = \frac{\pi D (\delta_0 + 10^{-6} u)^3}{12 \nu \rho_{WF} l} \quad [\text{m}^5/(\text{N} \cdot \text{sec})], \quad (8)$$

where  $\delta_0$  – the nominal size of the gap, m;  $\nu$  – the kinematic viscosity WF of the working fluid,  $\text{m}^2/\text{sec}$ ;  $\rho_{WF}$  – the density of the working fluid,  $\text{kg}/\text{m}^3$ ;  $l$  – the length of the annular gap, m.

To study an improved nonlinear mathematical model of the operation of the hydraulic drive of the mechanism of the garbage truck's sealing plate, taking into account the wear of its hydraulic cylinder in the form of a system of ordinary nonlinear differential equations with corresponding boundary conditions, the Runge-Kutta-Felberg numerical method of the 4<sup>th</sup> order with a variable integration step was used.

## Results

After substituting formula (8) into differential equation (2) and taking into account differential equation (7), the improved nonlinear mathematical model of the operation of the hydraulic drive of the garbage truck's sealing plate mechanism, taking into account the wear of its hydraulic cylinder, can be written as follows:

$$\left\{ \begin{aligned} Q_P &= \mu S_P \sqrt{\frac{2(p_1 - p_2)}{\rho_{WF}}} + \sigma(p_1 - p_2) + KW_1 \frac{dp_1}{dt}; \end{aligned} \right. \quad (10)$$

$$\left\{ \begin{aligned} \mu S_P \sqrt{\frac{2(p_1 - p_2)}{\rho_{WF}}} &= \frac{dx}{dt} S_{C1} + \frac{\pi D (\delta_0 + 10^{-6} u)^3}{12 \nu \rho_{WF} l} (p_2 - p_3) + KW_2 \frac{dp_2}{dt}; \end{aligned} \right. \quad (11)$$

$$\left\{ \begin{aligned} \frac{dx}{dt} S_{C2} &= \mu S_P \sqrt{\frac{2(p_3 - p_4)}{\rho_{WF}}} + \sigma(p_3 - p_4) + KW_3 \frac{dp_3}{dt}; \end{aligned} \right. \quad (12)$$

$$\left\{ \begin{aligned} \mu S_P \sqrt{\frac{2(p_3 - p_4)}{\rho_{WF}}} &= k_f \frac{p_4}{\mu_D} S_f + \sigma p_4 + KW_4 \frac{dp_4}{dt}; \end{aligned} \right. \quad (13)$$

$$\left\{ \begin{aligned} p_2 S_{C1} - p_3 S_{C2} &= m_p \frac{d^2 x}{dt^2} + \beta \frac{dx}{dt} + \left[ 8,661 \cdot 10^4 + 2,037 \cdot 10^7 \left( \frac{x}{x_{\max}} \right)^{12} \right] S_{P1} + F_{FR} + F_{TW}; \end{aligned} \right. \quad (14)$$

$$\left\{ \begin{aligned} \frac{du}{dt} &= 7,153 \cdot 10^{-7} e^{-1,047 \cdot 10^{-8} p_2 S_{C1}}; \end{aligned} \right. \quad (15)$$

$$\left\{ \begin{aligned} 0 \leq \{p_1, p_2, p_3, p_4\} &\leq p_{zk}; \quad 0 \leq x \leq x_{\max}. \end{aligned} \right. \quad (16)$$

A comparison of changes in the main parameters of the hydraulic drive of the garbage truck's sealing plate mechanism without taking into account wear and taking into account the wear of the hydraulic cylinder is shown in Fig. 2. The graphical dependencies shown in Fig. 2 are obtained for the drive parameters corresponding to the serial model of the KO-436 garbage truck that is manufactured by "Turbivskiyi Machine-Building Plant" (Public joint stock company «ATEKO»):  $W_1 = 1.48$  l;  $W_2 = 1.59$  l;  $W_3 = 1.59$  l;  $W_4 = 0.3$  l;  $S_p = 5.02 \cdot 10^{-5} \text{ m}^2$ ;  $S_f = 3.49 \cdot 10^{-2} \text{ m}^2$ ;  $k_f = 6.13 \cdot 10^{-9} \text{ m}$ ;  $\mu_e = 1.63 \cdot 10^{-2} \text{ N} \cdot \text{sec}/\text{m}^2$ ;  $\nu = 1.83 \cdot 10^{-5} \text{ m}^2/\text{sec}$ ;  $\rho_{WF} = 890 \text{ kg}/\text{m}^3$ ;  $\delta_0 = 0.136 \text{ mm}$ ;  $l = 35 \text{ mm}$ ;  $x_{\max} = 900 \text{ mm}$ ;  $m_p = 54 \text{ kg}$ ;  $\beta = 50 \text{ N} \cdot \text{sec}/\text{m}$ ;  $\sigma = 9.24 \cdot 10^{-11} \text{ m}^5/(\text{N} \cdot \text{sec})$ ;  $S_{C1} = 9.503 \cdot 10^{-3} \text{ m}^2$ ;  $S_{C2} = 3.142 \cdot 10^{-3} \text{ m}^2$ ;  $S_{P1} = 1.019 \text{ m}^2$ ;  $D = 110 \text{ mm}$ ;  $d = 90 \text{ mm}$ ;  $F_{TP} = 247.7 \text{ N}$ ;  $F_{TV} = 718 \text{ N}$ ;  $p_{zk} = 10 \text{ MPa}$ ;  $t_0 = 0 \text{ c}$ ;  $x_0 = 0 \text{ m}$ ;  $p_{10} = 0 \text{ MPa}$ ;  $p_{20} = 0 \text{ MPa}$ ;  $p_{30} = 0 \text{ MPa}$ ;  $p_{40} = 0 \text{ MPa}$ .

The calculations were performed with an integration step  $h = 10^{-4} \text{ sec}$  and a relative error  $\varepsilon = 10^{-16}$ . The stability of the solution to the system of differential equations was ensured by checking the identity of the results obtained at the values of the integration steps  $h$  and  $h/2$ .

In the blank field of the Figs. 2a and 2b it is shown the graphs of transient processes during the startup of the hydraulic drive of the garbage truck's sealing plate mechanism. As it can be seen from the Fig. 2, taking into account the wear of the hydraulic cylinder in the improved mathematical model significantly affects the main parameters of the hydraulic drive of the garbage truck's sealing plate mechanism.

The construction of a linearized mathematical model of the operation of the hydraulic drive of the garbage truck's sealing plate mechanism, taking into account the wear of the hydraulic cylinder, and its analytical solution in order to obtain dependencies for an improved methodology for engineering calculations require further research.

## Conclusions

An improved nonlinear mathematical model of the operation of the hydraulic drive of the garbage truck's sealing plate mechanism is proposed, which takes into account the wear of the hydraulic cylinder and allows to

numerically study the dynamics of this drive and determine that taking into account the wear of the hydraulic cylinder significantly affects the main parameters of the hydraulic drive of the garbage truck's sealing plate mechanism. Graphical dependencies have been plotted to compare changes in the main parameters of the hydraulic drive of the garbage truck's sealing plate mechanism without taking into account the wear of the hydraulic cylinder and with taking into account the wear.

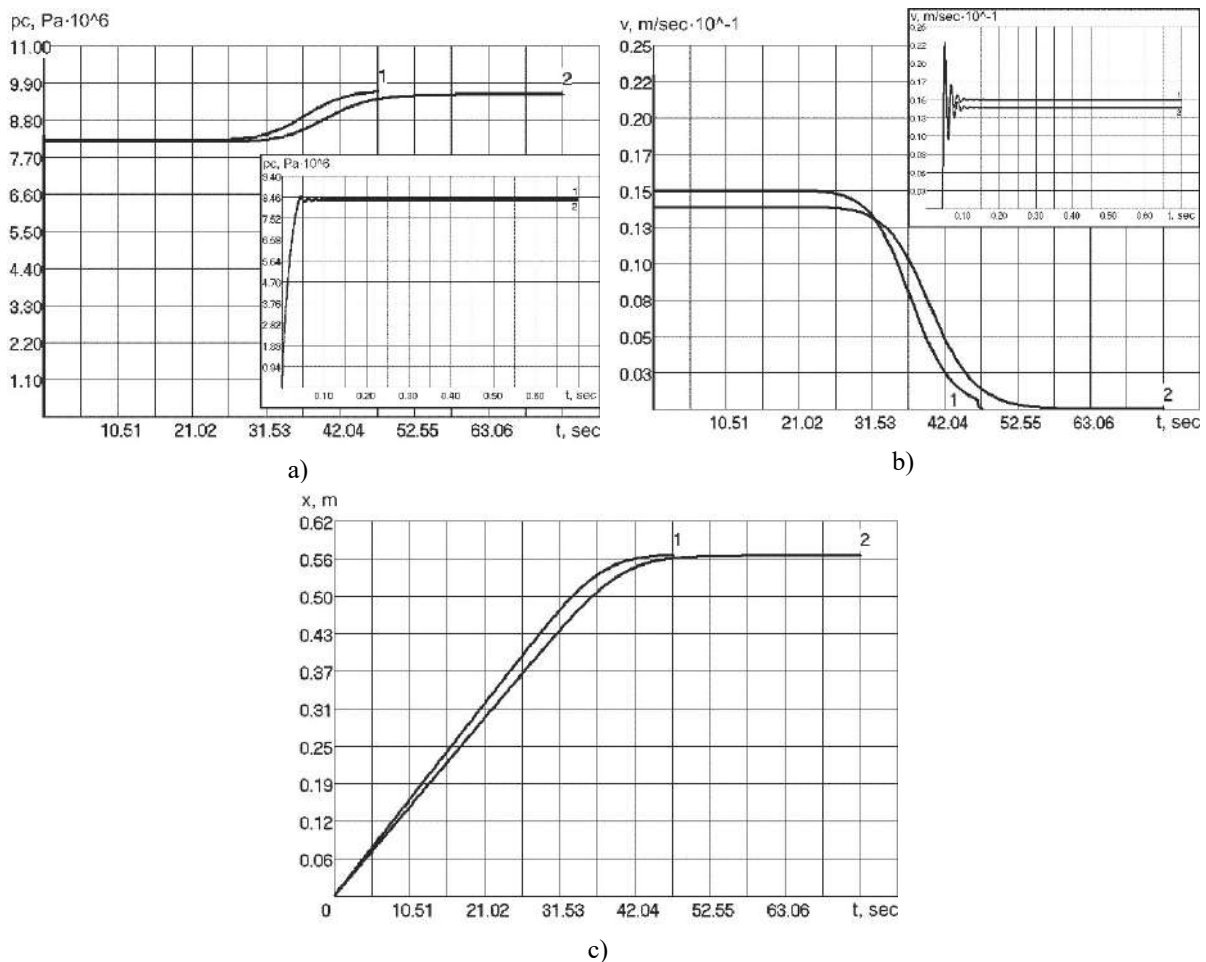


**Fig. 2. Comparison of changes in the main parameters of the hydraulic drive of the garbage truck's sealing plate mechanism: 1 – without taking into account the wear of the hydraulic cylinder; 2 – taking into account the wear of the hydraulic cylinder: a) change in pressure in the hydraulic cylinder; b) speed of the sealing plate; c) movement of the sealing plate**

It has been also established that the construction of a linearized mathematical model of the hydraulic drive of the garbage truck's sealing plate mechanism, taking into account the wear of the hydraulic cylinder, and its analytical solution in order to obtain dependencies for an improved methodology for engineering calculations require further research.

## References

1. Dykha O., Sviderskyi V., Holenko K. (2024) Pidvyshchennia antyfraktsiinykh kharakterystyk porshnevnykh ushchilnen kompresora kondytsionera avtomobilia [Increasing the anti-friction characteristics of car air conditioner compressor piston seals]. Herald of Khmelnytskyi National University. Technical sciences, 333(2), 314-321, <https://doi.org/10.31891/2307-5732-2024-333-2-50>.
2. Khomenko IM, Kindrachuk MV, Kobrynets AK (2010) Hranychnodopustymyi znos mashyn [Maximum permissible wear of machines]. Problems of friction and wear, 52, 28-37.
3. Petrov O., Kozlov L., Lozinskiy D., Piontkevych O. (2019) Improvement of the hydraulic units design based on CFD modeling. In: Lecture Notes in Mechanical Engineering XXII, 653-660, [https://doi.org/10.1007/978-3-030-22365-6\\_65](https://doi.org/10.1007/978-3-030-22365-6_65).
4. Tataryants M.S., Zavinsky S.I., Troshin A.G. (2015) Development of a methodology for calculating loads on the screw and energy consumption of screw presses. ScienceRise, 6 (2), 80-84, <https://doi.org/10.15587/2313-8416.2015.44378>.
5. Bereziuk O.V., Savulyak V.I., Kharzhevskiy V.O., Alekseev A.Ye. (2024) Determination of the regularity of the rate of wear of the working hydraulic cylinder of the mechanism of the sealing plate of the garbage

truck from the pressing force. *Problems of Tribology*, 29(1/111), 38-44, <https://doi.org/10.31891/2079-1372-2024-111-1-38-44>

6. Nosenko A.S., Domnickij A.A., Altunina M.S., Zubov V.V. (2019) Theoretical and experimental research findings on batch-operation bin loader with hydraulically driven conveying element. *MIAB. Mining Informational and Analytical Bulletin*, 11, 119-130, <http://dx.doi.org/10.25018/0236-1493-2019-11-0-119-130>.

7. Lobov N.V., Maltsev D.V., Genson E.M. (2019) Improving the process of transport of solid municipal waste by automobile transport. *Proceedings of IOP Conference Series: Materials Science and Engineering*. IOP Publishing, 1(632), 012033, <https://doi.org/10.1088/1757-899X/632/1/012033>.

8. Kotomchin A.N., Lyakhov Yu.G. (2019) Analysis of failures of knots and units of construction, road, lifting and transport machines and specialized motor transport on the example of MUE "Communal service". *Engineering & Computer science*, 3, 174-178.

9. Bereziuk O.V., Savulyak V.I., Kharzhevskiy V.O. (2023) Establishing the peculiarities of tire wear of garbage trucks during the transportation of municipal solid waste. *Problems of Tribology*, 28(1/107), 59-64, <https://doi.org/10.31891/2079-1372-2023-107-1-59-64>

10. Kabashev R.A. (1997) Road and construction machines: abrasive wear of the working parts of earthmoving machines. Almaty: Gylym.

11. Nurakov S.N., Savinkin V.V. (2008) About development methods for calculating the wear of the rod cylinder interface of hydraulic machines. *Proceedings of the Karaganda State Technical University*, 3 (32), 96.

12. Shalapai VV, Machuga OS (2023) Vraty potuzhnosti u hidrotsylindri vnaslidok protikannia hidravlichnoi ridyny cherez neshchilnist [Power loss in the hydraulic cylinder due to hydraulic fluid leakage through non-tightness]. *Comprehensive quality assurance of technological processes and systems – 2023: Proceedings of the XIII International Scientific and Practical Conference, May 25-26, 2023, Chernihiv. National University "Chernihiv Polytechnic"*, 287-289.

13. Kargin R.V., Yakovlev I.A., Shemshura E.A. (2017) Modeling of workflow in the grip-container-grip system of body garbage trucks. *Procedia Engineering*, 206, 1535-1539, <https://doi.org/10.1016/j.proeng.2017.10.727>.

14. Bereziuk O.V. (2005) Vibratsiinyi hidropriyvod plyty presuvannia tverdykh pobutovykh vidkhodiv u smittievozakh [Vibration hydraulic drive of the solid waste sealing plate in garbage trucks] *Diss. Cand. of Eng. Sciences: 05.02.03 – Drive systems*, Vinnytsia, 217.

15. Perekrestov A.V. (1983) Zadachi po obiemnomu hidropriyvodu [Problems on volumetric hydraulic drive]. Kyiv: Vyscha shkola 145.

**Березюк О.В., Савуляк В.І., Харжевський В.О., Алексєєв А.Є.** Удосконалена математична модель роботи гідроприводу механізму ущільнюючої плити сміттевоза із урахуванням зносу його гідроциліндра.

Дана стаття присвячена удосконаленню математичної моделі роботи гідроприводу механізму ущільнюючої плити сміттевоза із урахуванням зносу гідроциліндра. Запропонована удосконалена нелінійна математична модель роботи гідроприводу механізму ущільнюючої плити сміттевоза, яка враховує знос гідроциліндра і дозволяє чисельно дослідити динаміку даного приводу та визначити, що врахування зносу гідроциліндра суттєво впливає на основні параметри гідроприводу механізму ущільнюючої плити сміттевоза. Дане дослідження математичної моделі здійснювалося із застосуванням чисельного методу Рунге–Кутта–Фельберга четвертого порядку з адаптивним кроком інтегрування. Побудовано графічні залежності для порівняння зміни основних параметрів гідроприводу механізму ущільнюючої плити сміттевоза без урахування зносу гідроциліндра та з урахуванням зносу. Встановлено, що побудова лінеаризованої математичної моделі роботи гідроприводу механізму ущільнюючої плити сміттевоза із урахуванням зносу гідроциліндра та її аналітичне розв'язання з метою отримання залежностей для удосконаленої методики інженерних розрахунків вимагають проведення подальших досліджень.

**Ключові слова:** знос, швидкість зношування, гідроциліндр, механізм, ущільнююча плита, сміттевоз, зусилля пресування, тверді побутові відходи, математична модель.



## Modeling of contact interaction and wear of the trolleybus contact insert-wire tribopair

K.E. Holenko<sup>0000-0002-6140-4573</sup>, O.S. Kovtun<sup>0000-0002-1430-6479</sup>, O.V. Dykha<sup>\*0000-0003-3020-9625</sup>

*Khmelnytskyi national University, Ukraine*

*\*E-mail: [tribosenator@gmail.com](mailto:tribosenator@gmail.com)*

*Received: 02 April 2025; Revised 20 April 2025; Accept: 10 May 2025*

### Abstract

The article presents the results of numerical modeling of the contact interaction of the tribopair "contact insert - contact wire" of a trolleybus using the Ansys software environment. The main attention is paid to the analysis of the stress state and the prediction of wear of friction surfaces when modeling a stable frictional contact. Based on the constructed solid-state models of the contact insert and the MF-100 copper wire, a finite element mesh was formed and real conditions of operational loading were simulated. The distributions of contact pressure, frictional and equivalent stresses, as well as the nature of the contact spot were determined. Linear wear was calculated using the energy criterion, taking into account local frictional stresses and material hardness. The obtained results were compared with the available experimental data, which confirms the adequacy of the proposed model. The article also outlines the prospects for interpolation of short-term simulations into long-term operating modes by mathematical modeling of wear under variable load. The material is useful for predicting the service life of current collection devices and optimizing their geometry and materials.

**Keywords:** tribocouple, contact insert, contact wire, ANSYS, wear, friction stress, contact zone, modeling.

### Introduction

Wear of contact elements of electric transport, in particular contact inserts of trolleybus pantographs, remains one of the main reasons for the decrease in reliability and increase in operating costs of urban transport. During the movement of the trolleybus, the insert is constantly in contact with the wire network, which leads to intensive abrasive and adhesive wear. Change in the insert profile, loss of contact surface geometry and increase in sliding resistance reduce the quality of current collection, cause electrical sparks and deterioration of the operation of electrical equipment.

Traditionally, wear resistance assessment has been performed experimentally in laboratory or field conditions, but such methods are laborious, expensive and do not always allow to take into account the complex variability of operating modes characteristic of real conditions. Therefore, it is relevant to introduce numerical analysis tools, in particular the finite element method (FEM), which allow to model not only the mechanical interaction, but also the processes that directly affect wear, such as contact pressure, friction, local stresses, the shape of the contact spot and the geometry of the elements.

Of particular interest is the possibility of quantitative assessment of linear wear based on the distribution of frictional stresses obtained in Ansys, with the subsequent application of energy approaches to the calculation. This approach allows not only to take into account local friction characteristics, but also to predict the service life of the insert depending on the length of the run and the modes of movement of the trolleybus. This opens up prospects for integrating numerical modeling into regulatory procedures for assessing the wear resistance of current-collecting components and unifying approaches to their constructive optimization.

### Literature review

The problem of wear of tribosystem elements is key in transport engineering, in particular for current-collecting pairs of electric transport. A systematic study of wear mechanisms is given in the work P. Blau [1],



where transient friction modes and the influence of loading conditions on the nature of wear of materials are considered. G. Stachowiak and A. Batchelor [2] in their fundamental monograph classify in detail the types of wear — adhesive, abrasive, fretting, etc. — and consider mathematical models that describe the dependence of wear on contact pressure, sliding velocity and material properties.

Particular attention in the study of wear is paid to energy criteria. Meng and Ludema [3] summarized the main approaches to building wear models and emphasized their limitations under conditions of variable loading and unsteady contact. Their analysis of the forms and content of predictive equations highlights the need to use models that take into account local contact parameters. At the same time, modern software environments, as shown in [4], allow the use of these equations based on numerical modeling data - in particular, friction stresses and contact pressure.

Han et al. [5] presented a numerical analysis of a wear-sensitive contact problem using a fully discrete scheme to model an elastic body under friction and wear conditions. Their results demonstrate the effectiveness of the approach in predicting the evolution of the contact surface. Ravitej and Kumar [6] conducted a comparative study on the prediction of wear rate of hybrid composites by combining experimental analysis, finite element modeling, and machine learning, which allowed to improve the accuracy of predictions.

Ansys Inc. [7] provided an example of modeling the wear of a contact surface using the Archard wear model, demonstrating the process of sliding a hemispherical ring on a flat ring and evaluating the strains and normal stresses before and after wear. Lopez [8] provided an overview of contact modeling methods in Ansys Mechanical, including different contact types such as bonded, non-separated, frictionless, and rough, and discussed the contact algorithms used in Ansys to accurately model surface interactions.

Thus, modern literature confirms the effectiveness of combining classical energy models with numerical FEA data for wear analysis in tribopairs, which is a relevant and promising approach for modeling the insert and contact wire of a trolleybus.

### Purpose and objectives of the study

The aim of the work is to model the stress state and assess the wear of the tribopair "contact insert - contact wire" of a trolleybus using the Ansys environment.

To achieve the goal, the following tasks were set: to create geometric models of tribopair elements; to construct a finite element mesh taking into account the parameters of contact interaction; to simulate the distribution of pressure and stresses in the contact zone; to determine wear parameters using the energy approach; to compare the obtained results with experimental data; to formulate directions for further research taking into account variable load modes.

### Main material

#### Output data

Based on the working drawings, the following solid models were created: contact insert (Fig. 1) and cross-section of the MF-100 contact wire (Fig. 2).

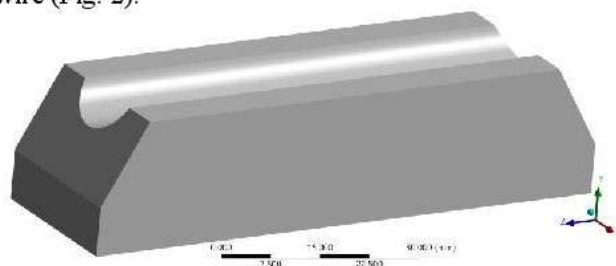


Fig. 1. Solid model of a trolleybus contact insert

The models were created in SolidWorks with working dimensions. The body length is 300 mm (solid model extrusion).

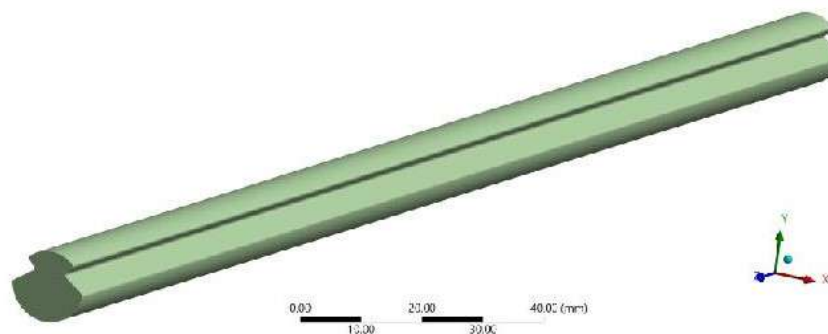
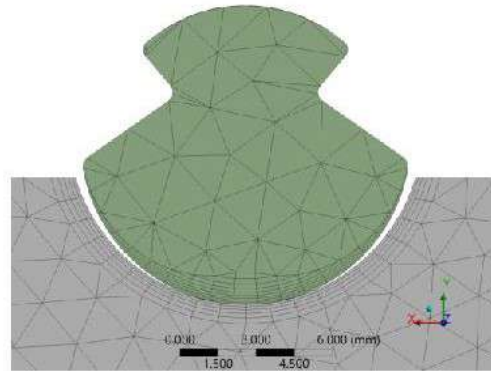


Fig. 2. Solid model of the contact wire

Based on the solid-state models of the insert and the contact wire, a finite element FEA mesh was built in the Ansys environment. The FEA mesh parameters are as follows: Body Sizing = 2.0 mm – the maximum size of the finite elements of the model bodies; Face Sizing = 1.0 mm – the size of the finite elements on the contact surfaces of the bodies; Inflation = 9 for the wire and 12 for the insert. The parameters also determine the number of layers of finite elements with the size Face Sizing deep into the wire body and insert.

Body materials. From the available Granta EduPack library, the only possible materials that are close to the target ones were selected: Carbon (CY) for the insert; Cooper C10100 for the wire. The mesh view is presented in Fig. 3.



**Fig. 3. FEA mesh of the contact model of the trolleybus and contact wire insert**

To simulate the contact conditions for this pair, a frictional contact mode Frictional with a friction coefficient of 0.13 was specified (Fig. 4).

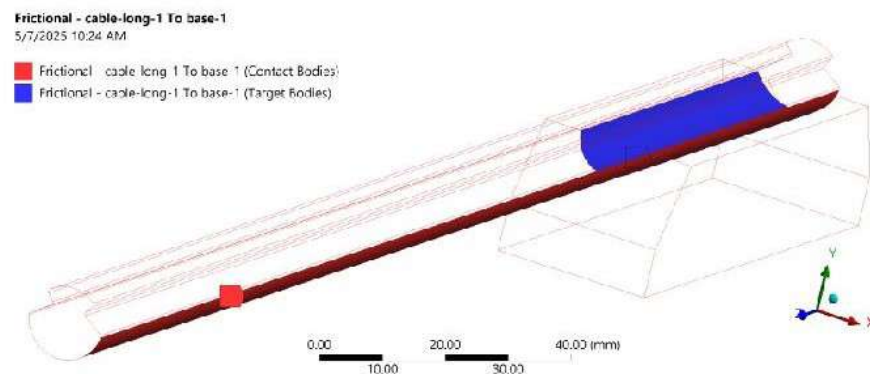


**Fig. 4. Frictional contact in the insert-wire pair**

To simulate contact pressure from the insert side, a uniformly distributed force of 0.5 MPa was applied to the wire perpendicular to the lower surface of the insert (Fig. 5).

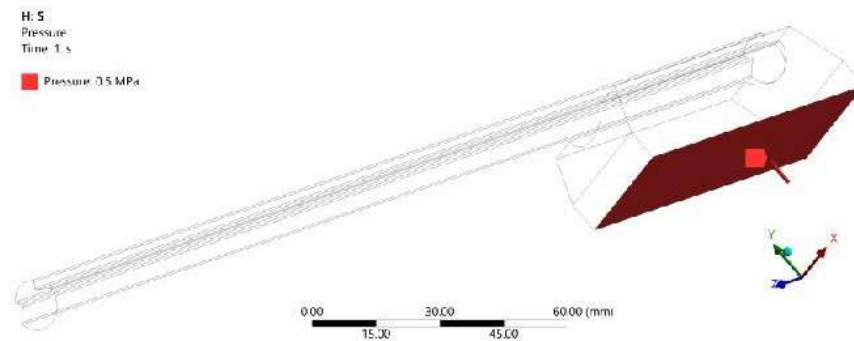


**Fig. 5. Modeling the load on the contact pair**

A steady state loading regime of 0.5 MPa was analyzed. The insert was displaced 200 mm along Z in both L- and S-modes.

### Results of calculation of tribocontact parameters

The equivalent Mises stresses for the insert and wire are shown in Fig. 6-7, respectively. For the insert maximum stresses  $\sigma$  are observed  $\max=16.236$  MPa at the moment of time  $t=2 \cdot 10^{-2}$  s; for wire  $\sigma_{\max}=14.33$  MPa at time  $t=0.12$  s.

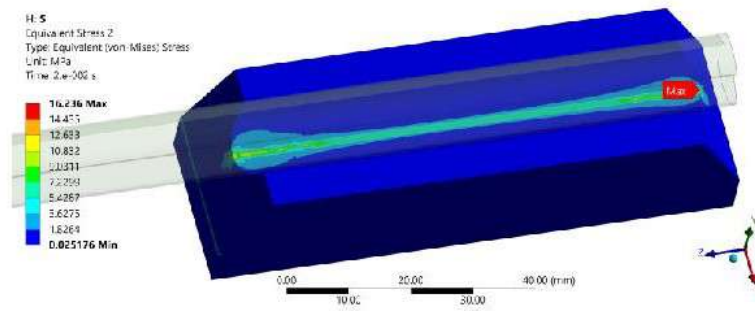


Fig. 6. Equivalent Mises stresses for the insert

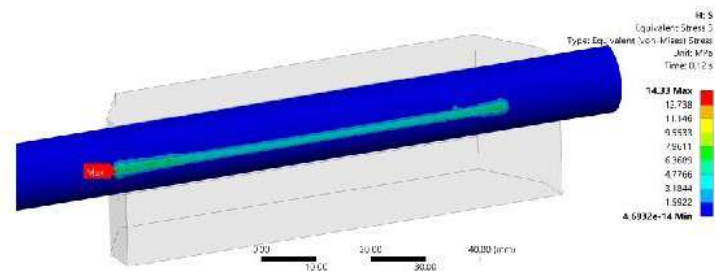


Fig. 7. Equivalent Mises stresses for a wire

Next, the characteristics of the dimensions of the contact zone (Contact Tool) were determined. A slip spot was recorded in the contact area, further from it the nature of the contact changes to a transitional one, and at the edges – to a gap (Fig. 8).

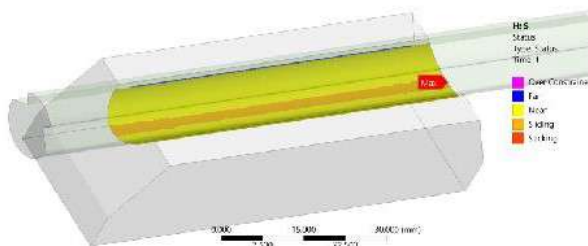


Fig. 8. Qualitative characteristic of the contact mode of the insert and wire

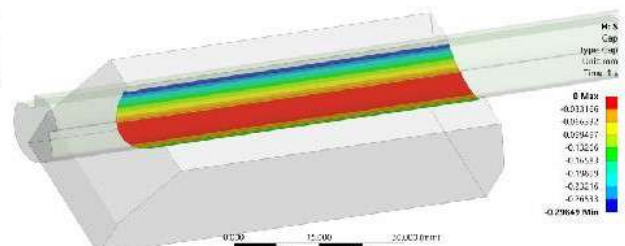


Fig. 9. The value of the contact gap between the insert and the wire

The contact gap varies from 0 to 0.29849 mm (Fig. 9). The maximum penetration is 0.0035762 mm at  $t=0.42$  s.

The maximum pressure in the contact area is 23.951 MPa at  $t=0.42$  s. The maximum average pressure value is 1.063 MPa at  $t=0.12$  s. The fluctuations of the average pressure are shown in the graph (Fig. 10).

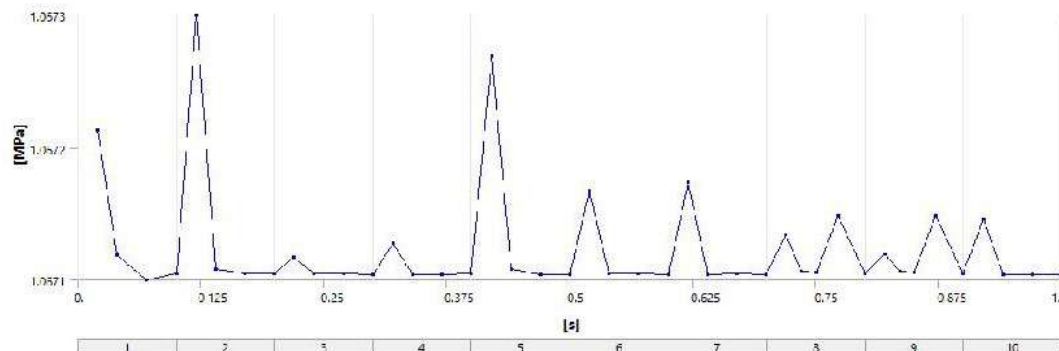


Fig. 10. Fluctuations in average pressure

Frictional stresses were used to calculate the wear characteristics in the insert-contact wire pair. Accordingly, the values of frictional stresses were further determined using the Ansys application package (Fig. 11).

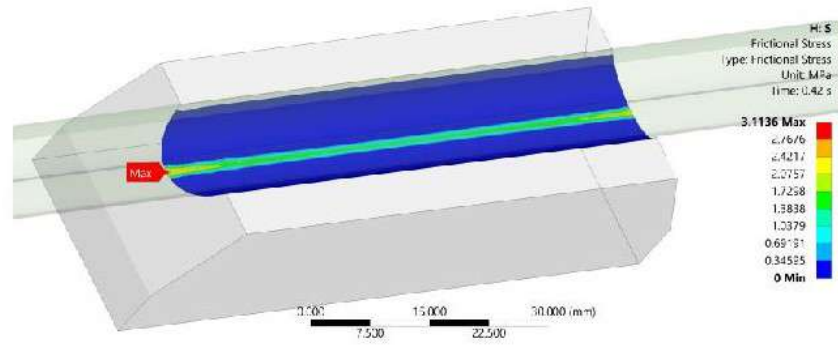


Fig. 11. Map of friction stresses on the surface of the contact insert

The maximum frictional stresses were  $\sigma_{max}=3.1136$  MPa at time  $t=0.42$  s.

The maximum value of the average frictional stress is  $\sigma_{max} = 0.13874$  MPa at  $t=0.12$  s. The fluctuations of the average frictional stress are shown in Fig. 12.

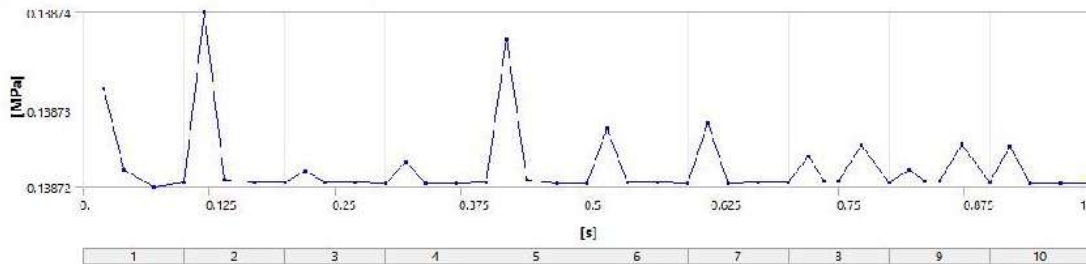


Fig. 12. Fluctuations of average friction stresses on the surface of the contact insert

### Calculation of insert wear

According to the energy approach, wear is the result of the expenditure of part of the mechanical friction energy on plastic deformation and detachment of particles from the contact surface.

The general equation:

$$V = \alpha \cdot E_{frict} = \alpha \cdot \int p \cdot \Delta u dA, \quad (1)$$

where:  $\alpha$  is the global efficiency coefficient of energy conversion into wear,  $\text{mm}^3/\text{J}$ ;  $E_{frict}$  is the friction energy (total or local),  $\text{N m}$  or  $\text{J}$ ;  $p$  is the contact pressure or normal force per area,  $\text{Pa}$ ;  $\Delta u$  is the relative shear displacement,  $\text{m}$ ;  $dA$  is the contact area element,  $\text{m}^2$ .

Simplified local formula for linear wear:

$$d(x, y) = \frac{\eta \cdot \tau(x, y) \cdot s(x, y)}{H}, \quad (2)$$

where:  $d(x, y)$  is the local wear depth,  $\text{mm}$ ;  $\eta$  is the local efficiency coefficient of energy conversion into wear ( $\approx 0.01-0.1$ );  $\tau$  is the tangential stress,  $\text{Pa}$ ;  $s$  is the sliding distance,  $\text{m}$ ;  $H$  is the material hardness,  $\text{Pa}$ .

Physical content:  $\tau \cdot s$  is the friction work per unit area,  $\text{J}/\text{m}^2$ ;  $\eta \cdot \tau \cdot s$  is the energy effectively spent on wear and tear (losses);  $H$  is the normalization of this energy due to the resistance of the material (the higher the hardness, the less wear).

Format for manual calculation:

$$d = \frac{\eta \tau_{avg} s_{total}}{H}, \quad (3)$$

where:  $\tau_{avg}$  is the average frictional stress value from Ansys,  $\text{Pa}$ ;  $s_{total}$  is the total sliding distance,  $\text{m}$ . According to FEA tests  $\tau_{avg} = 0.13873$  MPa for the entire surface, and the max value is 3.1136 MPa. However, we will be interested only in the central part, where the permanent contact is fixed - the red area with a gap value of 0 mm (Fig. 9). The approximate value in the red area is 0.4 MPa. For the hardness of the insert material  $\text{HRB} = 50...75$ , the value varies between  $H = 3.45 \cdot 50 = 172.5$  MPa and  $H = 3.45 \cdot 75 = 258.75$  MPa. We take the average value  $2.15 \cdot 10^8$  Pa. We consolidate the boundary conditions:  $\tau_{avg} = 0.4$  MPa;  $s_{total} = 0.2$  m;  $H = 2.15 \cdot 10^8$  Pa; Mileage = 100 km.

Wear per 1 sliding cycle (0.2 m):

$$d = \frac{\eta \cdot \tau_{avg} \cdot s_{total}}{H} = \eta \cdot \frac{0.4 \cdot 10^6 \cdot 0.2}{2.15 \cdot 10^8} = \eta \cdot 0,37209 \text{ mm}. \quad (4)$$

Number of cycles per 100 km:  $100,000/0.2=500,000$  cycles

Total wear:

$$d_{100km} = 0,37209 \cdot 500,000 \cdot \eta = 186,045 \cdot \eta \text{ mm}. \quad (5)$$

The result under the condition is:  $\eta = 10^{-6} d_{100km} = 0.186$  mm, which correlates with experimental data on wear "Performance characteristics of VKT-M inserts when working in conjunction with MF-100 copper wire": linear wear of inserts, mm/100 km of run is  $+(0.1 \dots 0.2)$  mm under dry sliding contact conditions. Given the value of mm  $\eta = 10^{-5} d_{100km} = 1.86$ .

Obviously, there is a question of interpolation of FEA test results and selection of a real value of the coefficient. Also, the question of the correspondence of the physical and mechanical properties of Granta EduPack materials in Ansys to real materials in operation. The subject of future research is interpolation of the insert loading modes: with constant and linearly increasing pressure. It can be assumed that when starting from stops, the pressure value changes (increases or decreases); under the conditions of linear movement of the trolleybus and a flat road surface, the pressure value can maintain a relatively constant value; in turns, the contact spot of the insert with the wire migrates to the inner sidewalls of the insert recess, so the wear area shifts, providing a greater overall resource. Interpolation of short FEA tests to long-term operating conditions requires the creation of a mathematical prediction model, which is an integral of various driving modes during the trolleybus working shift. Undoubtedly, studying the totality of these factors can help actualize the meaning of wear and tear and bring it closer to real conditions  $\eta$ .

## Conclusions

1. Numerical modeling of the contact interaction of the insert–wire tribopair was carried out, which allowed determining the stress-strain state and friction characteristics.
2. According to the results of FEA analysis, the values of stresses, pressures, and penetration in the contact zone were obtained, indicating the presence of a stable slip spot and a gap zone.
3. The application of the energy criterion allowed us to calculate the wear depth of the contact insert per cycle and per full mileage, which is consistent with experimental data.
4. It has been established that modeling in the Ansys environment provides a reliable assessment of wear conditions provided that the physical and mechanical parameters are correctly selected.
5. The need to develop a mathematical model for interpolation of short-term FEA tests for long-term operation, taking into account changes in load during trolleybus movement, is shown.

## References

1. Blau, PJ (1989). Friction and Wear Transitions of Materials: Break-In, Run-In, Wear-In. Noyes Publications. ISBN: 9780815511960.
2. Stachowiak, GW, & Batchelor, AW (2013). Engineering Tribology (4th ed.). Butterworth-Heinemann. ISBN: 9780123970473.
3. Meng, HC, & Ludema, KC (1995). Wear models and predictive equations: their form and content. Wear, 181–183, 443–457. [https://doi.org/10.1016/0043-1648\(95\)90158-2](https://doi.org/10.1016/0043-1648(95)90158-2)
4. Bhushan, B. (2013). Introduction to Tribology (2nd ed.). Wiley. ISBN: 9781119943925.
5. Han, D., Han, W., Jureczka, M., & Ochal, A. (2019). Numerical Analysis of a Contact Problem with Wear. arXiv preprint arXiv:1905.05541. <https://arxiv.org/abs/1905.05541>
6. Ravitej, YP, & Kumar, R. (2025). Wear Rate Prediction of Hybrid Composites: A Comparative Study Using Experimental Analysis, Finite Element Simulation, and Machine Learning. SSRN Electronic Journal. <https://doi.org/10.2139/ssrn.5177817>
7. Ansys Inc. (2024). Contact Surface Wear Simulation. PyMechanical Examples. [https://examples.mechanical.docs.pyansys.com/examples/technology\\_showcase/example\\_07\\_td\\_043.html#pymechanical](https://examples.mechanical.docs.pyansys.com/examples/technology_showcase/example_07_td_043.html#pymechanical)
8. López, S. (2024). Contact Modeling in Ansys Mechanical for Beginners. Ozen Engineering Blog. <https://blog.ozeninc.com/resources/understanding-contacts-in-ansys-mechanical> Ozen Blog+1LinkedIn+1

**Голенко К.Е., Ковтун О.С., Диха О.В.** Моделювання контактної взаємодії та зносу трибопари контактна вставка-провід тролейбуса

У статті представлено результати чисельного моделювання контактної взаємодії трибопари «контактна вставка – контактний провід» тролейбуса із використанням програмного середовища Ansys. Основну увагу приділено аналізу напруженого стану та прогнозуванню зношування поверхонь тертя при моделюванні сталого фрикційного контакту. На основі побудованих твердотільних моделей контактної вставки та мідного дроту МФ-100 сформовано кінцево-елементну сітку та змодельовано реальні умови експлуатаційного навантаження. Визначено розподіли контактного тиску, фрикційних та еквівалентних напружень, а також характер контактної плями. Розраховано лінійний знос за енергетичним критерієм із урахуванням локальних напружень тертя та твердості матеріалів. Отримані результати порівняно з наявними експериментальними даними, що підтверджує адекватність запропонованої моделі. Стаття також окреслює перспективи інтерполяції короточасних моделювань на довготривалі режими експлуатації шляхом математичного моделювання зносу при змінному навантаженні. Матеріал є корисним для прогнозування ресурсу струмомізмальних пристроїв та оптимізації їх геометрії й матеріалів.

**Ключові слова:** трибопара, контактна вставка, контактний провід, ANSYS, знос, напруження тертя, контактна зона, моделювання.



## Study of the influence of rapidly quenched aluminum alloy on the wear resistance of ultra-high-molecular-weight polyethylene

A.-M.V. Tomina<sup>0000-0001-5354-0674</sup>, D.V. Yakovenko<sup>\*0009-0003-1499-9054</sup>, V.F. Bashev<sup>0000-0002-3177-0935</sup>,  
S.I. Golovko<sup>0009-0004-3916-5205</sup>

*Dniprovsk State Technical University, Kamyanske, Ukraine*

*\*E-mail: [dimyak.pr@gmail.com](mailto:dimyak.pr@gmail.com)*

*Received: 15 April 2025; Revised 30 April 2025; Accept: 15 May 2025*

### Abstract

The article considers the influence of 5-30 wt.% dispersed (50-100  $\mu\text{m}$ ) AlMnCrVZrCuMgW alloy rapidly quenched from the liquid state on the wear resistance of ultra-high-molecular-weight polyethylene under different operating conditions. In particular, we studied the behaviour of the metal-polymer composite under the action of rigidly fixed abrasive particles and friction conditions without lubrication according to the “disk-pad” scheme. This simulates real operating conditions in tribological joints of mechanisms of modern machinery. The results of experimental studies showed that introducing the rapidly quenched AlMnCrVZrCuMgW alloy into the composition of the polymer material contributes to a significant improvement in its wear resistance in different modes. Thus, the abrasive wear index decreases 1,7 times compared to pure ultra-high-molecular-weight polyethylene. And the intensity of linear wear decreases more than 13 times. The maximum effect was achieved at an alloy content of 20 wt.%. This occurs because of the effective ratio of intermolecular interaction of the components and the uniform distribution of the filler in the polymer volume. The increase in wear resistance is due to the increase in the resistance of the ultra-high-molecular-weight polyethylene surface to mechanical stress. This is confirmed by an increase in the hardness of the material by 1,46 times. Morphological analysis of the friction surfaces revealed a decrease in the number and depth of the ploughing grooves, which is additional confirmation of the effective action of the AlMnCrVZrCuMgW rapidly quenched alloy as a strengthening phase.

**Keywords:** ultra-high-molecular-weight polyethylene, rapidly quenched alloy, abrasive wear index, linear wear intensity

### Introduction

In the constantly complicated operating conditions of mechanisms and equipment of modern machinery, increasing the wear resistance of parts of structural (protection of header bottoms, bearing housings, scrapers) and tribotechnical (sliding bearings, gears) purpose is of particular importance. This directly affects their reliability and durability. This is because traditional materials, particularly metals and alloys, are gradually losing their versatility due to several limitations, including susceptibility to corrosion, large mass, scarcity of raw materials and increasing cost of mechanical processing. This necessitates the search for alternative materials that would meet modern operational requirements and simultaneously be economically feasible. One of the effective solutions to this problem is the creation of polymer composite materials (PCMs) based on thermoplastic polymers filled with effective functional dispersed fillers (FLs). Such materials are characterized by high wear resistance, in particular in conditions of limited or complete absence of lubrication, as well as excellent resistance to X-ray and ultraviolet radiation, corrosion, moisture, and the action of aggressive media (acids, salts, organic solvents and alkalis). In addition, PCMs allow for the implementation of fast technological cycles of forming products without welding or mechanical joining being needed [1,2].

One of the commonly used polymers in the composition of PCMs is ultra-high-molecular-weight polyethylene (UHMWPE). This is due to its high-performance properties such as resistance to dynamic and fatigue loads. The use of functional dispersed FLs, in particular ordinary and oxidized graphite, hexagonal boron nitride [3, 4], graphene oxides, aluminium, zinc and zirconium [5, 6], molybdenum disulfide [7], carbon black [8], allows



obtaining PCMs with increased wear resistance, hardness, impact strength, and a low coefficient of friction. Significant interest among dispersed fillers is caused by rapidly quenched (r.q.) alloys based on aluminium. This is explained by the fact that their ultrafine-grained structure, which is formed during rapid cooling, contributes to obtaining fillers with high physical and mechanical properties. Given the above, searching for new PCM compositions based on UHMWPE remains an urgent task in materials science.

### The purpose of the work

Taking into account the above, this study focuses on investigating how a powder filler — an alloy composed of AlMnCrVZrCuMgW — affects the tribological performance of polymer composite materials based on UHMWPE, with the objective of enhancing their wear resistance under different frictional conditions.

### Objects and methods of research

UHMWPE of Jiujiang Zhongke Xinxing New Material Co., Ltd. [9] was chosen as a matrix for wear-resistant polymer composites. We chose dispersed (40-100  $\mu\text{m}$ ) r. q. eight-component AlMnCrVZrCuMgW alloy (Table 1) as the FL when creating new samples of metal-polymer composites (MPCs). This r. q. alloy is characterized by high wear resistance and hardness, thermal stability, and chemical inertness. These properties are due to the high level of microstresses in the crystalline fcc lattice of the aluminium-based substitution solid solution. They arise due to a significant difference in the atomic radii of aluminium and other alloying elements (Table 1). This makes the specified alloy an effective FL for creating MPC with high functional properties.

The production of UHMWPE samples and MPCs with a 5-30 wt.% alloy content was performed by the compression pressing method according to the regime given in [9]. The theoretical density of the AlMnCrVZrCuMgW alloy was calculated by the following formula to obtain samples of the required shape:

$$\rho_{\text{cm}} = x_1 \cdot \rho_1 + x_2 \cdot \rho_2 + \dots + x_n \cdot \rho_n$$

where  $x_n$  is a mass percentage of metal in aluminium;

$\rho_n$  is a tabular density (g/cm<sup>3</sup>) of this metal (Table 1).

Table 1

**Composition and properties of the components of the AlMnCrVZrCuMgW alloy**

Chemical element	Content, wt. %	Atomic radius, pm	Density, g/cm <sup>3</sup>
Al	87,6	142	2,70
Mn	6,0	127	7,21
Cr	2,0	128	7,19
V	0,3	134	6,11
Zr	0,6	160	6,52
Cu	0,4	128	8,96
Mg	2,8	160	1,74
W	0,3	139	19,25

The average density of the alloy was 3.14 g/cm<sup>3</sup>. The abrasive wear index for rigidly fixed abrasive particles (at a dispersion of 100  $\mu\text{m}$ ) was determined using the HECKERT experimental device at a constant load of 10 N. The study of the tribological properties of UHMWPE and MPCs based on it under friction conditions without lubrication was performed in rotational motion ( $v=380$  rpm) according to the "disk-pad" scheme in a pair with a steel cylindrical counterbody (steel 45,  $\varnothing 25$  mm, hardness 45-48 HRC and surface roughness  $R_a=0.32$   $\mu\text{m}$ ) at a constant sliding speed of 1.0 m/s and a load of 1.0 MPa on the SMC-2 friction machine. The hardness of UHMWPE and MPCs on the Rockwell HRR scale (pre- and total load were 98.1 N and 588.4 N, respectively) was determined using the 2074 TPR instrument. Morphological analysis of the friction surfaces of samples from UHMWPE and MPCs was performed using a BIOLAM-M optical microscope. Measurement of the surface roughness of the samples after friction ( $R_a$  scale,  $\mu\text{m}$ ) was done using a 170621 probe profilometer.

### Results analysis and discussion

In the course of research, we found that the new compositions of the MPCs are characterized by greater wear resistance compared to the UHMWPE (see Table 2). It is 1.7 times higher in the case of abrasive wear on rigidly fixed particles, and 13.2 times greater in the case of friction without lubrication according to the "disk-pad" scheme. The increase in wear resistance is because of the rise in the resistance of the MPCs to mechanical loads [9], which is confirmed by the increase in the hardness of the material and the decrease in the roughness of its surface after testing by 1.46 times [9].

Table 2

Operational properties of UHMWPE and MPCs based on it

FL content, wt.%	Abrasion index*, $V_i$ , mm <sup>3</sup> /m	Intensity of linear wear **, $I_h \cdot 10^{-7}$	Hardness HRR, Hardness units***	Roughness*** Ra, $\mu$ m	
				under the influence of rigidly fixed abrasive particles	under friction conditions without lubrication
0	1,48	15,8	32	2,78	2,14
5	1,40	10,6	35	2,53	2,02
10	1,31	6,2	39	2,35	1,89
15	1,22	2,7	43	2,13	1,75
20	0,86	1,2	47	1,92	1,63
25	1,06	3,1	45	2,16	1,77
30	1,14	5,5	40	2,43	1,82

\*average of three study cycles

\*\*average of three experiments

\*\*\*average of 12 measurements

It should be noted that with an increase in the number of test cycles (Fig. 1), a decrease in the abrasive wear index is observed for both UHMWPE and MPCs based on it. This is explained by the gradual filling of the micro-irregularities of the abrasive surface with finely dispersed wear products, which leads to the effect of the so-called "greasing" of the surface.

A comparison of the morphology of the friction surfaces (Fig. 2) under different operating conditions showed that the MPCs have a more homogeneous and less damaged surface compared to pure UHMWPE. In particular, we observe a decrease in the number of deep grooves and microcracks on the friction surface of the composite with an effective FL content of 20 wt.%, which indicates higher resistance to mechanical wear. There are signs of intense plastic deformation and destruction of the structure because of friction on the surface of pure UHMWPE under friction conditions without lubrication, in contrast to the MPCs [10].

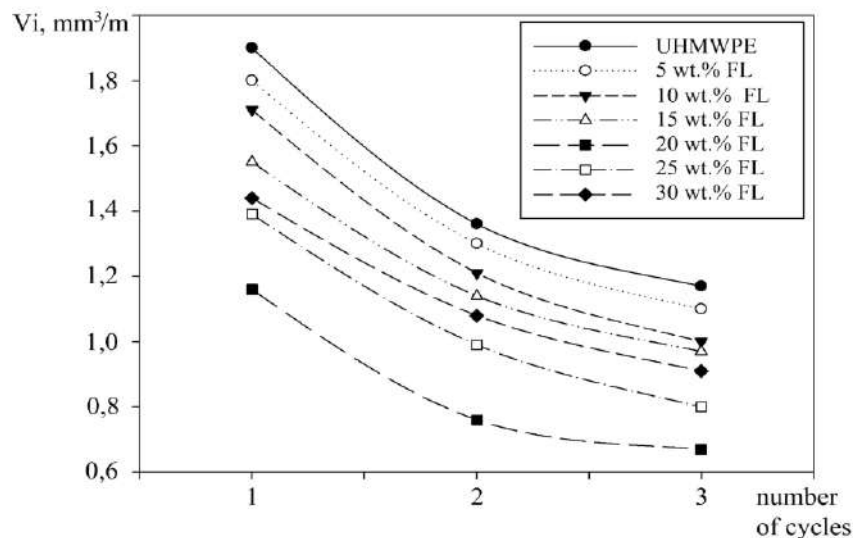
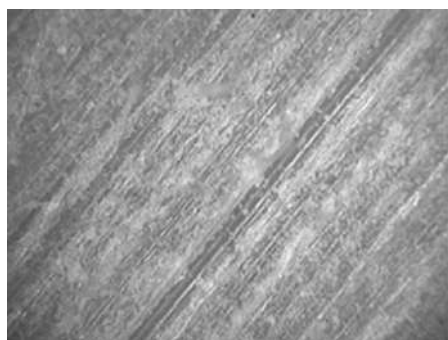
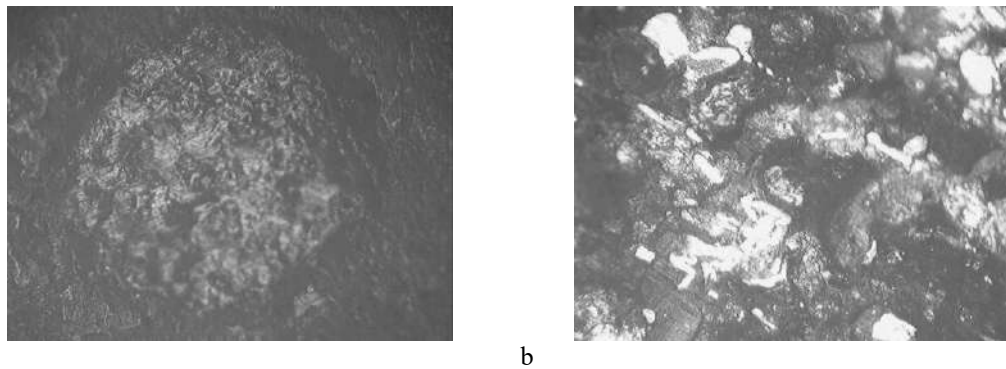


Fig. 1. Dependence of the abrasive wear index ( $V_i$ , mm<sup>3</sup>/m) of ultra-high-molecular-weight polyethylene and MPCs based on it on the number of study cycles



a



**Fig.2. Friction surfaces ( $\times 200$ ) of pure UHMWPE (a) and MPC (b) based on it, containing 20 wt.% FL in different operating modes: under the action of rigidly fixed abrasive particles (1) and under friction conditions without lubrication according to the “disk – pad” scheme**

It is worth noting that there is a decrease in the wear of the MPCs in the filling range of 5-20 wt.%. This is due to the uniform distribution of FL in the UHMWPE. However, with a further increase in the alloy content to 25-30 wt.%, there is a reverse trend, and the wear resistance decreases. This may occur because aggregates of filler particles form, the homogeneity of the MCP structure is disrupted, and the stress concentrators appear due to the above [11]. As for the friction coefficient, its average 15% increase was recorded, which is typical for composites with a metal FL.

### Conclusions

It was found that the introduction of 5-30 wt.% AlMnCrVZrCuMgW alloy contributed to an increase in the wear resistance of the UHMWPE during abrasive wear on rigidly fixed particles by 1.7 times, and by 13.2 times under friction conditions without lubrication according to the "disk-pad" scheme, reaching minimum values at 20 wt.% FL. We recommend using a composite with an effective FL content of 20 wt.% for the manufacture of parts of structural (protection of the bottoms of headers, bearing housings, scrapers) and tribotechnical (sliding bearings, gears) purpose of elements of mechanisms and equipment of modern machinery.

### References

1. O.S. Kabat, N.G. Bannyk, O.M. Voronyi Polymer composite materials of special purpose for the aerospace and rocket industry. *Science and Innovation*. 2025. Vol.21, No 1, P. 95 – 103. [10.15407/scine21.01.095](https://doi.org/10.15407/scine21.01.095)
2. R. Hsissou, R. Seghiri, Z. Benzekri, M. Hilali, M. Rafik, A. Elharfi Polymer composite materials: A comprehensive review. *Composite Structures*. 2021. Vol.262, P. 113640. <https://doi.org/10.1016/j.compstruct.2021.113640>
3. P. Gangwani, J. Kovač, N. Emami, M. Kalin Effect of multi-scale fillers on the tribological behavior of UHMWPE composites in water-lubricated contacts. *Tribology International*. 2024. Vol.196, P.109669. <https://doi.org/10.1016/j.triboint.2024.109669>
4. Q. Gao, S. Liu, K. Hou, Z. Li, J. Wang Graphene-based nanomaterials as lubricant additives: a review. *Lubricants*. 2022. 10, P. 273–310. <https://doi.org/10.3390/lubricants10100273>
5. L.F.M. Rocha, S.B. Cordeiro, L.C. Ferreira, F.J.H. Ramos, M.F. Marques Effect of Carbon Fillers in Ultrahigh Molecular Weight Polyethylene Matrix Prepared by Twin-Screw Extrusion. *Materials Sciences and Applications*. 2016. Vol.7, No.12, P. 863–880. <http://dx.doi.org/10.4236/msa.2016.712066>
6. J. Zhen, Han Y., L. Zhu, W. Hou, Y. Liu, W. Huang, L. Yang, L. Yuan, Z. Jia, R. Zhang MoS<sub>2</sub>/CF synergistic enhancement to improve the friction and wear properties of UHMWPE composites. *Tribology International*. 2023. Vol.179, P.108097. <https://doi.org/10.1016/j.triboint.2022.108097>
7. A.I. Misiura, Ye.P. Mamunia, M.P. Kulish, A.M. Pylypenko Polymer composites based on new carbon fillers. VI All-Ukrainian Scientific Conference "Current Problems of Chemistry: Research and Prospects", October 5, 2022, Zhytomyr. URL: <http://eprints.zu.edu.ua/id/eprint/35069>
8. J. Somberg, G. Gonçalves, N. Emami Graphene oxide versus graphite and chemically expanded graphite as solid lubricant in ultrahigh molecular weight polyethylene composites. *Tribology International*. 2023. Vol.187, P. 108643. doi:10.1016/j.triboint.2023.108643
9. V.F. Bashev, A.-M.V. Tomina, K.A. Mykyta, T.V. Kalinina, S.I. Riabtsev, O.I. Kushnerov The influence of a rapidly-quenched filler on the wear resistance of ultrahigh molecular weight polyethylene. *Functional Materials*. 2024. Vol.31, No.3. P. 387-390. <https://doi.org/10.15407/fm31.03.387>
10. A.I. Burya, Ye.A. Yeriomina The Effect of Various Metallic Filling Materials on the Wear Resistance of Aromatic-Polyamide-Based Composite Materials. *Journal of Friction and Wear*. 2016. Vol. 37, No 2. P. 151–154.

11. O. Kabat, V. Sytar, O. Derkach, K. Sukhyu Polymeric composite materials of tribotechnical purpose with a high level of physical, mechanical and thermal properties, Chemistry and Chemical Technology. 2021. Vol.15, No.4. P. 543–550. 10.23939/CHCHT15.04.543

**Томіна А-М.В., Яковенко Д.В., Башев В.Ф., Головко С.І.** Дослідження впливу швидкозагартованого алюмінієвого сплаву на зносостійкість надвисокомолекулярного поліетилену

У статті розглянуто вплив дисперсного (50-100 мкм) швидкозагартованого з рідини сплаву AlMnCrVZrCuMgW у кількості 5-30 мас.% на зносостійкість надвисокомолекулярного поліетилену за різних режимів експлуатації. Зокрема, досліджено поведінку металополімерного композиту під дією жорстко закріплених часток абразиву, а також в умовах тертя без змащення за схемою «диск – колодка», що моделює реальні умови експлуатації у трибологічних з'єднаннях машин і механізмів сучасної техніки. Результати експериментальних досліджень показали, що введення швидкозагартованого сплаву AlMnCrVZrCuMgW до складу полімерного матеріалу сприяє істотному покращенню його зносостійкості у різних режимах. Так, показник абразивного стирання зменшується у 1,7 рази порівняно з чистим надвисокомолекулярним поліетиленом, а інтенсивність лінійного зношування – більш ніж у 13 разів. Максимального ефекту досягнуто при вмісті сплаву 20 мас.%, що зумовлено ефективним співвідношенням міжмолекулярної взаємодії компонентів і рівномірним розподілом наповнювача в об'ємі полімеру. Підвищення зносостійкості обумовлено зростанням опору поверхні надвисокомолекулярного поліетилену до механічного навантаження, що підтверджується збільшенням твердості матеріалу у 1,46 рази. Морфологічний аналіз поверхонь тертя виявив зменшення кількості та глибини борозен проорювання, що додатково є підтвердженням ефективної дії швидкозагартованого сплаву AlMnCrVZrCuMgW як зміцнювальної фази. Металополімерний композит із ефективним вмістом наповнювача 20 мас.% може бути рекомендований для виготовлення деталей конструкційного (захист днищ жаток, корпуси підшипників, чистики) та триботехнічного (підшипники ковзання, шестерні) призначення елементів машин і механізмів сучасної техніки. Використання таких матеріалів забезпечить підвищення довговічності на надійності трибологічних з'єднань машин і механізмів техніки, що зазнають інтенсивного зношування під час експлуатації.

**Ключові слова:** надвисокомолекулярний поліетилен, швидкозагартований сплав, показник абразивного стирання, інтенсивність лінійного зношування.



## Morphological Analysis of Surface Degradation in Phenolic Friction Composites Using Image Processing Techniques

F.F. Yusubov\*<sup>0000-0002-2095-2469</sup>, V.K. Valiyev<sup>0000-0002-9684-6494</sup>, U.B. Akbarova

*Azerbaijan State Oil and Industrial University, Baku, Azerbaijan*

E-mail: [fikratyusub@gmail.com](mailto:fikratyusub@gmail.com)

Received: 27 April 2025; Revised 10 May 2025; Accept: 7 June 2025

### Abstract

This study investigates the surface degradation of phenolic-based brake friction composites under corrosive NaCl environments, emphasizing morphological analysis through digital image processing. The specimens were subjected to both vapor-phase and immersion conditions to simulate real-world corrosion scenarios. Surface changes were characterized via optical microscopy, Otsu-based grayscale binarization, and roughness profiling. The results indicated that vapor-phase exposure caused more uniform corrosion, but with smoother surfaces, while immersion led to localized and irregular damage. Post-corrosion dry friction tests showed a marked reduction in the coefficient of friction, attributed to surface smoothing and lubricious corrosion product formation.

**Key words:** composites, brake pads, corrosion, surface morphology, cracks, microstructural degradation

### Introduction

Brake systems are essential components in all vehicles, ensuring safety by slowing down or stopping motion through friction. The effectiveness of these systems largely depends on the performance of brake pads, which press against rotating surfaces like discs or drums to generate the necessary braking force. They must maintain stable friction and structural integrity under significant contact pressures and repeated braking cycles [1]. Brake pads are exposed to various environmental factors, including moisture, road salts, and oils, which demand excellent chemical and corrosion resistance. To meet these challenges, brake pad materials must combine high wear resistance with reliable performance over extended periods [2].

The performance of a brake pad is largely influenced by its surface characteristics. A rough or micro-textured surface enhances initial contact with the brake disc, affecting the coefficient of friction and contributing to effective heat dissipation [3]. However, this surface can change over time due to wear or corrosion, which can alter frictional properties. The interplay between the surface's ability to maintain stable friction and its resistance to environmental and operational stresses is critical to the brake pad's overall performance and longevity. Surface corrosion of brake pads significantly influences both material integrity and braking performance. Unlike the more extensively studied corrosion of brake discs, brake pad corrosion occurs at the interface where tribological and chemical processes intersect [4,5]. Moisture and chlorides infiltrate the porous composite matrix, initiating micro-galvanic corrosion between dissimilar phases, such as metallic inclusions and ceramic particles. This degradation not only leads to material loss but also alters the surface texture—reducing effective contact area, generating corrosion products with lubricious or abrasive properties, and destabilizing the friction coefficient [6]. Additionally, the formation of surface pits and cracks can accelerate mechanical wear, especially during repeated braking cycles under load. Despite its practical relevance, the interplay between corrosion-induced surface transformation and wear evolution in composite brake pads remains insufficiently characterized, with limited data available on how these processes co-evolve over time and affect braking reliability under real-world service conditions.

Although previous studies have investigated the corrosion mechanisms in braking couple materials, a systematic comparison of different corrosion conditions and their respective impacts on the tribological behavior of brake pad materials has not been considered [7-9]. Typically, brake pad materials are composed of both metallic and non-metallic components, which generally makes them less susceptible to corrosion. However, in aggressive



environments and under various operating conditions, long-term use of the material—combined with factors such as moisture exposure and interaction duration—can lead to changes in the surface structure of the material [10].

This study aims to bridge these gaps by providing a detailed analysis of the corrosion behavior and friction performance of a brake friction composite under aggressive NaCl environments, offering insights into how material composition and environmental conditions influence both surface degradation and tribological properties.

### Materials and methods

The brake friction composites were formulated using 25% barite, 25% phenolic resin, 7% aluminum oxide, 5% synthetic wollastonite, 10% lead, 10% tin, 7% copper-graphite (composed of 80% Cu and 20% C), and 5% silicon dioxide, along with minor additions of magnesium disulfide and molybdenum oxide, with brass chips incorporated as an alloying element. The specimens were fabricated via ball milling and dry mechanical mixing, followed by pre-forming under 10 MPa and hot pressing at 25.5 MPa.

The specimens were exposed to corrosion through both vapor-phase and direct immersion methods using sodium chloride (NaCl) solutions. For the immersion test, the samples were completely submerged in a 3.5 wt.% NaCl solution at 28°C, ensuring uniform and thorough exposure to the corrosive environment. The corrosion rate of the material was calculated using the formula below, which evaluates degradation over time based on the specimen's weight loss. The formula is expressed as:

$$\text{Corrosion rate (g/cm}^2 \cdot \text{day)} = \frac{\text{Weight loss (g)}}{\text{Surface area (cm}^2) \times \text{Time (days)}}$$

Here, the weight loss refers to the difference between the initial and final mass of the sample, measured in grams (g). The surface area is the exposed area of the sample, given in square centimeters (cm<sup>2</sup>), and time represents the exposure duration in days.

Dry friction tests were conducted using an MMW-1 testing machine at room temperature. During the tests, a load was applied from the lower side of the rotating disc onto the cylindrical composite specimen, which rotated in a clockwise direction (Fig. 1). Dry friction testing was carried out using cylindrical composites (12.7 × 4.8 mm) against a low-carbon steel disc as the counterface, under operating conditions of 5.75 MPa contact pressure, 1.74 m/s sliding velocity, and a total sliding distance of 1.57 km.

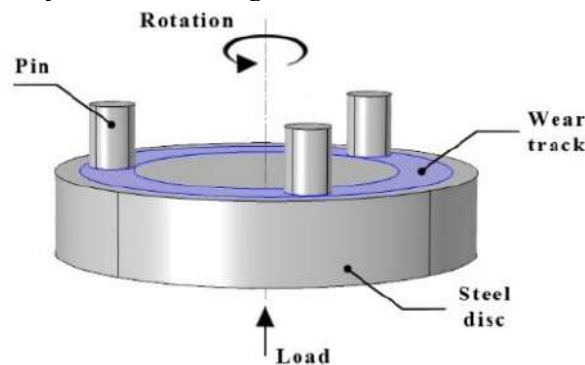


Fig. 1. Diagram of the pin-on-disc wear test setup

Surface roughness was analyzed using a digital image-based technique applied to optical micrographs of the composite surfaces. Grayscale images were first converted to two-dimensional intensity arrays, where pixel brightness values were interpreted as proportional to relative surface height—based on the assumption that elevated regions scatter more light and appear brighter in reflected light microscopy [11]. From each grayscale image, horizontal and vertical surface profiles were extracted along the central axes. These profiles were treated as pseudo-topographical lines, and roughness parameters were computed according to ISO 4287 standard.

### Results and discussion

Table 1 summarizes the corrosion performance of the brake friction composite samples after 7 days of exposure to sodium chloride (NaCl) environments, using both vapor-phase and immersion methods. In the NaCl vapor test, the initial sample weight was 0.7457 g, which decreased to 0.7430 g, resulting in a weight loss of 0.0027 g. This corresponds to a corrosion rate of 0.017 g/cm<sup>2</sup>/day. In comparison, the NaCl immersion test showed a significantly lower weight loss of 0.0007 g, with the sample's weight decreasing from 0.6129 g to 0.6122 g. The corrosion rate for immersion was 0.0044 g/cm<sup>2</sup>/day, which is approximately four times lower than that of the vapor test. The obtained results indicate that the vapor-phase environment induced more aggressive corrosion of the composite material compared to the immersion condition. This increased corrosion activity may be attributed to greater salt deposition and enhanced oxygen availability in the vapor environment, both of which can accelerate surface oxidation and overall corrosion processes.

Table 1

## Corrosion test results

Corrosion method	Duration (days)	Initial weight (g)	Final weight (g)	Weight loss (g)	Corrosion rate (g/cm <sup>2</sup> /day)
NaCl vapor	7	0.7457	0.7430	0.0027	0.017
NaCl immersion	7	0.6129	0.6122	0.0007	0.0044

Based on the Otsu thresholding results of the brake pad composite surfaces, a clear progression in surface degradation is evident across the three conditions. Fig. 2, illustrating the uncorroded surface, clearly reveals distinct constituent phases, as well as a relatively intact and homogeneous material structure. In contrast, image, taken after exposure to NaCl vapor, reveals an increased presence of darkened zones (Fig.3). These regions correspond to corrosion-induced changes such as pitting, phase separation, or surface roughening due to salt deposition and reaction with moisture in the air. The third image, depicting the surface after full immersion in NaCl solution, displays the most extensive dark areas, signifying severe corrosion (Fig 4.). Immersion leads to accelerated electrochemical reactions, especially in the presence of conductive phases like copper-graphite and metallic additives (lead, tin, brass chips). The barite and oxide fillers, typically inert, may also suffer from interfacial degradation when immersed. This escalating surface deterioration from air exposure to full immersion confirms the corrosive aggressiveness of NaCl environments, particularly when liquid water facilitates deeper penetration and reaction with the composite matrix.

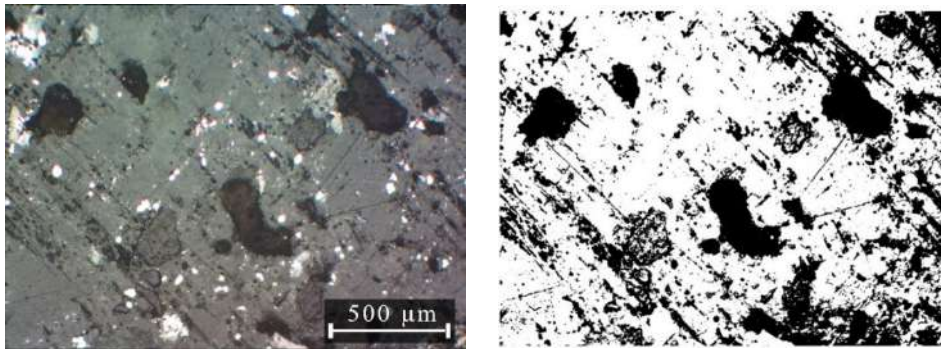


Fig. 2. a) Brake pad surface before corrosion b) image binarized using Otsu's method

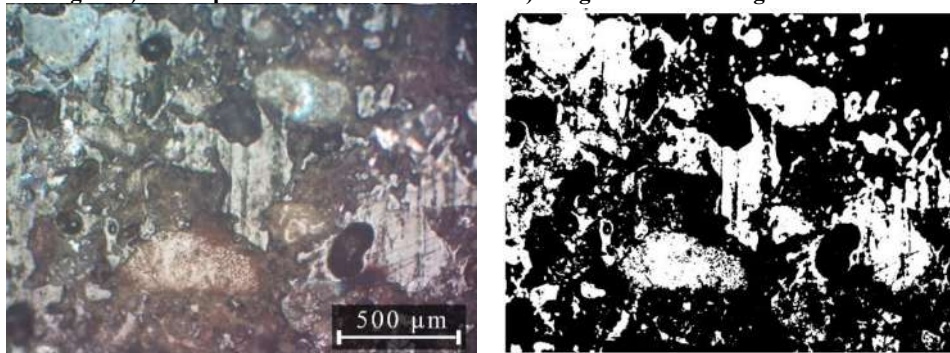


Fig. 3. a) Corroded surface after NaCl immersion exposure; b) image binarized using Otsu's method

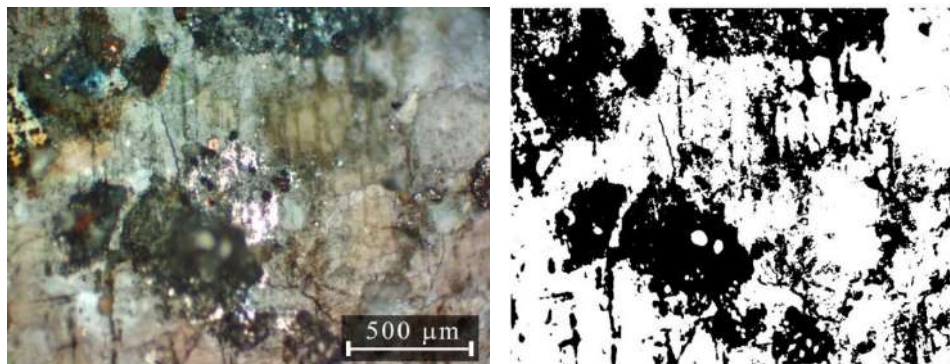


Fig. 4. a) Surface morphology following NaCl vapor exposure b) image binarized using Otsu's method

To better understand the surface characteristics and quantitatively assess the extent of surface damage, the following dimensionless parameters were used for evaluation: the ratio of the area of segmented cracks to the total

image area ( $P_1$ ), the ratio of the perimeter of segmented cracks to the total area ( $P_2$ ), and the ratio of the skeletonized crack length to the total area ( $P_3$ ):

$$P_1 = \frac{A_c}{S_t}$$

where  $A_c$  is the area of segmented cracks and  $S_t$  is the total area of the image. This expression characterizes the extent of wear relative to the total surface.

$$P_2 = \frac{P_c}{S_t}$$

where  $P_w$  is the perimeter of the segmented cracks

$$P_3 = \frac{L_c}{S_t}$$

where is the total length (or area, depending on pixel definition) of the skeletonized cracks. This parameter measures the crack length in relation to the total image area. The results are presented in Table 2.

Table 2

#### Quantitative morphological parameters of segmented corroded regions

Test condition	P <sub>1</sub> : Area ratio	P <sub>2</sub> : Perimeter ratio	P <sub>3</sub> : Skeleton ratio
Before corrosion	21.62%	6.61%	0.00%
NaCl vapor	63.30%	1.69%	0.00%
NaCl immersion	32.30%	4.34%	0.00%

Prior to corrosion, the area ratio is relatively low at 21.62%, suggesting limited defect coverage, while a higher perimeter ratio of 6.61% reflects natural surface texture rather than damage-induced complexity. The skeleton ratio being 0.00% confirms the absence of connected or continuous damage structures. Upon exposure to NaCl vapor, the area ratio dramatically rises to 63.30%, indicating widespread corrosion coverage, albeit with a lower perimeter ratio of 1.69%, implying smoother and more uniform surface attack. Despite the broader damage, the skeleton ratio remains 0.00%, pointing to isolated rather than networked corrosion features. Under NaCl immersion, a moderate area ratio of 32.30% is observed—less extensive than vapor exposure, but accompanied by a higher perimeter ratio (4.34%), suggesting more irregular or pitted corrosion. The absence of interconnected skeleton structures across all cases implies that while corrosion is present and advancing, it has not yet reached a critical state of structural connectivity that would signal severe cracking or mechanical failure.

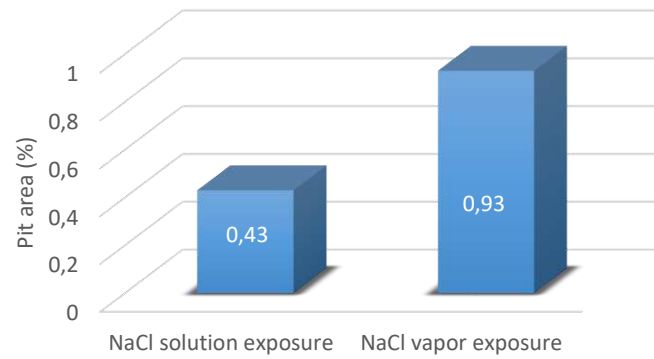
The surface roughness analysis of brake friction composites before and after corrosion revealed distinct degradation patterns depending on the exposure method (Table 3). The initial (uncorroded) surfaces exhibited moderate roughness values ( $R_a \approx 50\text{--}54$  a.u.;  $R_z \approx 224\text{--}229$  a.u.), attributed to inherent heterogeneity from hard ceramic inclusions and metallic fillers.

Table 3

#### Surface roughness before and after corrosion

Test condition	R <sub>a</sub> (H)	R <sub>z</sub> (H)	R <sub>a</sub> (V)
Before corrosion	53.97	224.2	50.40
NaCl vapor corrosion	64.85	206.6	49.60
NaCl immersion corrosion	56.92	243.8	48.52

Following NaCl vapor exposure, the horizontal  $R_a$  increased by approximately 20%, indicating a more uniformly textured surface, while  $R_z$  decreased slightly, suggesting reduced peak-to-valley variation. This behavior is likely due to surface oxidation and the formation of corrosion products that smoothed out deeper surface features. In contrast, immersion in 3.5 wt.% NaCl solution at 28°C resulted in the highest  $R_z$  values (up to 243.8 a.u.), indicative of localized pitting and more severe surface attack. The relatively moderate  $R_a$  under immersion conditions suggests that the roughness increase is dominated by isolated but deep defects rather than widespread surface roughening. These results reflect the influence of composite constituents such as lead, tin, copper-graphite, and brass chips, which are prone to galvanic and chloride-induced corrosion, particularly under full immersion. To calculate the pit area, pits were extracted from Otsu-binarized images (Fig.2-4), and the results are presented in Fig. 5.



**Fig. 5. Pit area comparison between different corrosion conditions**

Although the immersion sample appeared more extensively corroded based on surface analysis, quantitative pit analysis revealed that vapor exposure resulted in approximately twice the amount of actual pitting. This suggests that vapor corrosion is more localized and severe, leading to deeper pit formation.

The friction test results reveal a distinct contrast between non-corroded and corroded brake friction composites. As shown in Fig. 6, the non-corroded samples exhibited a relatively high and stable friction coefficient, averaging around 0.385, with values ranging from approximately 0.367 to 0.402. This consistent behavior suggests strong mechanical interlocking and effective contribution from hard fillers such as barite, aluminum oxide, and silicon dioxide, along with lubricating agents like copper-graphite and magnesium disulfide. In contrast, the corroded composites (Fig. 7), which were exposed to corrosive conditions, demonstrated a lower average friction coefficient of approximately 0.285, with more pronounced fluctuations ranging between 0.263 and 0.301. This reduction in friction performance is likely attributed to the degradation of active components, surface smoothing, or formation of lubricious corrosion products such as oxidized lead, tin, or copper compounds.

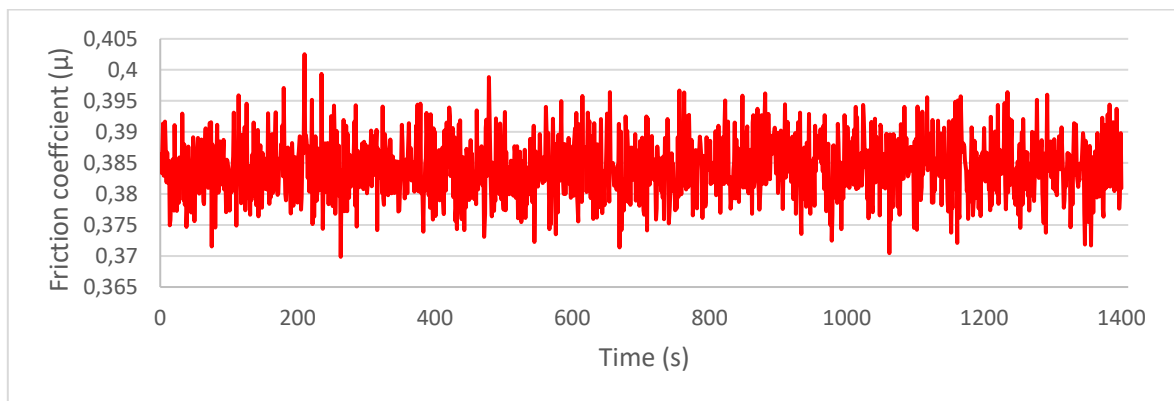


**Fig. 6. Friction test results of non-corroded friction composites**

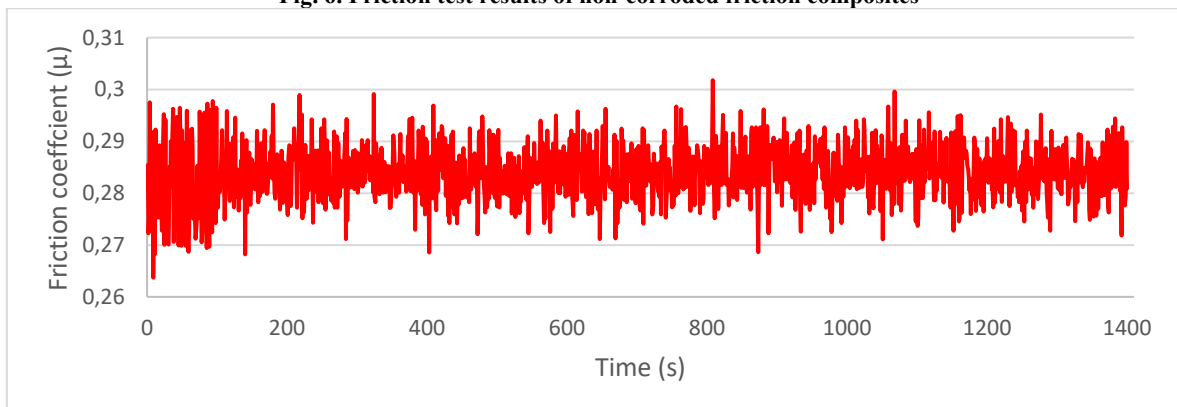


**Fig. 7. Friction test results of corroded friction composites**

Despite the presence of lubricating and corrosion-inhibiting constituents such as graphite,  $\text{MoO}_3$ , and  $\text{MgS}_2$ , morphological analysis revealed notable surface degradation. Table 4 presents the shape-based descriptors of the corroded brake pad surface after the friction test, including the area ratio ( $P_1$ ), perimeter ratio ( $P_2$ ), and skeleton ratio ( $P_3$ ).

**Table 4. Shape-based descriptors of the corroded brake pad surface after the friction test**

Descriptor	Symbol	Value
Area ratio	$P_1$	0.1013
Perimeter ratio	$P_2$	9.0220
Skeleton ratio	$P_3$	0.1125

The area ratio ( $P_1 = 10.13\%$ ) reflected a modest but significant presence of corrosion-affected regions, while the high perimeter ratio ( $P_2 = 9.02$ ) indicated the presence of sharp, fragmented corrosion fronts—potentially originating from localized electrochemical reactions. Notably, the skeleton ratio ( $P_3 = 0.1125$ ) suggested a branching corrosion network, possibly facilitated by microstructural heterogeneity and preferential attack near soft metallic constituents. These observed morphological features align with further analysis of the surface, revealing clear signs of localized corrosion.

The worn surface exhibited pronounced micro-topographical irregularities following exposure to corrosion, as revealed by optical microscopy (Fig. 8). The micrograph clearly shows corrosion-induced degradation, characterized by localized white patches and grooved textures—features indicative of corrosion-assisted wear mechanisms. The directionality of the grooves corresponds to the sliding direction during dry friction testing, suggesting a synergistic interaction between mechanical wear and chemical attack. Given the composite's heterogeneous composition—including metallic phases such as Cu, Pb, and Sn, as well as ceramic reinforcements like  $\text{Al}_2\text{O}_3$  and  $\text{SiO}_2$ —the corrosion attack likely proceeded in a non-uniform manner.

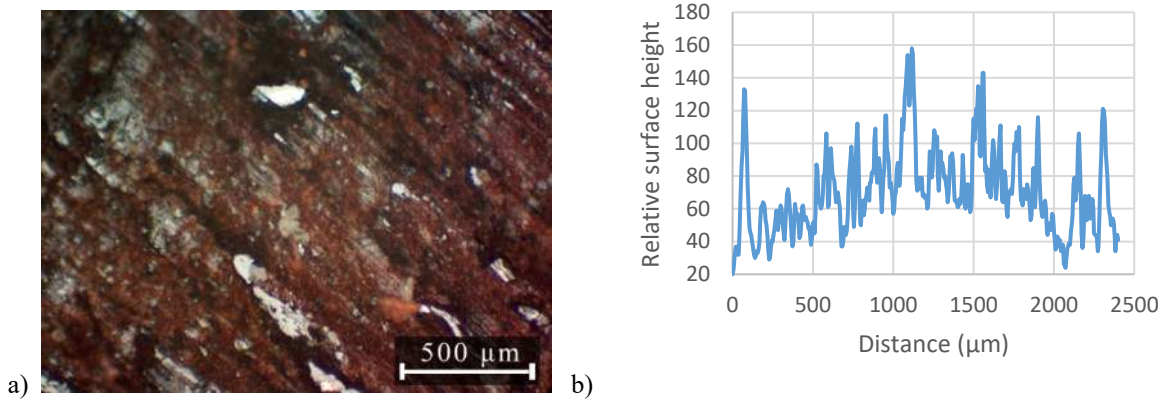


**Fig. 8. a) Worn surface of the brake friction composite after NaCl vapor-induced corrosion and b) corresponding surface roughness profile**

To further analyze the damaged surface, a three-dimensional topographical reconstruction was performed using grayscale intensity values extracted from the optical micrograph (Fig. 5b). The simulated surface topography indicates concentrated wear along specific paths, likely resulting from the combined effects of mechanical loading and corrosive product formation. The presence of low-hardness constituents such as lead and tin may have contributed to smearing effects, while the hard ceramic particles ( $\text{Al}_2\text{O}_3$ ,  $\text{SiO}_2$ ) likely facilitated micro-cutting. Surface roughness profile, which exhibits significant variation in relative surface height—from approximately 20  $\mu\text{m}$  to 160  $\mu\text{m}$ . These fluctuations reflect an uneven degradation pattern, where deeper valleys correspond to regions of severe material loss due to pitting corrosion, while elevated areas may represent corrosion-resistant phases or embedded hard particles such as  $\text{Al}_2\text{O}_3$  or copper-graphite. The overall high surface roughness is consistent with the pitting and delamination phenomena typically associated with chloride-induced corrosion.

## Conclusions

This study evaluated the surface degradation and frictional performance of phenolic-based brake friction composites under corrosive NaCl environments, simulating both vapor-phase and immersion conditions. The main findings are summarized as follows:

1. The corrosion rate under vapor-phase conditions was  $2.31 \text{ mg/cm}^2/\text{day}$ , about 28% higher than the  $1.80 \text{ mg/cm}^2/\text{day}$  measured in immersion.
2. Vapor-phase NaCl exposure led to smoother and more uniform corrosion, reducing surface roughness from  $4.3 \mu\text{m}$  to  $2.1 \mu\text{m}$ , whereas immersion in NaCl caused more localized and aggressive attack, increasing roughness to  $5.6 \mu\text{m}$ .
3. Dry friction tests showed a 15% drop in the average coefficient of friction (COF) after vapor-phase corrosion (from 0.41 to 0.35) and a 9% drop after immersion (to 0.37). Friction fluctuations, indicated by a 26% increase in the coefficient of friction standard deviation, worsened after vapor exposure due to surface smoothing and corrosion debris formation.

## References

1. Mulani, S.M., Kumar, A., Shaikh, H.N.E.A., Saurabh, A., Singh, P.K. and Verma, P.C., 2022. A review on recent development and challenges in automotive brake pad-disc system. *Materials Today: Proceedings*, 56, pp.447-454.
2. Kchaou, M., Sellami, A., Elleuch, R. and Singh, H., 2013. Friction characteristics of a brake friction material under different braking conditions. *Materials & Design* (1980-2015), 52, pp.533-540.
3. Österle, W., Kloß, H., Urban, I. and Dmitriev, A.I., 2007. Towards a better understanding of brake friction materials. *Wear*, 263(7-12), pp.1189-1201.
4. Bandiera, M., Mauri, A., Bestetti, M., di Milano, P., Bonfanti, A., Mancini, A. and Bertasi, F., 2020, June. Corrosion phenomena in braking systems. In *Nace Corrosion* (pp. NACE-2020). NACE.
5. Hamid, M.A., Kaulan, A.M., Syahrullail, S. and Bakar, A.A., 2013. Frictional characteristics under corroded brake discs. *Procedia Engineering*, 68, pp.668-673.
6. Mandziy, Teodor, et al. "Evaluation of the Degree of Degradation of Brake Pad Friction Surfaces Using Image Processing." *Lubricants* 12.5 (2024): 172.
7. Motta, M., Fedrizzi, L. and Andreatta, F., 2023. Corrosion stiction in automotive braking systems. *Materials*, 16(10), p.3710.
8. Park, C.W., Shin, M.W. and Jang, H., 2014. Friction-induced stick-slip intensified by corrosion of gray iron brake disc. *Wear*, 309(1-2), pp.89-95.
9. Sergienko, V.P., Kozhushko, V.V., Bukharov, S.N. and Merinov, V.K., 2023. Effect of corrosion inhibitors in compositions of friction composites on corrosion resistance of the metal counterbody and noise generation during friction. *Journal of Friction and Wear*, 44(5), pp.259-265.
10. Lenik, K., Paszeczko, M., Durjagina, Z., Dziedzic, K. and Barszcz, M., 2008. The surface self-organization in process friction and corrosion of composite materials. *Archives of Materials Science and Engineering*, 30(1), pp.9-12.
11. Otsu, Nobuyuki. "A threshold selection method from gray-level histograms." *Automatica* 11.285-296 (1975): 23-27.

**Ф.Ф. Юсубов, В.К. Валієв, У.Б. Акбарова.** Морфологічний аналіз деградації поверхні фенольних фрикційних композицій з використанням методів обробки зображень

У цьому дослідженні вивчається деградація поверхні гальмівних фрикційних композицій на основі фенолформальдегідної смоли в корозійних середовищах NaCl із акцентом на морфологічний аналіз за допомогою цифрової обробки зображень. Зразки піддавалися впливу як парової фази, так і занурення для імітації реальних умов корозії. Зміни поверхні характеризувалися за допомогою оптичної мікроскопії, бінаризації за методом Отсу у відтінках сірого та профілювання шорсткості. Результати показали, що вплив парової фази спричиняє більш рівномірну корозію зі згладженою поверхнею, тоді як занурення призводить до локалізованих і нерегулярних пошкоджень. Післякорозійні випробування на сухе тертя виявили суттєве зниження коефіцієнта тертя, що пояснюється згладженням поверхні та утворенням мастильних продуктів корозії.

**Ключові слова:** композиційні матеріали, гальмівні колодки, корозія, морфологія поверхні, тріщини, мікроструктурна деградація.



## Study of the concentration effect and structure of multilayer spherical carbon nanoclusters on the carrying capacity of alternative fuels

Ie.V. Polunkin<sup>0000-0001-9724-8835</sup>, S.M. Pleskun\*<sup>0009-0001-6034-7175</sup>

*Institute of Bioorganic Chemistry and Petrochemistry named VP Kukhar of the National Academy of Sciences of Ukraine*

E-mail: [albazdan7@gmail.com](mailto:albazdan7@gmail.com)

Received: 05 May 2025; Revised 15 May 2025; Accept: 10 June 2025

### Abstract

The paper presents the results of tribological studies of the influence of nanoscale additives on the properties of ethanol and biodiesel fuels. The non-monotonic extreme nature of the dependence of the carrying capacity of liquid fuels on the content of nanoscale particles is revealed; this indicator changes most maximally in the region of ultra-low concentrations of nanoparticles (several ppm).

The possibility of improving the synthesis and modification of carbon spheroidal nanoclusters by conducting high-frequency high-voltage synthesis in various organic solvents has been shown, which allowed to increase significantly the set of starting materials for the synthesis with the inclusion of various elements in the structure of CNSs. In order to increase the yield of carbon nanospheres during synthesis in the liquid phase, a reactor with a given angle of the interelectrode space was made for the first time for use in the synthesis process of "Jacob's ladder".

Chemical analysis and structural studies of synthesized samples of nanoscale objects of different chemical structures were carried out using IR and Raman spectroscopy, and electron microscopy.

For the first time, the hypothesis proposal has been made that individual carbon nanoparticles, obtained by high-voltage high-frequency plasma-chemical synthesis, which appear as spheroidal objects in electron microscopic images, are actually twisted coils of linear chain molecules of the polyyne type – carbynes.

**Keywords:** fullerene-like carbon nanoparticles, plasma discharge, high-voltage high-frequency plasma chemical synthesis, carrying capacity, alternative fuels.

### Introduction and literature review

In addition to the main function of motor fuels – the ability to transform the chemical energy accumulated in them into thermal and mechanical work of engines, they must provide high lubricating properties [1].

According to the generally accepted definition, "the lubricating properties of fuels and lubricants are their ability to reduce friction and wear of contact surfaces moving relative to each other when a load is applied to the friction pair."

In modern internal combustion engines running on liquid fuels (gasoline, diesel and jet), fuel acts as a lubricant for plunger pumps, injector elements and other parts of the fuel supply control equipment. The condition of this equipment determines fuel consumption, reliability, service life and functional suitability of the engines as a whole.

Therefore, the problem of assessing the anti-wear properties of modern motor fuels (both traditional hydrocarbon and biofuels) is very important for developing the composition of fuels, creating new anti-wear additives, and recommendations for their use.

The final, most reliable tests of batches of motor fuels for compliance with anti-wear properties before their practical implementation are carried out on real engines. However, this requires significant consumption of motor fuel (tens of tons) and is long-term.

For screening non-engine assessment of anti-wear properties of liquid motor fuels at the initial stages, more than 10 tribological testing methods are used in world practice [2–3]. These methods differ in friction contact schemes, friction pair materials, test time and load. When conducting tribological tests, the anti-wear properties of



diesel fuels are characterized by the values of the following indicators: friction coefficient, average diameter of wear spots (under selected standardized conditions), as well as by the value of the bearing capacity (critical load before seizure).

In our studies, the impact of nanoscale additives on the anti-wear properties of biofuels was assessed by the change in bearing capacity.

The bearing capacity of fuels determines the range of loads at which, under given standard conditions, the fluid friction mode is implemented until the fluid layer ruptures and metal contact of friction surfaces occurs with their microdamage - burrs.

The characteristic of bearing capacity for a liquid is, in its physical content, analogous to the corresponding characteristic of dynamic strength for solids; they both reflect the ability of materials to resist external loads on them.

Carbon nanospheres (CNSs) ideally have a structure in the form of concentric fullerene-like shells. In addition to the six-membered  $C_6$  rings, the shells also include  $C_5$  and  $C_7$  rings [4].

But in real spherical carbon nanoobjects, the regular shell spherical structure is disrupted; they consist of individual graphene fragments – petals.

Currently, various methods for the synthesis of CNSs have been developed: pyrolytic deposition from the gas phase, hydrothermal synthesis, template synthesis. However, despite the significant number of publications on the synthesis methods of carbon nanospheres, they mainly concern large-sized nanospheres. The number of publications on the synthesis of CNSs with sizes smaller than 100 nm is very limited [5].

The main methods for obtaining such nanospheres are arc discharge between carbon electrodes in the gas phase, as well as in a liquid, for example, in water or benzene, the particle size in this case is 5–100 nm [6]. High-temperature annealing of detonation nanodiamonds creates spheroidal particles with well-defined shells and a narrow size distribution of 2–10 nm [7].

There is no commonly accepted model for the primary structure of individual spherical nanoparticles at the moment. Most researchers who have obtained CNSs by thermal transformation of nanodiamonds [8] believe that individual nanoparticles that form spheroidal agglomerates consist, in turn, of multilayered partially closed defective graphene shells – petals of irregular shape, the interplanar distance between which is  $\sim (0.332 \pm 0.001)$  nm (the interplanar distance of graphite is 0.3354 nm). In the middle of the particle there is a disordered core. It is believed that this core is in a liquid state [9].

In the previous stages of our research, the modification of carbon nanospheres was carried out by treating the mixed synthesis product (in the form of carbon black) with various chemical reagents and subsequent isolation of the desired target nanoparticles by extraction in various solvents, filtration and vacuum distillation of solvents [10]. The structure and size of the nanoobjects selected for further research were controlled using SEM and TEM electron microscopy and Raman scattering spectroscopy.

We have improved the synthesis and modification of carbon spheroidal nanoclusters - high-frequency high-voltage synthesis was carried out in various organic solvents. This allowed us to increase significantly the set of starting materials for the synthesis of CNSs with the inclusion of atoms of various elements in the structure.

## Purpose

The aim of the work is to develop methods for the synthesis of nanosized objects with different chemical structures and to identify the mechanisms of action of small concentrations of nanoclusters on the magnitude of the carrying capacity of individual liquid substances and practically important liquid petroleum products.

## Results

Brominated CNSs were obtained by a one-step synthesis from solutions of bromo- and fluorocarbons in hydrocarbon solvents without using an additional CNSs halogenation step.

The synthesis of carbon nanomaterials in the liquid phase is carried out using dielectric liquids. These can be organic solvents, as well as liquid gases (nitrogen, argon, helium). During these processes, a suspension of individual nanoparticles with a defined spatial structure, as well as associates of such nanostructures, is formed in the liquid. The content of various modifications of individual nanoparticles, their sizes and the sizes of associates of these objects depend on the energy conditions of the arc discharge process and on the liquid in which the synthesis takes place.

Plasma-chemical liquid-phase synthesis of carbon nanoparticles was carried out in a glass reactor. The plasma discharge in aliphatic and aromatic solvents was generated by a bipolar power source - a high-voltage high-frequency generator using tungsten open electrodes. The electrodes were placed in the volume of liquid - the starting material. The frequency of the voltage pulses was 25 kHz. The generator voltage  $U = 4$  kV.

Also, to increase the yield of carbon nanospheres during liquid-phase synthesis, a reactor with a given angle of the interelectrode space was first made for use in the Jacob's ladder synthesis process.

plasma-chemical liquid-phase synthesis modes for the production of spheroidal carbon nanomaterials was carried out using individual hydrocarbon compounds in the liquid state (hexane, octane, benzene, bromomethane), mixtures (hexane with bromomethane), and fluorocarbon derivatives.

The synthesis products were isolated from the liquid phase by centrifugation (30 min at 4000 rpm). Then the powders were additionally dried in vacuum and fractionated by extraction in low-boiling solvents and filtered on filters with a pore diameter of 250 nm and the solvent was distilled off.

Electronic images of the CNSs samples are shown in Fig. 1. High-resolution microscopic images of the CNSs were obtained using a JEOL JEM-2100F transmission electron microscope (TEM) with an electron accelerating voltage of 200 kV. For this, carbon nanosphere samples were dispersed in a dimethyl ketone medium using an ultrasonic disperser, and then applied to a special substrate.

The obtained carbon nanomaterials are spheroidal nanoparticles with sizes of ~ 10–30 nm with a complex hierarchical structure.

We were the first to propose the hypothesis that individual carbon nanoparticles obtained by high-voltage high-frequency plasma-chemical synthesis, which appear as spheroidal objects in electron microscopic images, are actually twisted coils of linear chain molecules of the polyene type - carbynes.

This opinion is confirmed by in particular, the results of IR spectroscopic analysis of these materials. Their IR spectra (Fig. 2) show a rather intense band at  $1737\text{ cm}^{-1}$ , which is characteristic of linear carbynes with double cumulated bonds  $=C=C=C=C=C=$ , and is absent in the spectra of cyclic molecules of the benzene type.

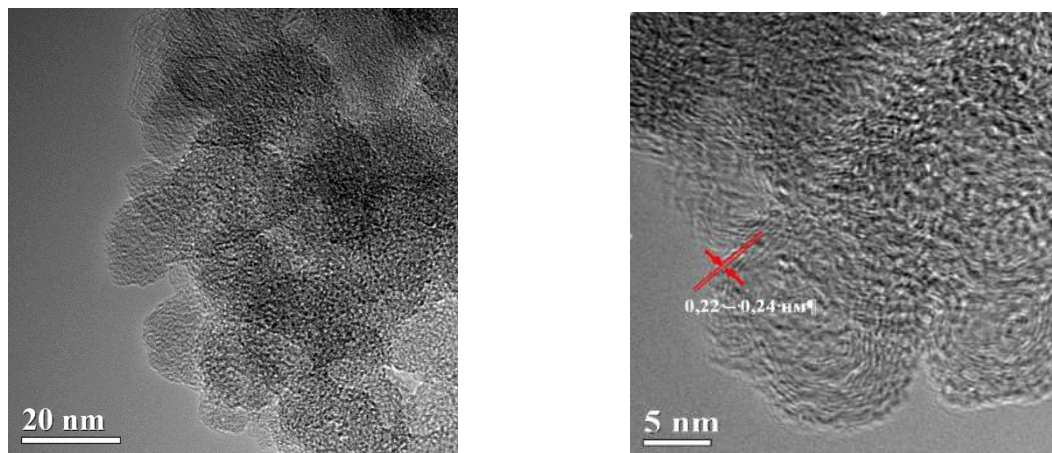


Fig. 1. TEM image of carbon nanospheres

Fig. 1 presents the results of the study of the structure of the synthesized compounds by transmission electron microscopy. The synthesized nanospheres of the type consist of carbyne threads woven into a ball with a diameter of 2.2 - 2.4 nm, which coincides with the diameter of the polycumulene chain. Indeed, the absorption band at 1737 nm present in the IR spectra of the obtained nanocarbon compounds is present in the IR spectrum of polycumulenes and is not observed in the spectrum of graphene.

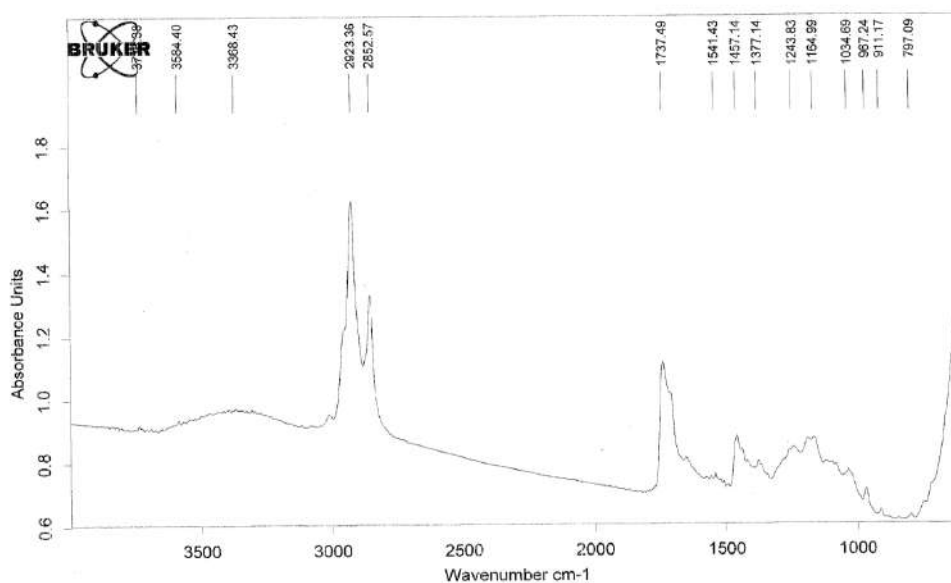


Fig. 2. IR spectrum of carbon nanospheres

To identify the structural features, degree of ordering, and homogeneity of the obtained carbon materials, laser Raman spectroscopy was used.

Raman spectroscopic studies of samples of synthesized nanomaterials were carried out at the V.E. Lashkaryov Institute of Semiconductor Physics of the NAS of Ukraine (senior scientific collaborator Kolomys O.F.).

Raman spectra were recorded in a wide range of wavenumbers at 150–3500  $\text{cm}^{-1}$  using a LabRAM laser spectrometer (Yobin Yvon) with a 632.8 nm He-Ne laser excitation line.

Raman spectroscopy is one of the vibrational spectroscopy methods that does not require the destruction of samples for analysis and is widely used in the study of various allotropic modifications of carbon. A characteristic feature of the Raman spectra of carbon materials is the presence of a G-band at 1500–1600  $\text{cm}^{-1}$ . The vibrations that are reflected in the spectrum by the G (graphite) - band are considered to be associated with vibrations of carbon atoms in the plane of graphene cycles (tangential vibrations).

Depending on the structural perfection and curvature of such layers, the G-band can vary in frequency and shape. In the spectra of pure graphite, it has a narrow and undivided shape due to the symmetry and unstrained state of the bonds between carbon atoms in the flat graphene layers of this material.

In the Raman spectra of onions (spheroidal multilayer carbon clusters), in addition to the band characteristic of vibrations of  $sp^2$ -bonds in ordered carbon materials, a band also appears at about 1320  $\text{cm}^{-1}$ . The intensity of the band at 1320  $\text{cm}^{-1}$  may be different in magnitude compared to the intensity of the band at a frequency 1590  $\text{cm}^{-1}$ .

The Raman-active oscillation bands at a frequency 1590  $\text{cm}^{-1}$  are usually designated G (graphite) - band, and the band at 1320  $\text{cm}^{-1}$  is designated as D (disorder) - band. The D (disorder) - band is due to various structural defects and limited crystallite sizes, i.e. it is associated with the disordering of carbon nanomaterials. The intensity of this band characterizes the defectivity, i.e. the degree of symmetry violation of the ideal graphite layer with  $sp^2$ -hybridization of carbon atoms. Therefore, the ratio of the intensities of the D/G bands characterizes the relative content in the studied sample of the amount of materials with disordered and ordered structures.

The presence of these two bands in the Raman spectrum of a chemical substance is a kind of characteristic mark that indicates the content of carbon with  $sp^2$ - and  $sp^3$ -hybridization in the substance, that is, carbon nanomaterials with a spheroidal shell structure.

Below are the Raman scattering spectra (Fig. 3) of bromine-containing carbon nanoclusters, which we obtained by the method of plasma-chemical synthesis in the liquid phase.

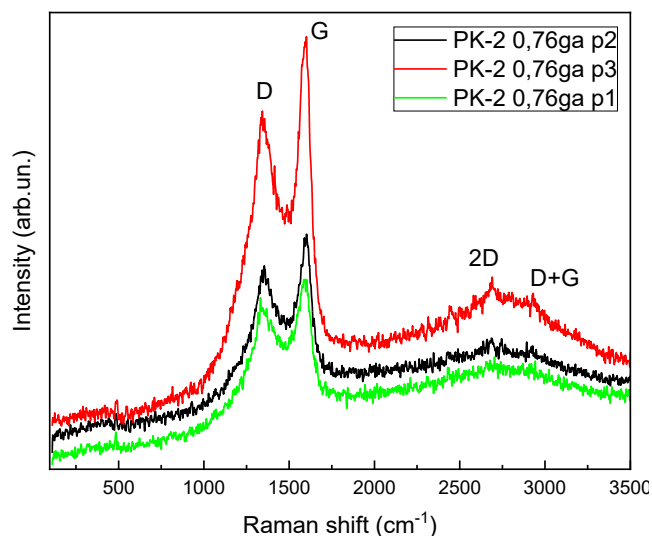


**Fig. 3. Raman spectrum of carbon nanoclusters obtained by plasma-chemical synthesis of bromine-containing hydrocarbons in the liquid phase**

The presence of two characteristic vibration bands in the Raman spectra of the products synthesized by us (at about 1500  $\text{cm}^{-1}$  and 1300  $\text{cm}^{-1}$ ) is confirmation that spheroidal carbon nanoparticles were indeed obtained using the plasma-chemical synthesis method.

### **Tribological studies of the effect of small concentrations of nanoparticles in liquid motor fuels**

The comparison of the bearing capacity of fuels was determined on a four-ball tribometer by the magnitude of the critical load according to the ASTM D2783 method [11].

This indicator represents the maximum value of the axial load, up to which there is no metal contact and no scoring during sliding friction of standardized metal balls made of steel ShKh15 (microhardness 64-66 HRC, hardness parameter  $R_a < 0.25 \mu\text{m}$ , ball diameter – 12.7 mm) in test liquid medium. Test conditions: rotation speed

of the upper loaded ball relative to three stationary balls – 1500 rpm, temperature 20 °C, test time – 10 s. At each load, at least three tests were performed.

Fig. 4 shows that the carrying capacity of ethanol is changing non-monotonically with increasing concentration of bromine-containing CNSs.

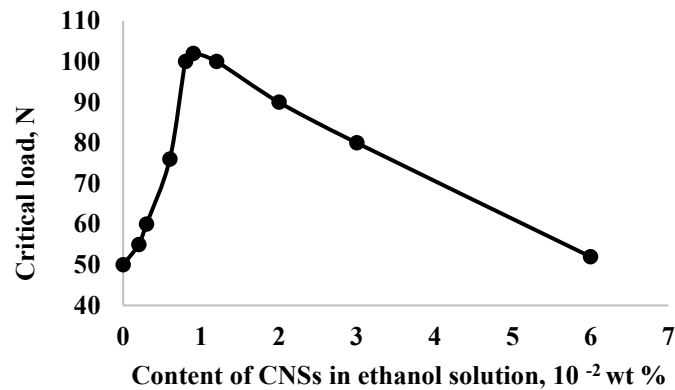


Fig. 4. Non-monotonic dependence of the carrying capacity of ethanol solutions on the concentration of bromine-containing CNSs

The critical load value for blended biodiesel fuel (80% commercial petroleum diesel fuel DSTU 7688:2015 + 20% ethyl esters of vegetable oils) at different concentrations of spheroidal carbon nanoclusters is shown in Fig. 5.

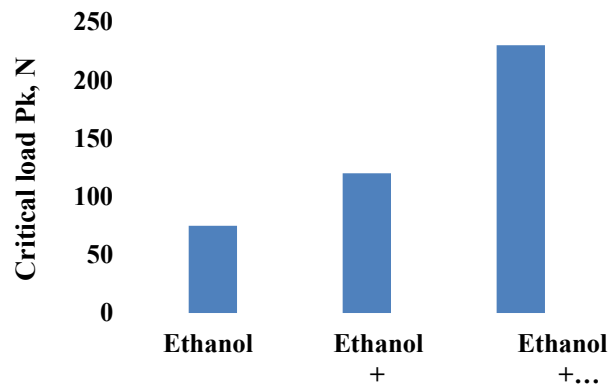


Fig. 5. Maximum increase in the carrying capacity of ethanol fuel by additives of bromine- and fluorine-containing carbon spheroidal nanoclusters (at optimal concentrations in the range of 10<sup>-4</sup>-10<sup>-3</sup>% by weight)

The critical load value for blended biodiesel fuel (80% commercial petroleum diesel fuel DSTU 7688:2015 + 20% ethyl esters of vegetable oils) at different concentrations of spheroidal carbon nanoclusters is shown in Fig. 6.

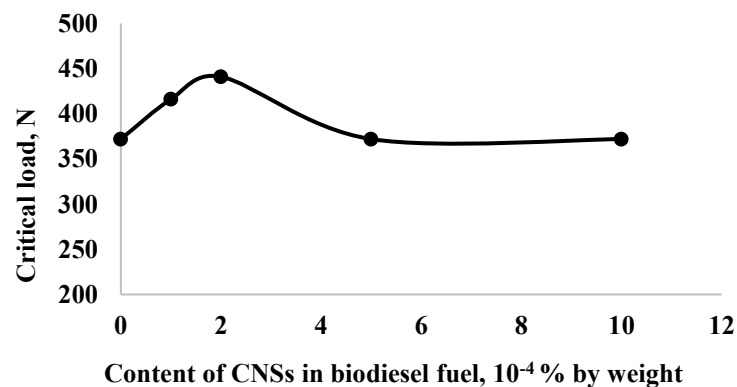


Fig. 6. Effect of carbon bromine-containing nanospheres on the carrying capacity of blended biodiesel B20 (80% diesel fuel + 20% ethyl esters)

According to the results of tribological studies, the concentration dependences of the bearing capacity of ethanol solutions and biofuels on the content of nanoparticles - carbon nanoclusters and metal complexes - are of an extreme nature.

The maximum effect of increasing the critical load index is observed in the range of small concentrations of nanoclusters in solutions (less than  $10^{-2}$  % by weight).

The magnitude of the effect of increasing the carrying capacity for a given solution depends on the polarity (polarizability) of the nanoparticles. The most significant increase in the carrying capacity of ethanol solutions (by 2–3 times) was observed for fluorine-containing carbon nanospheres.

### Conclusions

1. The chemical analysis of the synthesized samples and structural studies using IR and Raman spectroscopy, electron microscopy confirms the formation of nanosized objects of different chemical structure (carbon spheroidal nanoclusters).

2. Tribological studies of the influence of nanoscale additives on the properties of ethanol solutions and biodiesel fuels were conducted. It was shown that the introduction of small concentrations (several ppm) of nanoscale additives allows to increase the carrying capacity of biofuels by 2–3 times. A non-monotonic extreme nature of the dependence of the carrying capacity of liquid fuels on the content of nanoscale additives was revealed; this characteristic changes most maximally in the region of small concentrations of nanoparticles, when the concentration threshold values are exceeded, the efficiency of the action of nanoparticles decreases.

3. The extreme non-monotonic nature of the dependence of solution parameters on the concentration of nanoparticles is explained by the formation of regions of heterogeneity in solutions.

### References

1. Бойченко С.В. Рациональне використання вуглеводневих палив. К.: НАУ, 2001. 216 с.
2. Сіренко Г. О., Кириченко В. І., Сулима І. В. Фізико-хімія паливно-мастильних матеріалів. Івано-Франківськ, 2017. 508 с.
3. Hsieh P.Y., Bruno T.J. A perspective on the origin of lubricity in petroleum distillate motor fuels. *Fuel Processing Technology*. 2015. Vol. 129. P. 52–60.
4. Ugarte D. Curling and closure of graphitic networks under electron-beam irradiation. *Nature*. 1992. Vol. 359. P. 707–709.
5. Bartelmess J., Giordani S. Carbon nano-onions (multi-layer fullerenes): Chemistry and applications. *Beilstein J Nanotechnol*. 2014. Vol. 5. P. 1980–1988.
6. Schwenke A.M., Hoepfner S., Schubert U.S. Synthesis and modification of carbon nanomaterials utilizing microwave heating. *Advanced Materials*. 2015. Vol. 27, N 28. P. 4113–4141.
7. Isakova V.G., Petrakovskaya E.A., Isakov V.P. The research of powder fullerene and ultra-dispersed diamonds composites with metal and oxide nano-particles. *The Physics of Metals and Metallography*. 2006. Vol. 102, N 1. P. 51–60.
8. Marco Zeiger, Nicolas Jäckel, Vadym N. Mochalin, Volker Presser Review: carbon onions for electrochemical energy storage *J. Mater. Chem. A*, 2016, 4, 3172–3196. <https://doi.org/10.1039/c5ta08295a>.
9. Banhart, F., Ajayan, P. Carbon onions as nanoscopic pressure cells for diamond formation. *Nature* 382, 433–435 (1996). <https://doi.org/10.1038/382433a0>.
10. Pleskun S.M., Polunkin E.V., Pyliavskiy V.S. Gas phase synthesis of carbon nanospheres, structure and properties Proceedings of the International conference «Current problems in catalysis» CPC2023. P 113–114.
11. Yadav G., Tiwari S., Jain M.L. Tribological analysis of extreme pressure and anti-wear properties of engine lubricating oil using four ball tester. *Materials Today*. 2018. Vol.5, N 1. Part 1. P. 248–253.

**Полункін Є.В., Плєскун С.М.** Дослідження концентраційного впливу та структури багат шарових сферичних карбонових нанокластерів на величину несучої здатності альтернативних палив

В роботі показано результати трибологічних досліджень впливу нанорозмірних присадок на властивості етанольних та біодизельних палив. Виявлено немонотонний екстремальний характер залежності несучої здатності рідких палив від вмісту нанорозмірних часток; найбільш максимально цей показник змінюється в області надмалих концентрацій наночастинок (декілька ppm).

Показано можливість вдосконалення синтезу та модифікацію карбонових сфероїдальних нанокластерів шляхом проведення високочастотного високовольтного синтезу в різних органічних розчинниках, що дозволило значно збільшити набір вихідної сировини для синтезу з включенням атомів різноманітних елементів в структуру КНС. Для збільшення виходу карбонових наносфер при синтезі в рідинній фазі вперше був зроблено реактор з заданим кутом міжелектродного простору для використання в процесі синтезу «драбина Якоба».

Проведено хімічний аналіз та структурні дослідження синтезованих зразків нанорозмірних об'єктів різної хімічної будови методами ІЧ- та КР- спектроскопії, електронної мікроскопії.

Вперше висунуто припущення, згідно якого окремі карбонові наночастинок, які отримували високовольтним високочастотним плазмохімічним синтезом, що в електронномікроскопічних зображеннях виглядають як сфероїдальні об'єкти, в дійсності є скрученими клубками лінійних ланцюжкових молекул поліінового типу – карбінів.

**Ключові слова:** фулереноподібні карбонові наночастинок, плазмовий розряд, високовольтний високочастотний плазмохімічний синтез, несуча здатність, альтернативні палива



## Research into the possibility of improving the quality of electric arc coatings by nitriding

A. Lopata<sup>\*10000-0001-5266-6486</sup>, V. Lopata<sup>20000-0002-1578-1298</sup>, I. Kachynska<sup>10009-0006-7623-2897</sup>,  
A. Solovykh<sup>30000-0001-5780-3582</sup>

<sup>\*1</sup>*G. S. Pisarenko Institute for Problems of Strength of National Academy of Sciences of Ukraine*

<sup>2</sup>*E.O. Paton Electric Welding Institute of the National Academy of Sciences of Ukraine*

<sup>3</sup>*Central Ukrainian National Technical University*

\*E-mail: [lopata-sasha@ukr.net](mailto:lopata-sasha@ukr.net)

Received: 10 May 2025; Revised 25 May 2025; Accept: 12 June 2025

### Abstract

An effective way to effectively change the characteristics of electric arc coatings made from crushed materials can be achieved by creating high-quality surface balls in them due to the use of different methods. chemical-thermal treatment. Research was carried out on the development and testing of the concept of molding chemical dry coatings based on the combined process of electrode deposition with technological processing of pulsed ion nitriding. It has been shown that duplex (combined) technology, which combines electric arc filing and nitriding, allows one to obtain a significant effect on non-structural properties, increased hardness, heat transfer and wear resistance of the part-coating system with a reduced degree of deformation of the part. An assessment was made of the possibility of moving the electric arc coatings from martensitic steels (40X13, 95X18), ferrite (Sv-08G2S) and austenitic (X18H10T, 12X18H10T) classes. further processing of nitriding.

**Keywords:** combined methods of applying wear-resistant coatings, electric arc spraying, chemical-thermal treatment, nitriding, wear and corrosion resistance, strengthening protective coatings

### Introduction

The use of coatings makes it possible to increase the wear and corrosion resistance of working surfaces of machine parts and mechanisms, in particular ship parts, and so to reduce the costs of alloyed steels and alloys [1].

The coatings application is associated with implementation of a fundamentally new approach, according to which the strength and carrying capacity of a part is provided by its basic material, whereas the resistance to corrosion, wear, and other factors may be increased *via* using hardening protective coatings. There are many alternative methods for producing coatings, from which it is advisable to choose an optimal, easy to implement, and inexpensive one [2]. Of the variety of methods for hardening coating deposition, the most common technologies used to restore and improve the performance properties of parts are gas-thermal spraying techniques [2], among which the cheapest and simplest method is electric arc spraying (EAS), whose current improvement is aimed at modifying and activating the spraying process [3]. A significant increase in the properties of EAS coatings is possible through combining arc spraying with ultrasonic [3], electric-spark [2], laser [10-14], electron-beam [2], and other processing techniques [2]. High wear resistance, hardness, and other surface properties of EAS coatings from iron based alloys can be provided by methods of chemical heat treatment [2]. The use of a combination of techniques for EAS and subsequent chemical heat treatment opens up great opportunities in creating composite coatings with special properties. Methods for improving the quality of electric arc coatings *via* subsequent heat treatment or modification are easily implemented in practice, in particular when part dimensions permit it. Such combined technologies do not require additional expensive equipment and operations, which predetermines a reduction in the cost of hardening processes.

Thus, an effective way to solve the problem of increasing the performance characteristics of EAS coatings from wire materials may be the formation of high strength surface layers through the use of various methods for chemical heat treatment. Combining coating with surface modification and treatment of produced coatings allows



the development of new combined methods for surface engineering. Among a large number of techniques for diffusional alloying of surface layers, nitriding methods are notable for high manufacturability, environmental safety, and economic efficiency [20]. Therefore, for the subsequent modification of EAS steel coatings, pulse ion nitriding (PIN) was chosen [15, 16].

**The aim of the work** was to develop a new combined method of surface engineering for the formation of hardening protective coatings on the basis of combination of EAS followed by treatment with PIN.

### Materials and procedures

For coating deposition, an apparatus for activated arc spraying ADN-10 was used. Coating materials were 0.8-2.8 mm diameter wire from steel of the martensitic (40Kh13, 95Kh18), ferritic (Sv-08G2S), and austenitic (Kh18N10T, 12Kh18N10T) grades. A feature of martensitic and austenitic steels is the ability to phase transformations and structural changes during deposition and treatment of coatings. This allows improvement of physic mechanical and performance properties of hardened surfaces and an increase in their wear and corrosion resistances. The PIN process lasted 2 h in the temperature range 600 - 800 K.

Microstructure was examined on etched and unetched thin sections using a light microscope «MeF-3» (Firm "Reichert", Austria) with magnifications  $\times 100$ ,  $\times 200$ , and  $\times 500$ . The microhardness was measured on a Micromet II microhardness meter with a load of 100 g from the coating surface edge to the base through the transition zone. A quantitative stereological analysis of coating porosity was carried out on a certified automatic image analyzer "Mini-Magiscan" (Firm "Joyce Loebel", England) using the program "Genias 26". The main stages of the image analysis were: image calibration, image fixation, segmentation, and porosity. The study was performed on a CamScan scanning electron microscope (Oxford Instruments, England) with an X-ray energy dispersive analyzer. The morphology (topography) of the coating surface was examined in the regime of reflected electrons at an accelerating voltage of 10–20 kV.

### Research results and discussion

As a result of the research, an assessment was made for possibility to improve the quality of EAS coatings by subsequent PIN. Data on microhardness are summarized in Table 1.

Table 1

**The effect of PIN temperature on the microhardness of EAS coatings**

Material of coating	Microhardness, GPa, at different temperatures of nitriding, K						
	600	620	650	670	700	720	770
Martensitic steel	8.6	11.3	12.9	14.0	15.9	12.7	11.3
Austenitic steel	5.6	6.2	8.0	8.9	11.1	12.0	11.8

The results of the study of structural parameters and phase composition of ion-modified coatings under various conditions are presented in Tables 2 and 3.

Table 2

**Structure parameters of EAS coatings from austenitic steels after PIN**

Conditions of PIN		Thickness of layer, $\mu\text{m}$	Phase composition
AEAS	N <sup>+</sup> 620 K	5-10	$\alpha$ -Fe, $\gamma$ -Fe, $\gamma$ N, Fe <sub>3</sub> O <sub>4</sub> , $\epsilon$ -(Fe,Cr) <sub>3</sub> N
	N <sup>+</sup> 670 K	10-15	$\alpha$ -Fe, Fe <sub>3</sub> O <sub>4</sub> , $\epsilon$ -(Fe,Cr) <sub>3</sub> N, $\gamma'$ -Fe <sub>4</sub> N
	N <sup>+</sup> 720 K	15-20	$\alpha$ -Fe, Fe <sub>3</sub> O <sub>4</sub> , $\epsilon$ -(Fe,Cr) <sub>3</sub> N, $\gamma'$ -Fe <sub>4</sub> N, CrN
	N <sup>+</sup> 770 K	25-30	$\alpha$ -Fe, Fe <sub>3</sub> O <sub>4</sub> , $\gamma'$ -Fe <sub>4</sub> N, CrN

Table 3

**Structure parameters of EAS coatings from austenitic steels after PIN**

Conditions of PIN		Thickness of layer, $\mu\text{m}$	Phase composition
AEAS	N <sup>+</sup> 620 K	3-5	$\alpha$ -Fe, $\gamma$ -Fe, Fe <sub>3</sub> O <sub>4</sub> , $\gamma$ N,
	N <sup>+</sup> 670 K	3-5	$\alpha$ -Fe, $\gamma$ -Fe, Fe <sub>3</sub> O <sub>4</sub> , $\gamma'$ N,
	N <sup>+</sup> 720 K	10-15	$\alpha$ -Fe, $\gamma$ -Fe, Fe <sub>3</sub> O <sub>4</sub> , $\gamma'$ N, $\gamma'$ -Fe <sub>4</sub> N, CrN
	N <sup>+</sup> 770 K	15	$\alpha$ -Fe, $\gamma$ -Fe, Fe <sub>3</sub> O <sub>4</sub> , $\gamma'$ -Fe <sub>4</sub> N, CrN

According to the data obtained, as the temperature of PIN increases, the modified layer depth increases as well (up to 50 μm). In addition, the microhardness of the layer significantly increases and, as the result of treatment at 670...720 K, reaches the level of maximum values (14.0...15.9 GPa). The main phases present in the nitrogen-modified layers on martensitic steel coatings are the nitrides ε - (Fe, Cr)<sub>3</sub>N and γ'-Fe<sub>4</sub>N. After ion treatment at 720 and 770 K, a sharp decrease in the high-nitrogen ε-nitride content and formation of CrN are recorded in nitrides layers, while the layer microhardness decreases to 11,3...12.7 GPa. For the layers formed by PIN on EAS coatings, a relatively high microhardness and a large depth of the dopant penetration are characteristic. In addition, a distinctive feature of nitride layers on the electric arc coating is the presence of particles of the α'' - (Fe, Cr)<sub>3</sub>N phase in them along with a reduced content of the γ'-Fe<sub>4</sub>N nitride phase and a relatively higher content of CrN.

The increased diffusion permeability of the coatings is caused by high concentration of defects (vacancies, dislocations, pores) contained in them, which were formed under the conditions of very rapid crystallization of molten drops in the course of EAS. At the same time, the presence of the thermodynamically stable chromium-doped Fe<sub>3</sub>O<sub>4</sub> oxide in the form of films, separating the sprayed particles, makes diffusion of nitrogen from the upper layer of particles to the underlying layers difficult. The greatest depth of PIN is achieved in EAS coatings with a reduced content of oxide films. PIN of EAS coatings from austenitic steel leads to the formation of modified layers, 3...5 to 15...25 μm thick (Table 3). Therefore, the coatings were formed by activated electric arc spraying (AEAS), providing a porosity of less than 7% (Fig. 1, b).

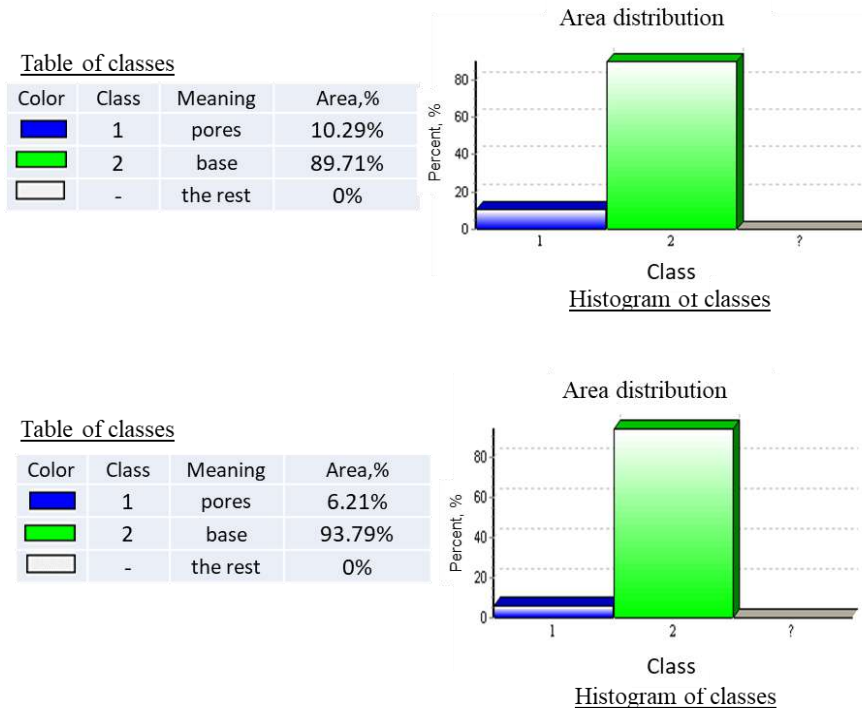


Fig. 1. Porosity distribution in coatings obtained by: (a) EAS and not recommended for treatment by PIN; (b) AEAS and recommended for treatment by PIN

The studies showed (Table 4) that at a layer density of more than 94%, this effect does not arise.

Table 4

**Results for topography of layer surfaces after PIN at 580 K**

Method of spraying	Material for spraying	Porosity of layer, %	Surface microtopography
EAS	Ferritic steels	≈ 10 ≥ 8	Bulging Bulging
Activated EAS		≈ 6 ≈ 5	smooth and unchanged smooth and unchanged
EAS	Martensitic steels	≈ 10 ≥ 8	Bulging Bulging
Activated EAS		≈ 6 ≈ 5	smooth and unchanged smooth and unchanged

The main reason for the relatively small depth of nitrogen saturation of electric arc coatings (15...30 μm) compared with that for cast steels is the presence of a large number of oxide films in the coating, which act as a barrier to the PIN process. Oxides are inevitably formed both during the flight of molten particles and in the course

of their crystallization on the surface of a part. For the same reason, it is almost impossible to strengthen coatings with porosity over 6% without formation of defective areas, since their pore walls are covered with a thin layer of iron oxides.

The formation of oxide films can be eliminated *via* spraying steel wires with the products of propane and air combustion, that is, *via* using AEAS. The consumption of propane and air combustion products during AEAS is 30–40 m<sup>3</sup>/h. In the course of the subsequent heating up to the nitriding temperature, which is in the range of 530–640 K (depending on the steel grade), the process of hardening and release of gaseous products to vacuum occur. It was established experimentally that the higher the nitriding temperature, the shorter the time interval between the temperature of PIN hardening and the start of surface saturation with nitrogen (Fig. 2). The samples after chemical heat treatment were cooled with the container to room temperature.

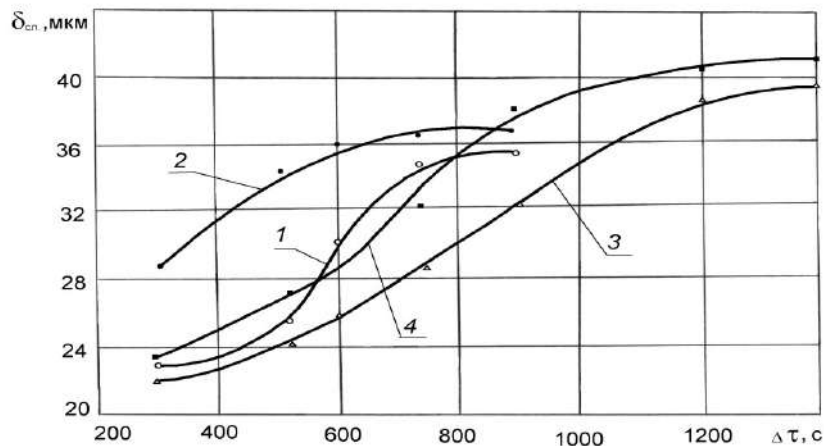


**Fig. 2. Dependence of the nitrided layer thickness on the time interval between heating up to PIN temperature and the start of surface saturation with nitrogen for coatings from martensitic steels (1,2) and austenitic steels (3,4) at: (1) 680 K; (2) 710 K; (3) 50 K; (4) 680 K**

As a result of tribological tests (pressure 0.64 MPa, dry friction) of coatings after various PIN modes, it was established that an increase in the PIN temperature for 40Kh13 steel coatings leads to a sharp increase in their wear resistance. The coatings treated with nitrogen ions at 670–770 K (Fig. 3) have the highest wear resistance. The wear rate of the counterbody (hardened steel 60G, HV = 78–80 GPa) slightly decreases during the EAS–PIN transition.

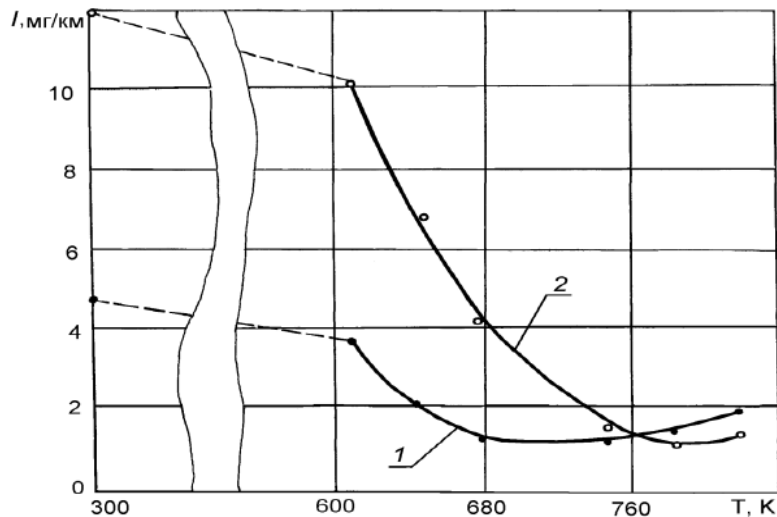


**Fig. 3. The effect of PIN temperature on the wear rate under dry friction for coatings from martensitic steel (1); austenitic steel. (2)**

Nitriding of Kh18N10T steel coatings at 500–520 K, which results in the formation of a modified 3–5 μm thick gradient layer, was not accompanied by increase in the wear resistance of steel surface under conditions of contact interaction without lubrication. At higher temperatures (670, 720 and 770 K), the wear resistance of coatings increases markedly. The increased wear resistance of EAS coating nitrided at 770 K is due to its significant depth and high microhardness.

It should be noted that a nitrogen-modified layer has an uneven thickness. The areas in the form of layers are detected in the coating depth and at the boundary with the substrate. The revealed morphology of modified interlayers in the depth of the deposited layers indicates a boundary mechanism of diffusion of interstitial atoms in the coatings. The results of metallographic analysis also indicate the preservation of oxide films in a modified

coating from steel 40Kh13. By changing the process temperature as well as the potential ratio of nitrogen, one can control the depth of diffusion layer and its hardness. It was established (Fig. 4 c, d) that after nitriding of electric arc coatings from steel 40Kh13, an anomalous structure is formed, which was not before observed in these systems. It is a composite type structure consisting of a steel matrix and solid nitrides, the appearance of which is due to intense diffusion along the boundaries of conglomerates of deformed wire particles. The microhardness of the diffusion layers on coatings is higher than that of the similar layers on cast steel 40Kh13 and reaches 10 GPa.

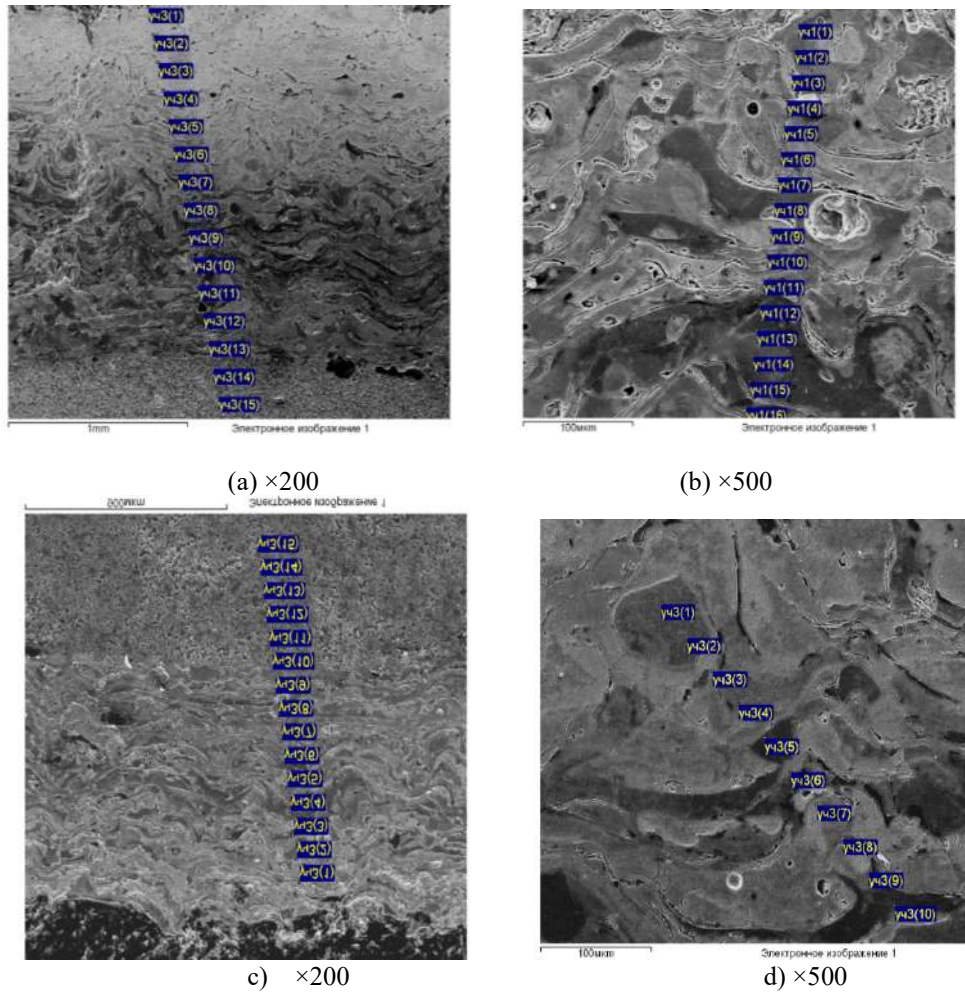
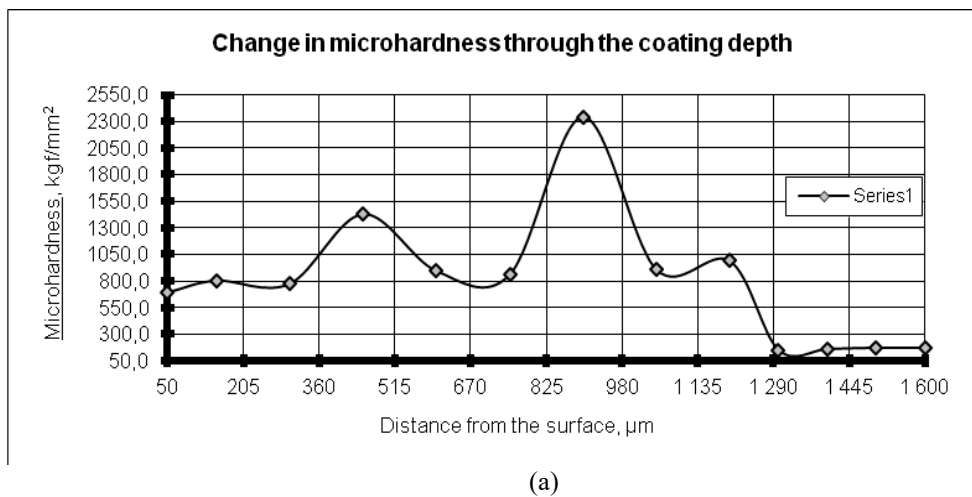
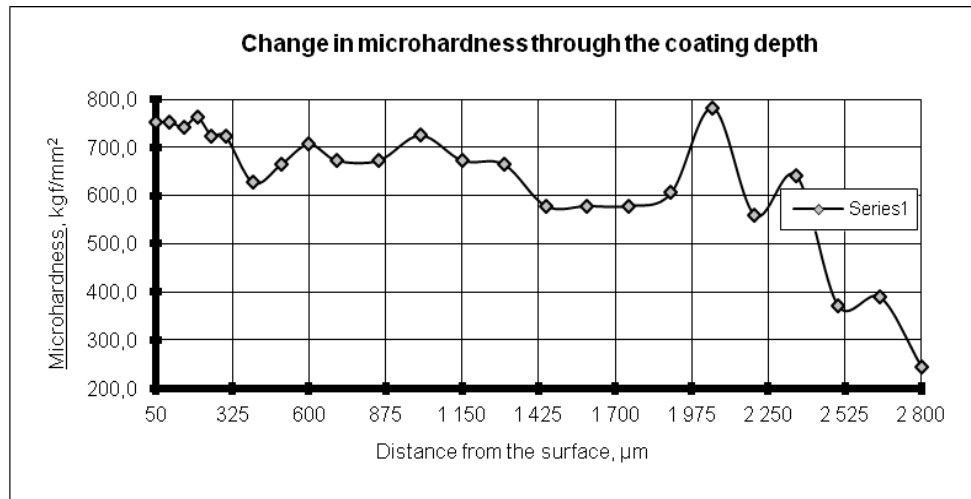


Fig. 4. Microstructure of sprayed coatings from the steels: (a, b) Sv-08G2S and (c, d) 40Kh13

The results of microhardness measurements of EAS coatings conducted on a microhardness tester “Micromet II” with a load of 100 g are presented in Fig. 5. Nitrogen saturation of the 40Kh13 steel coatings under the chosen conditions leads to the formation of a modified 150–200 μm thick surface layer (Fig. 4) with a microhardness of 6.5...7.0 MPa (Fig. 5).



(a)



(b)

Fig. 5. The microhardness distribution in EAS coatings from steel 40Kh13: the initial state; (b) after PIN treatment

The investigation for adhesion of EAS coatings showed that PIN can markedly increase the adhesion strength (Table 5). This increase is characteristic for coatings having porosity in the range of 5–14%; the further increase in porosity leads to decrease in adhesion.

The adhesion increase in the EAS coatings after PIN is due to the evolution of diffusion processes at the coating-substrate boundary, the recovery of oxides on the substrate surface, and the relaxation of internal stresses in the coating.

Table 5

The effect of porosity on the adhesion strength of EAS coatings (with no sublayer)

Material of coating	Adhesion strength, MPa, at different porosity, %					
	≤ 4	5–9	7–10	10–14	12–16	13–17
Sv-08G2S	38	49	61	53	40	36
40Kh13	37	43	55	47	43	35
40Kh13	41	55	67	63	50	39

The treatment of EAS coatings with PIN leads to a sharp increase in their wear resistance. Thus, the wear rate of coatings from steel 40Kh13 under dry friction decreases from 350 down to 19 μm/km. At the stage of steady friction, the wear rate of coatings after PIN treatment decreases to 5–6 μm/km. At the same time, the wear resistance of the modified layer from steel 40Kh13 is 1.6 times higher than that of cast steel 45 in the thermally hardened state (Fig. 6).

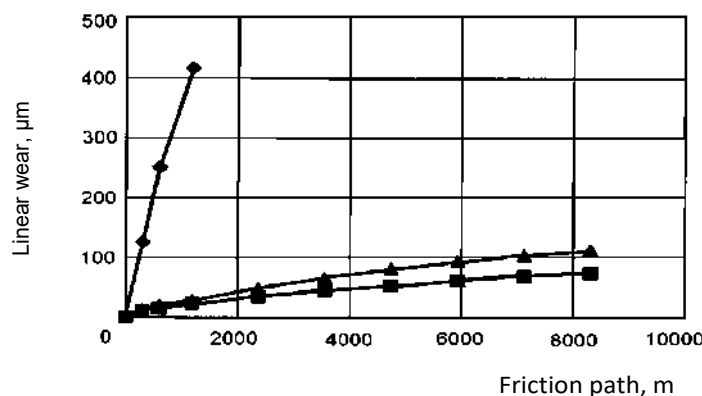
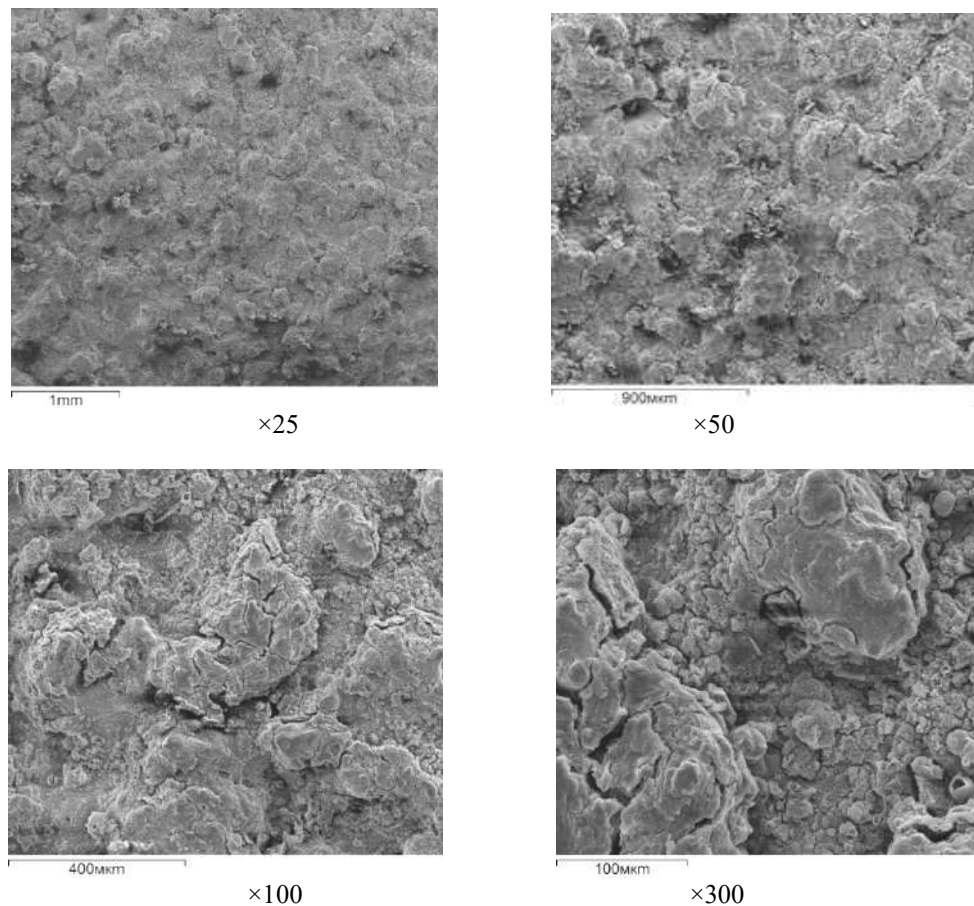


Fig. 6. Dependence of the linear wear on the dry friction path for coatings from steel Sv-08G2S: ■ coating Sv-08G2S + PIN; ▲ cast steel 45 (quenching and tempering); ♦ coating Sv-08G2S (initial state)

The findings of the surface topography examination for EAS coatings after PIN are presented in Fig. 7.



**Fig. 7. Surface topography of EAS coatings after PIN**

### Conclusions

This study was devoted to developing and testing techniques for formation of hardened protective coatings on the basis of combination of EAS with subsequent PIN.

The possibility to improve the quality of EAS coatings from steels of martensitic (40Kh13, 95Kh18), ferritic (Sv-08G2S), and austenitic (Kh18N10T, 12Kh18N10T) grades thanks to subsequent ion-nitriding treatment has been evaluated.

The phase composition and microhardness of coatings obtained *via* spraying wires from ferritic, austenitic, and martensitic steels have been investigated. As a result of experimental studies of the influence of modifying effects of PIN on the physicomechanical properties of EAS steel coatings. It was established that in order to increase the efficiency of the modification process, porosity of coatings should be not more than 7%, which allows the formation of surface layers with a microhardness of 6.5 - 15.0 GPa and a thickness of 20-50  $\mu\text{m}$ .

It was shown that the EAS method combined with subsequent PIN allows the formation of coatings with a surface layer with a hardness of 6.5 to 15.0 GPa and a thickness of 20 to 50  $\mu\text{m}$ .

The wear resistance of EAS coatings from 40Kh13 and Kh18N10T steels after PIN increases by eight times. The amount of oxides in the coatings does not change after PIN treatment and favorably affects the performance of the coatings under the conditions of dry friction in air.

Saturation with nitrogen of EAS coatings from wire steel 40Kh13 leads to the formation of a diffusion 40-50  $\mu\text{m}$  thick layer, the microhardness of which is 6.5 – 15 GPa. Herein the adhesion strength of the coatings increases by 1.6 times, and wear resistance does by 15–20 times.

It was shown that a duplex technology, combining EAS and PIN, allows one to obtain a significant effect concerning the bearing capacity, increase in hardness, adhesion strength, and wear resistance of the part-coating system along with reducing the probability of the part deformation. Discrete-pulse energy input at PIN increases the rates of heating and nitrogen diffusion by 2.5 times and shortens nitriding time by 2.6 times compared to the classical chemical heat treatment. The PIN process does not provide a uniform heating of the whole part, but only the surface layer of the required depth for hardening. PIN changes neither the shape and dimensions of the part, nor the roughness of its surface, so it can be used as a finishing treatment. The cyclical nature of the heating process makes it possible to reduce the power supply by 2.5 times.

## References

1. Ageev M.S., Lyashenko B.A. Application of hybrid technologies for renovation and resource increase of ship machinery and mechanisms. Bulletin of Brest State Technical University. Journ. "Machinostroyeniye", 4(94), 2015 – P. 18-22.
2. Coatings and their technology application // In the book "Strength of materials and structures", ed. V.T. Troshchenko - K.: Academperiodika, 2006. –P. 981-1074.
3. Sergeev V.V., Spiridonov Yu.L., Farakhshin I.I. Restoration of crankshafts of domestic and foreign diesel engines by arc metallization // Welding production. 2, 2004. P. 26-44.
10. Podchernyaeva I.A. Laser melting of gas thermal coatings based on cortinite // Technol. and management, 2, 1992. P. 42-43.
11. Antsiferov V.N., Shmakov A.M., Ivshina N.N. Laser treatment of plasma-sprayed powder steel coatings // Powder Metallurgy, 10, 1992. P. 25-28.
12. Liang G., Li C., Su J. et al. Microstructure of plasma coating on aluminum alloy after laser treatment // Chin. J. Nonferrous Metals - 1998-8, No. 1. –C.28-32.
15. Pokhmurska G.V., Dovgunik V.M., Student M.M. Wear resistance of laser-modified electric arc coatings from powdered wire FMI-2 // FKHM, 39, 4, 2003. P. 61 - 64.
13. Pokhmurska G.V., Dovgunik V.M., Student M.M. Wear resistance of laser-modified electric arc coatings from powdered wire FMI-2 // FKHM, 39, 4, 2003. P. 61 - 64.
14. Glebova MA, Kornev A. B., Glebov V.V. et al. Improving the quality of gas-thermal coatings by heat treatment with high-frequency currents and laser beams. Svaroch. Pr. № 6, 2004. P. 43 - 46.
15. Lyashenko B.A., Ageev M.S. On reducing volume and complexity of the finishing machining of hardening coatings. "Tool world". №1-4, 2015. P. 81-84.
16. Lyashenko B.A. Ageev M.S. Control of diffusion saturation of porous coatings under thermal cyclic ion nitriding. Proc. of 17th International conference "Surface Engineering and Product Renovation", Odesa, 2017. P. 111-114.

**Лопата О.В., Лопата В.М., Качинська І.Р., Солових А.Є.** Дослідження можливості підвищення якості електродугових покриттів шляхом обробки азотуванням

Ефективним способом вирішення завдань щодо зменшення витрат характеристик електродугових покриттів із дротяних матеріалів може виникнути утворення в них високоміцних поверхневих шарів за рахунок використання різних методів хіміко-термічної обробки. Були проведені дослідження з розробкою та апробуванням концепції формування зміцнювальних захисних покриттів на основі поєднання процесу електродного напилення з технологічною обробкою імпульсним іонним азотуванням. Показано, що дулексна (комбінована) технологія, що поєднує електродугове напилення та азотування, дозволить отримати значний ефект за несучою здатністю, підвищення твердості, міцності зчеплення та зносостійкості системи деталь-покриття при зниженні ймовірності деформації деталі. Була проведена оцінка можливості підвищення якості електродугових покриттів з мартенситного сталей (40X13, 95X18), феритного (Св-08Г2С) і аустенітного (X18H10T, 12X18H10T) класів шляхом подальшої обробки азотуванням.

**Ключові слова:** комбіновані методи нанесення зносостійких покриттів, хіміко-термічна обробка, електродугове напилення, азотування, зносо- та корозійну стійкість, зміцнюючі захисні покриття



## Optimization of discrete structure of electrospark coatings

V. Antonyuk<sup>10000-0003-0690-2411</sup>, L. Lopata<sup>\*20000-0002-2053-9252</sup>

<sup>1</sup>National Technical University of Ukraine "Igor Sikorsky, Polytechnic Institute", Kyiv, Ukraine

<sup>2</sup>G. S. Pisarenko Institute for Problems of Strength of National Academy of Sciences of Ukraine

\*E-mail: [beryuza@ukr.net](mailto:beryuza@ukr.net)

Received: 10 May 2025; Revised 29 May 2025; Accept: 14 June 2025

### Abstract

The presented article considers the disadvantages of chromium coatings and shows the possibility of their elimination by obtaining coatings of discrete structure. The principle of coatings of discrete structure allows to organically combine physical processes underlying pulse hardening methods with a discrete structure determining their service properties. It is shown and substantiated that the method of electric spark alloying is the most suitable for applying discrete coatings, since this process is discrete by its nature. The advantage of discrete coatings is the absence of a softening effect when a brittle crack passes from the coating to the base metal due to excessively high adhesive strength. High cohesive and adhesive resistance of individual discrete sections of the coating is achieved by limiting normal stresses in the coating and tangential stresses in the plane of adhesive contact with the base by changing the size and shape of an individual section. This article is devoted to determining the optimal parameters of a discrete structure. The required coating design is determined by a calculation method based on a model that describes the stress-strain state of the coating.

**Keywords:** chromium plating, spark alloying, discrete coating, stress-strain state, cohesive and adhesive strength, thermomechanical resistance, coating continuity, wear

### Introduction

In increasing the durability of special equipment parts, priority is given to hardening coatings on the inner surface of the parts. However, most coatings are destroyed during operation, which is associated with insufficient adhesive and cohesive strength, the occurrence and development of a network of cracks and the weakening of the coating during operation. Argon-arc surface hardening is considered as an alternative to coatings for hardening the inner surface of special equipment parts [1]. In research and industrial practice, chromium coatings applied by the electrolytic method are most common for increasing the durability of special equipment parts. However, with sufficient erosion-corrosion resistance of the Cr coating, it is not possible to eliminate cracking and peeling [2]. Most studies are devoted to improving the application technology and eliminating the disadvantages of Cr coatings.

### The aim of the work

Increasing the durability and bearing capacity of coatings by using a discrete structure.

### Research results and discussion

The main disadvantages of chromium coatings include brittleness at temperatures  $T < (0,1 \dots 0,2)T_{\text{m}}$  and extreme sensitivity to interstitial impurities both during its application and during operation. As a consequence, there is low resistance to mechanical and thermal shocks.

One of the disadvantages of electrolytic coatings is hydrogenation of the surface layer of the part. This leads to the phenomenon of hydrogen embrittlement and hydrogen corrosion. As a consequence, there is a decrease in the strength and ductility of the part. Thus, the fatigue limit of steels can decrease by 50% [3].



Therefore, along with the problems associated with the development and use of galvanic coatings, there is a need to assess the effect of coatings on reducing the strength and ductility of the base material. It is noted [4] that the most sensitive characteristic is the relative narrowing  $\psi$ . Electrolytic Cr coating leads to a decrease in  $\psi$  by 1.4 times. Heat treatment at 200°C promotes a slight increase in  $\psi$  from 33 to 39% (for the original sample without coating  $\psi = 45\%$ ). This is explained by the removal of hydrogen from the coating during heat treatment.

Technological difficulties in chroming are associated with the impossibility of maintaining a ratio between the anode and cathode areas, in which the former would exceed the latter, as well as the unequal resistance of the electrolyte along the length of the barrel inside the channel [5].

Another important circumstance in chroming the barrel bore is the need to ensure a uniform coating thickness along the entire length of the barrel. For rifled barrels, it is difficult to achieve a uniform Cr coating and high adhesive strength in the area of the mating of the lands and rifling. To eliminate these shortcomings, a number of technological methods are used to improve the dissipation capacity of the electrolyte, including current "push". To ensure a high-quality Cr coating, it is necessary to strictly control the composition of the electrolyte, its temperature and current density. A temperature deviation of 2...3°C leads to a significant change in the properties of Cr deposits. The presence of chemically active products in the gas environment, in particular nitrogen and its compounds, leads to the formation of brittle compounds. This leads to cracking and peeling of coatings under the influence of thermomechanical loads. Therefore, one of the ways to increase the durability and stability of chromium coatings is to alloy them with elements such as V, Nb, Mo, Ni and other elements.

The most effective materials for protection against thermomechanical wear are Ni and W. Alloying with Ni (0.1...0.3%) leads to an increase in the plasticity of the coatings, to a decrease in carbon deposits and a network of cracks during operation [6]. Alloying of Cr coatings is carried out by introducing alloying additives into the electrolyte. Thus, electrodeposition of Cr-Ni alloy is carried out from a diluted chromium plating electrolyte containing additives of nickel salts. However, simultaneous electrodeposition of Cr with other metals in practice is associated with great technological difficulties. Continuous monitoring and stabilization of the electrolysis process in terms of current, concentration and temperature of the electrolyte and other parameters are necessary [5,7]. In the search for ways to improve the properties of electrolytic Cr coating, a trend has emerged for multi-stage application: the use of additional electrospark alloying (ESA) treatment after electrodeposition.

The use of the ESA method without a continuous corrosion-resistant sublayer does not provide positive results [8]. Therefore, in the works [7, 9], the ESA method was used on pre-electrodeposited high-density Cr and NiCr alloys that protect the steel base from high-temperature gas corrosion.

### Research results and discussion

The ESA method is used to apply wear-resistant materials: hard alloys, W + Co, Ni-W-Co, etc. [7, 9]. The ESA method is most suitable for the task of strengthening the internal surfaces of special equipment parts.

The ESA method uses serial industrial equipment.

ESA treatment increased the wear resistance and durability of special equipment parts by 2 times according to the results of operational tests in comparison with standard chrome plating [9].

The mechanism of destruction of the Cr coating and the electric spark coating during operation is associated with the formation and development of a network of regular cracks, their merging and subsequent chipping of sections of the coatings [7]. This circumstance was the basis for the creation of the principle of discrete coatings with increased thermomechanical resistance [10, 11]. The discrete coating consists of individual sections, the dimensions of which are similar to the network of regular cracks in a continuous coating. The formation of a network of regular cracks occurs as a phenomenon of self-regulation and a decrease in the level of the stress-strain state of the coating. The discrete structure of the coating (applied from the same material as the continuous coating with equal thicknesses) allows for a multiple increase in the load-bearing capacity of the coated part, especially in the area of high loads and deformations of the base material [11]. High cohesive and adhesive resistance of individual discrete sections of the coating is achieved by limiting normal stresses in the coating and tangential stresses in the plane of adhesive contact with the base by changing the size and shape of an individual section.

The ESA method is the most suitable for applying discrete coatings, since ESA is discrete by nature. A single electric discharge ensures stability of the dimensions and properties of an individual discrete section of the coating. By changing the pulse frequency or the speed of relative movement of the electrode and the part, it is possible to regulate the number of discrete sections on the working surface of the part, as well as the continuity of the coating. The discrete structure of the coating allows (unlike the traditional continuous coating) to successfully apply surface plastic deformation (SPD). The use of SPD for continuous coatings is impossible due to their cracking and peeling. Discrete coatings can combine ESA and SPD in one technological cycle. In this case, SPD is the final dimensional processing and ensures the required surface purity of the discrete coating. Continuous coatings applied by the ELA method require final mechanical processing due to their high roughness.

When applying a discrete coating in one pass of the electrode, the productivity of the ESA method increases many times. The advantage of discrete coatings also lies in the absence of a softening effect when a brittle crack passes from the coating to the base metal due to excessively high adhesive strength. In [12], a criterion relationship for adhesive strength and the need to optimize it under the condition of crack transition from the coating to the base were established. The negative role of excessively high adhesive strength is confirmed by such a wear

mechanism during operation as the detachment of Cr coating particles with the tearing out of metal from deep layers [8]. This article is devoted to determining the optimal parameters of a discrete structure. The required coating design can be determined by a calculation method based on a model that describes the stress-strain state of a continuous coating [13]. We select the size of the discrete section based on the regular step of the crack that occurs due to cohesive cracking of the coating.

The criterion for selecting the parameters of the discrete structure is the minimum stress level during operation, on which the wear resistance of the part surface depends. Total effective stress value in the coating:

$$\sigma_c^{ef} = \sigma_c^{op} + \sigma_c^r \quad (1)$$

where:  $\sigma_c^{op} = \sigma_c^m + \sigma_c^t$  - operational stresses in the coating;

$\sigma_c^m$  - stress in the coating from mechanical load;

$\sigma_c^t$  - stress in the coating under the influence of temperature gradient;

$\sigma_c^r$  - residual (technological) stresses in the coating.

The stresses in the coating from the mechanical load are determined from the dependence [13]:

$$\sigma_c^m = \frac{1}{h_c} \cdot \frac{\varepsilon_{crit}}{\left( \frac{1}{E_c h_c} + \frac{1}{E_b H_b} \right)} \cdot \left[ 1 - \frac{ch(ky)}{ch(kl)} \right] \quad (2)$$

where:  $\varepsilon_{crit}$  - critical deformation of the base, above which cohesive cracking of the coating begins;

$H_b, h_c$  - thickness of the base and coating respectively;

$E_b, E_c$  - elastic moduli of the base and coating;  $l$  - base size;

$k$  - a coefficient that depends on the ratio of the elastic properties of the base and the coating:

$$k^2 = 2 \frac{G_b G_c}{G_b h_c + G_c H_b} \left( \frac{1}{E_c h_c} + \frac{1}{E_b H_b} \right) \quad (3)$$

where:  $G_b, G_c$  - shear moduli of the coating and base.

The nature of the stress distribution in a discrete section of the coating with a length of  $2l$  is shown in Fig. 1.

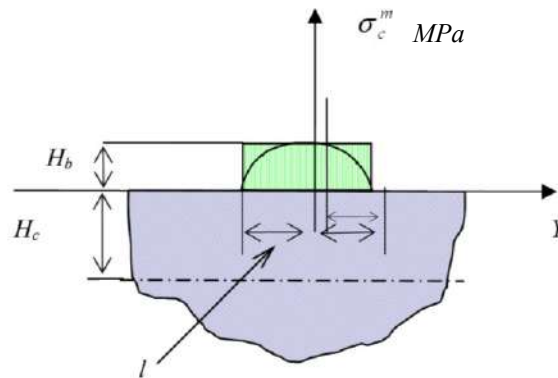


**Fig. 1. Distribution of stresses  $\sigma_c^m$  along the length of the coating**

The stress  $\sigma_c^m$  under the action of a temperature gradient in different variants of Cr coating for shooting conditions are given in [14]. Residual stresses in the coating  $\sigma_c^r$  were determined by the radius of curvature of a flat sample after coating application. Using the method for calculating thin plates for bending, we determine  $\sigma_c^r$ :

$$\sigma_c^r = \frac{4E_b H_b^3}{6(1 - \mu^2)(H_b + h_c)Rh_c} \quad (4)$$

where:  $\mu$  - base material coefficient;  $R$  - radius of curvature of the sample.

In a linear stress state and  $h_c \ll H_b$ , dependence (4) turns into the well-known Stoney formula [15]:

$$\sigma_c^r = \frac{E_b H_b^2}{6Rhc} \tag{5}$$

Since we assume that the cohesive strength of the coating  $\sigma_c^{coh} = \varepsilon_{crit} E_c$  is distributed according to the normal law with a standard deviation of  $0.1 \sigma_c^{coh}$ , then the crack is most likely to occur in the section  $y = 0$  (Fig. 1) at  $\sigma_c^{ef} = 0.9 \sigma_c^{coh}$ .

Then the distance between cracks  $C_c$  will be determined:

$$C_c = \frac{1}{k} \ln \left( 0,1 + \frac{h_c \cdot (\sigma_c^t + \sigma_c^r)}{\varepsilon_{kp}} \cdot \left( \frac{1}{E_c h_c} + \frac{1}{E_b H_b} \right) \right) \tag{6}$$

The values of residual stresses  $\sigma_c^r$  during the coating application varied in the range of 350...500 MPa. Temperature stresses  $\sigma_c^m$  varied in the range of 140...180 MPa. The dependences of the discrete section size on the coating thickness for different values of  $\varepsilon_{kp}$ ,  $\sigma_c^r$  and  $\sigma_c^m$  are shown in Fig. 2 and Fig. 3.

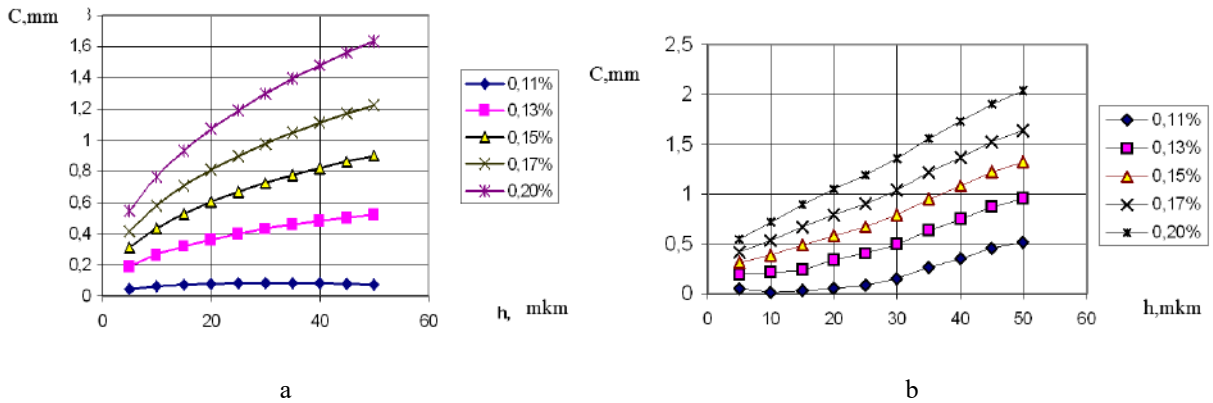


Fig. 2. Dependence of the size of the discrete section  $C_c$  on the coating thickness  $h_c$  for  $\varepsilon_{crit} = 0,11 \dots 0,20\%$ ;

a)  $\sigma_c^r = 500$  MPa;  $\sigma_c^m = 160$  MPa; b)  $\sigma_c^r = 400$  MPa;  $\sigma_c^m = 160$  MPa.

The surfaces of the dependence of the size of the discrete section  $C_c$  on the coating thickness  $h_c$  and the critical deformation of the base  $\varepsilon_{crit}$  are shown in Fig. 4.

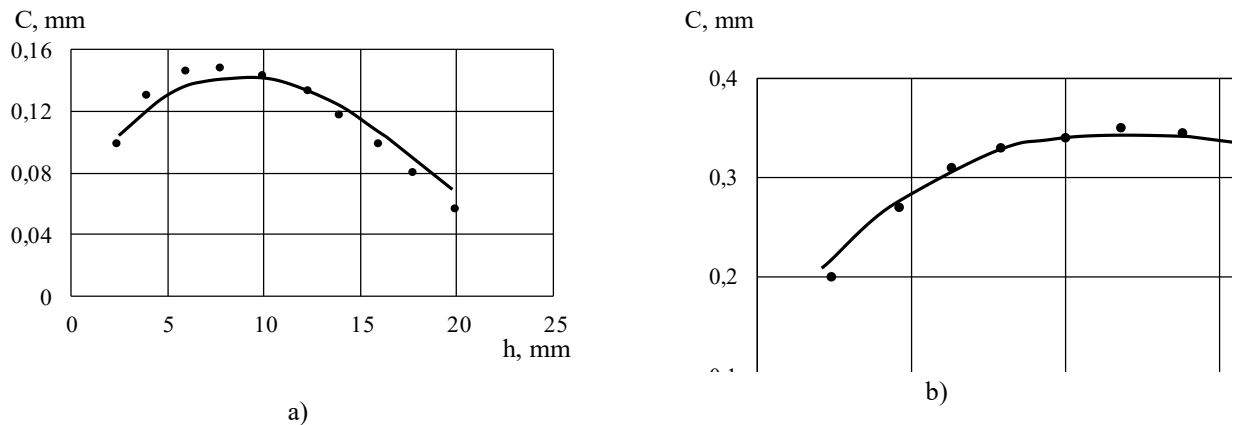
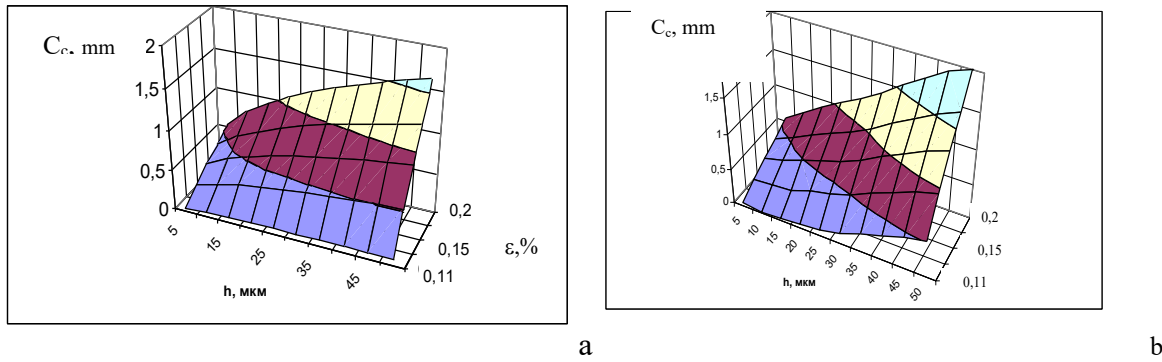


Fig. 3 Dependence of the size of the discrete section  $C_n$  on the coating thickness  $h_c$  at  $\sigma_c^r = 350$  MPa;  $\sigma_n^m = 180$

MPa: a)  $\varepsilon_{crit} = 0.11\%$  b)  $\varepsilon_{crit} = 0.13\%$



**Fig.4** Dependence of the size of the discrete section of the section  $C_c$  on the coating thickness  $h_c$  and the critical deformation of the base  $\epsilon_{crit}$ : a)  $\sigma_c^r = 500$  MPa; b)  $\sigma_c^r = 400$  MPa

An experimental test of the optimal size of the discrete section  $C_c$  of the discrete coating was carried out under sliding friction. The dependence of the weight wear on the continuity of the discrete coating  $\psi$  is shown in Fig. 5. A steel sample served as a counterbody.

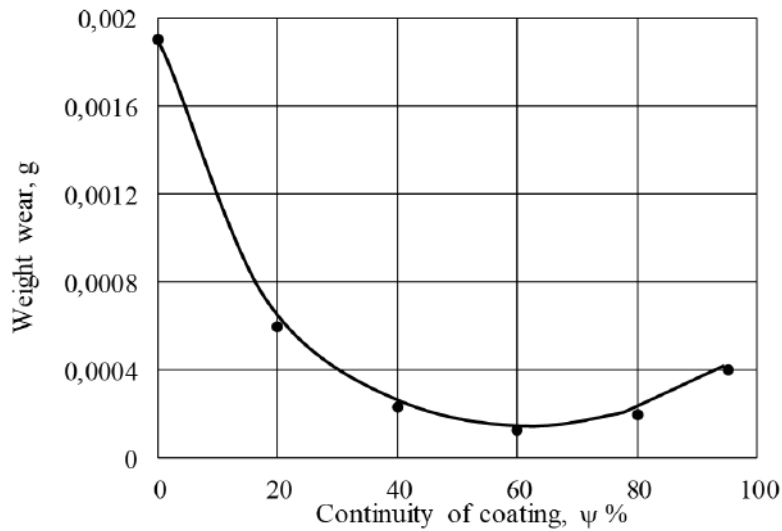


**Fig. 5.** Dependence of weight wear on the continuity of the coating  $\psi$

Minimum wear occurs at  $\psi = 60\%$ , which corresponds to the coating area in the form of discrete circular sections with a diameter size equal to  $C_c$ .

A change in the continuity  $\psi$  of the discrete coating changes the wear mechanism. At  $\psi < 40\%$ , the adhesive wear mechanism is observed. In the range  $\psi = 50 \dots 70\%$ , the most preferable type of wear occurs - abrasive. At  $\psi > 70\%$ , wear by peeling and chipping of coating particles is observed. This is confirmed by studying the profilograms of the friction surfaces (Fig. 6).

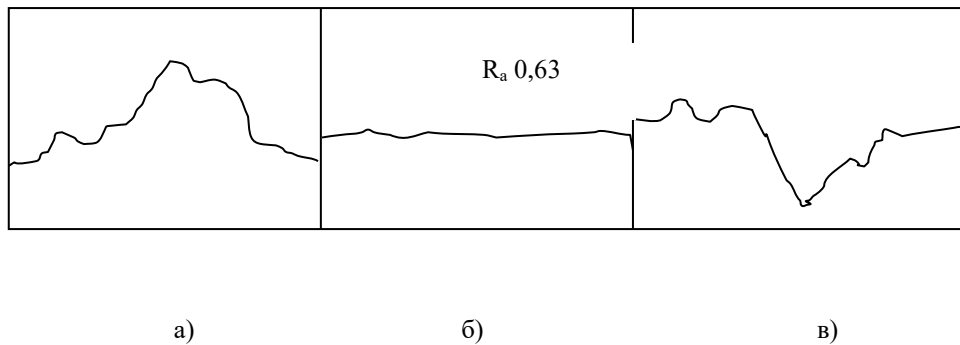


**Fig. 6.** Friction surface profile of a discrete coating: a)  $\psi < 40\%$ ; б)  $\psi = 50 \dots 70\%$ ; B)  $\psi > 70\%$

## Conclusions

The technological processes of ESA are based on the concept of obtaining continuous layers, which is achieved by multiple passes of the electrode along the surface being hardened. This leads to a decrease in the productivity of the hardening process, to a decrease in a number of physical and mechanical properties of the alloyed layer, and in some cases even leads to its destruction.

The principle of discrete structure coatings made it possible to organically combine the physical processes underlying pulsed hardening methods with a discrete structure that determines their service properties.

## References

1. Bondarenko L.I., Puzrin L.G. Argono-dugovaya poverhnostnaya zakalka kak sredstvo uprochneniya artillerijskih stvolov. Artillerijskoe i strelkovoje vooruzhenie: Sb. st., vyp.2 Kiev, GNTC ASV, 2000. S.105-107.
2. Schlett V., Stuke H., Weiss H. Morphology and erosive wear of Fe-Cr-coatings for gun bores deposited by physical vapor deposition. Vac. Sci and Tehnol. 1986, A4, №6. P. 3032-3037.
3. Novikov N.V., Bidnyj A.A., Lyashenko B.A. i dr. Metody uprochneniya poverhnostej mashinostroitelnyh detalej. Kiev, ISM AN USSR. 1989. 112 s.
4. Aleksandrovskij A.N., Yakovenko P.M. Vliyanie galvanicheskikh hromovyh i hromnikelevykh pokrytij na prochnost obrazcov iz stali 38HN3MFA. Artillerijskoe i strelkovoje vooruzhenie: Sb. st. Kiev, GNTC ASV, 1999. S.145-147.
5. Komnackij A.L., Gladkij E.D., Roik T.A. Nekotorye mehanicheskie osobennosti processa hromirovaniya poverhnosti kanala stvola kalibra 30 mm. Artillerijskoe i strelkovoje vooruzhenie: Sb. st. Vyp.6. Kiev, GNTC ASV, 2002 S. 31-34.
6. Aleksandrovskij A.N., Melnik V.P., Dudnik M.I. Sluzhebnye svojstva legirovannyh elektroliticheskikh hromovyh pokrytij. Artillerijskoe i strelkovoje vooruzhenie: Sb. st. Kiev: GNTC ASV, 1999. S. 153-156.
7. Lapshin S.P., Provolockij A.E., Dudnik M.I. i dr. Issledovanie elektroerozionnogo uprochneniya vnutrennih poverhnostej trub specialnogo naznacheniya. Sb. trudov 1-j Mezhdunar. konf. «Artillerijskie stvolnye sistemy, boepripasy, sredstva art. razvedki i upravleniya ognem». Kiev, GNTC ASV. 1997. S. 260-271.
8. Provolockij A.E., Lapshin S.P., Melnik V.P. Ob elektroiskrovom uprochnenii Stvolov. Artillerijskoe i strelkovoje vooruzhenie: Sb. st. Kiev, GNTC ASV. 1999. S. 172-175.
9. Lyashenko B.A., Kuzema Yu.A., Digam M.S. Uprochnenie poverhnosti metallov pokrytiami diskretnoj struktury s povyshennoj adgezionnoj i kogezionnoj stojkostyu. Kiev, IPP AN USSR. 1984. 57 s.
10. Lyashenko B.A., Movshovich A.Ya., Dolmatov A.I. Uprochnyayushie pokrytayah diskretnoj struktury. Tehnologicheskie sistemy. 2001. № 4 (10). S. 17-25.
11. Lyashenko B.A., Cygulev O.V., Kuznecov P.B. Neobhodimo li vseгда povyshat adgezionnyuyu prochnost zashitnyh pokrytij. Problemy prochnosti. 1987. № 5. S. 70-74.
12. Umanskij E.S., Lyashenko B.A. Usloviya adgezionnoj i kogezionnoj ravnoprochnosti zharostojkikh pokrytij, Kosmicheskikh issledovaniy na Ukraine. 1975. Vyp.6. S. 58-64.
13. Lyashenko B.A., Alekseyuk M.M., Kuzovkov E.G. Povyshenie dolgovechnosti detalej mashin putem racionalnogo konstruirovaniya zashitnyh pokrytij. Sb. trudov 1-j Mezhdunar. konf. «Artillerijskie stvolnye sistemy, boepripasy, sredstva art. razvedki i upravleniya ognem». Kiev, GNTC ASV, 1997. S. 118-132.
14. Lyashenko B.A., Rutkovskij A.V., Soroka E.B., Lipinskaya N.V. O snizhenii ostatocnyh napryazhenij v vakuum-plazmennyyh pokrytayah. Probl. prochnosti. 2001. №4. S.62-67.

**Англошук В.С., Лопата Л.А. Оптимізація дискретної структури електроіскрових покриттів**

У наведеній статті розглянуто недоліки хромових покриттів та показано можливість їх усунення шляхом отримання покриттів дискретної структури. Принцип покриттів дискретної структури дозволяє органічно поєднати фізичні процеси, що лежать в основі імпульсних методів зміцнення, з дискретною структурою, що визначає їх службові властивості. Показано та обґрунтовано, що метод електроіскрового легування є найбільш підходящим для нанесення дискретних покриттів, бо цей процес є дискретним за своєю природою. Перевага дискретних покриттів полягає у відсутності розміцнювального ефекту при переході крихкої тріщини з покриття в основний метал за рахунок надмірно високої міцності адгезійної. Висока когезійна та адгезійна стійкість окремих дискретних ділянок покриття досягається шляхом обмеження нормальних напруг у покритті та дотичних у площині адгезійного контакту з основою за рахунок зміни розмірів та форми окремої ділянки. Ця стаття присвячена визначенню оптимальних параметрів дискретної структури. Необхідна конструкція покриття визначається розрахунковим методом на основі моделі, що описує напружено деформований стан покриття.

**Ключові слова:** хромирование, электроискровое легирование, дискретное покрытие, напряженно-деформированное состояние, когезионная и адгезионная прочность, термомеханическая стойкость, сплошность покрытия, износ



## The influence of hydrogen saturation on the wear mechanism of steel

V.V. Shchepetov<sup>10000-0003-1644-6042</sup>, S.S. Bys<sup>20000-0002-7518-3310</sup>, M.R. Byalik<sup>20009-0009-6987-341X</sup>,  
V.Yu. Medvedchuk<sup>20009-0005-9661-3251</sup>, Ya.S. Bys<sup>20009-0007-0143-1303</sup>

<sup>1</sup> Institute of Technical Thermophysics of the National Academy of Sciences of Ukraine, Kyiv

<sup>2</sup> Khmelnytskyi National University, Khmelnytskyi

\*E-mail : [serhiibys@gmail.com](mailto:serhiibys@gmail.com)

Received: 10 May 2025; Revised 30 May 2025; Accept: 15 June 2025

### Abstract

The tribological characteristics of hydrogenated steel 60C2 with different structural states were compared with the obtained results of studies of friction surfaces by physicochemical methods, which allowed us to draw a conclusion about the relationship between friction and wear indicators with the processes occurring on the surface of the material during friction, and the significant influence of hydrogen present in the contact zone on them. It was proven that during friction on the contact surface of hydrogenated steel 60C2, regardless of its structural state, the process of formation of secondary structures occurs, which determine the process of friction and wear of the material. Reduction of the wear intensity of steel 60C2 with a tempered martensite structure (300°C) is accompanied by the formation of secondary structures on the surface, which have a higher resistance and shield the base material from direct contact and destruction. In addition, the saturation of the material with hydrogen changes the nature and mechanism of formation of secondary structures, which in turn leads to a change in the mechanism of friction and wear of the material.

**Keywords:** friction, wear, hydrogen, surface structures.

### Introduction

Under friction, in almost any conditions, thanks to tribochemical processes in the contact zone, hydrogen is released due to the decomposition of hydrocarbons in lubricants, fuel, plastics, wood and other environments, as well as the diffusion of hydrogen present in the steel under the influence of various processes in the surface layer zone [1]. In this case, under the influence of hydrogen, not only mechanical but also tribological characteristics of materials change significantly [1-4]. There is some information in the literature on the effect of hydrogen on the properties of materials, but they are advisory in nature and do not allow for a full characterization of its effect on a specific material. In view of the fact that parts made of 60C2 steel are used in friction pairs under conditions that do not exclude hydrogenation of the material, it became necessary to conduct studies on friction and wear taking into account the effect of hydrogenation, to analyze the change in the physicochemical situation in the contact zone under the influence of hydrogen.

**The purpose of the work** is was the study of the mechanisms of wear of materials, using the example of steel 65G, when they are hydrogenated. As well as the processes occurring on surfaces during their friction under hydrogenation conditions.

### Materials and research methods

For the research, steel 60C2 was selected, used in industry (sealing and spring rings, in the manufacture of wire tools, springs for automobiles and rolling stock, etc.).

Various structural states of steel were achieved by quenching from 870°C and their subsequent tempering at different temperatures (200, 300, 400 and 500°C) for two hours.



Tribological studies of metals under dry sliding friction conditions were carried out on a universal friction machine model 2168. Tests were carried out using the disk-finger friction scheme on standard samples.

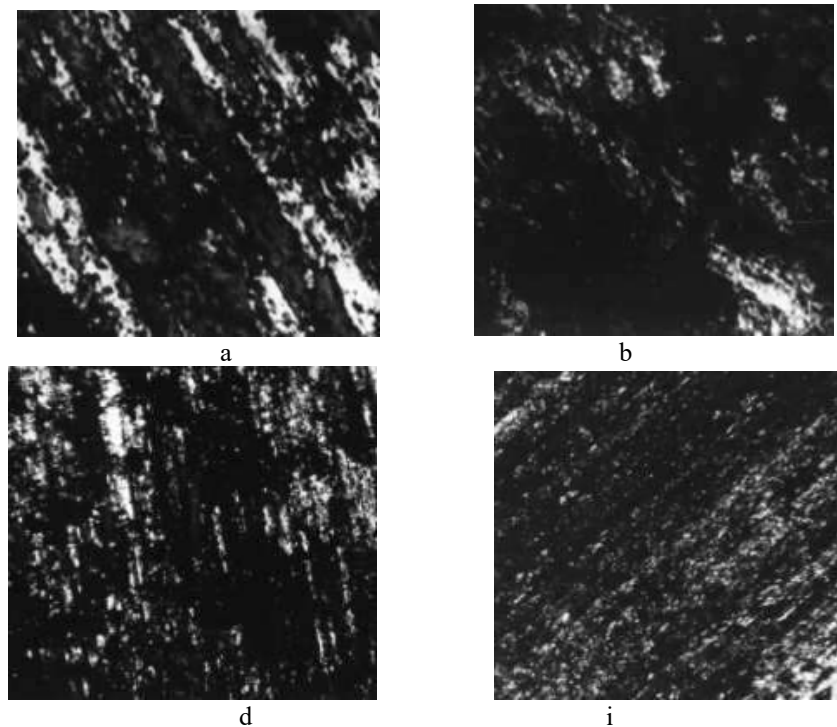


**Fig. 1. Friction surfaces of 60C2 steel with different structural states, studied in air at constant pressure (10 MPa): a - tempering structure 200°C (0.2 m/s); b - 300°C (0.2 m/s); d - 400°C (0.2 m/s); i - 500°C (0.4 m/s) (×152)**

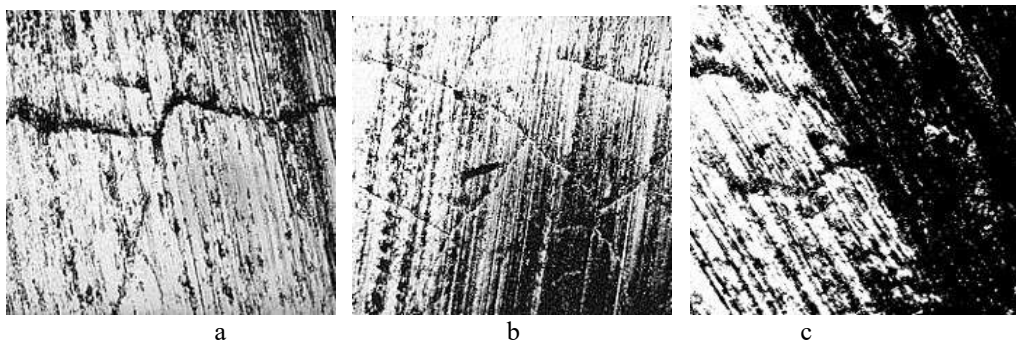
To study the effect of hydrogen on the characteristics of 60C2 steel with different structural states, samples were saturated with hydrogen using the cathodic polarization method in a 10% H<sub>2</sub>SO<sub>4</sub> solution for 1 hour.

With the development of regularities, a complex of modern physico-chemical methods of structural-phase analysis, which is important for the examination of surface balls, is lost and worn out. In this case, the comprehensive research methodology included metallography; scanning electron microscopy (scanning electron microscope JSM-840); X-ray structural phase analyzer (DRON-UM1 diffractometer).

### Research results and their discussion

The laws of transformation of mechanical energy into internal energy during friction are determined by loading conditions, the structure of materials and the action of the environment. At this stage of the work, the goal was achieved - determining the effect of hydrogen on the structure, phase composition of the surface layer of contact pairs, the degree of plastic deformation. This will allow a qualitative assessment of the results of tribological tests.

The performed macroscopic studies of the surface allow us to draw a conclusion about the qualitative and quantitative difference of the films formed on the friction surfaces of 60C2 steel tested in air (fig. 1) and after hydrogenation (fig. 2), depending on the test conditions. The friction surfaces of the samples tested after hydrogenation are covered with a network of microcracks (fig. 2 a, c, d), whereas they are absent when tested in air (fig. 1). Micro cracks formed on the surface films and in the near-surface layer of the material, which indicates embrittlement of the material surface under the influence of hydrogen.



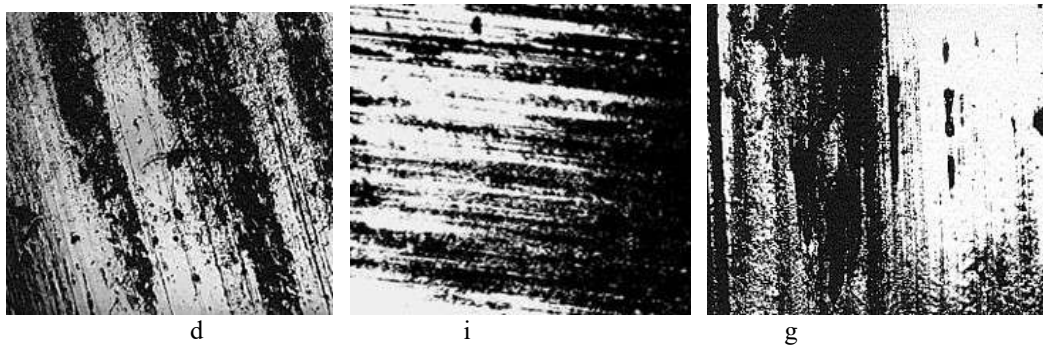


**Fig. 2.** Friction surfaces of 60C2 steel with different structural states,  $P=10$  MPa, saturated with hydrogen at different current densities: a - tempering structure 300°C (0.4 m/s, 1 A/dm<sup>2</sup>); b - 400°C (0.2 m/s, 1 A/dm<sup>2</sup>); in - 500°C (0.4 m/s, 1 A/dm<sup>2</sup>); g - 300°C (0.2 m/s, 4 A/dm<sup>2</sup>); d - 400°C (0.2 m/s, 4 A/dm<sup>2</sup>); f - 500°C (0.4 m/s, 4 A/dm<sup>2</sup>) ( $\times 152$ )

Comparing the results obtained in the study of the wear intensity of 60C2 steel in different structural states with the corresponding friction surfaces, a certain pattern can be seen between them - an increase in the number of cracks on the friction surfaces is accompanied by an increase in the wear intensity of the material and vice versa - a decrease in the number of cracks on the friction surfaces is associated with a decrease in the wear intensity of the material.

During friction, the surface is deformed due to tangential stresses, the relaxation of which, when tested in air, occurs due to an increase in plastic deformation of the contact points. In our opinion, hydrogen present in the contact zone activates the processes of self-organization of the surface and promotes the formation of fairly brittle films, which, under the action of the touch. The stresses are destroyed, forming a network of microcracks, and intensifies the wear process.

On friction surfaces of steel 60C2 with a higher tempering structure (400°C and above) (fig. 2 c-e), saturated with hydrogen, a less intense formation of cracks was noted, which can be explained by an increase in the plasticity of the material and completely different conditions for the formation of microfilms, and with an increase in the friction speed and pressing force (fig. 2 g, e), surface cracks were not detected.

To explain the processes occurring during friction and wear of hydrogenated steel 60C2 with different structural states, a study of the chemical composition of friction surfaces and secondary structures was conducted.

In fig.3 shows the nature of the distribution of elements on the friction surface of hydrogenated steel 60C2, with a tempering structure of 300°C, for different speeds of sliding friction. From which it follows that the chemical composition of the friction surface depends on the structural state and changes under the influence of hydrogen.

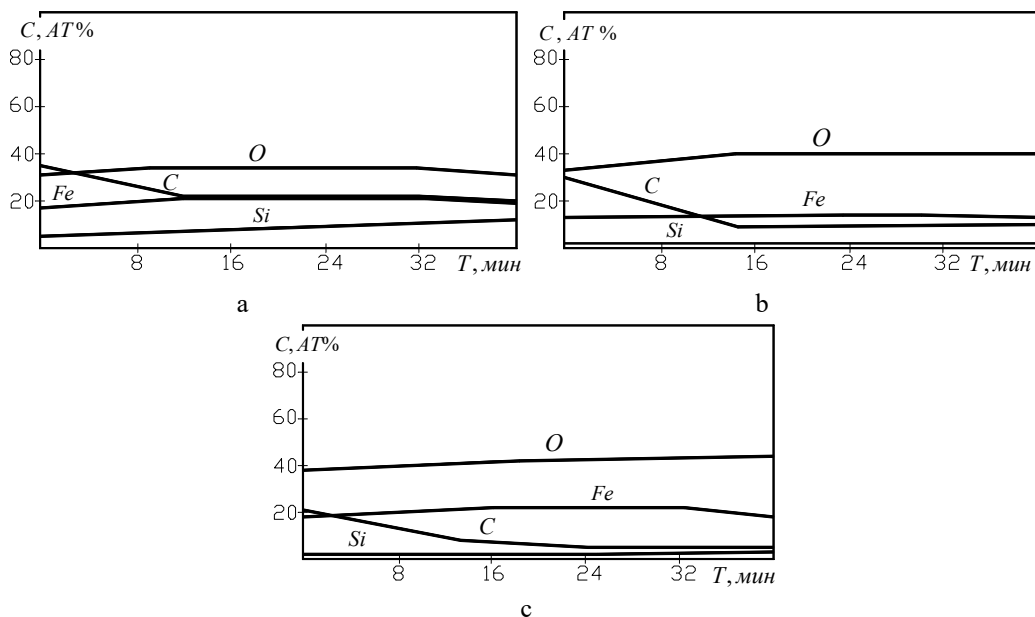


**Fig. 3.** Distribution of chemical elements of hydrogenated steel 60C2 by the depth of the friction surface, depending on the etching time, at  $P = 10$  MPa: a -  $V = 0.2$  m/s; b -  $V = 0.3$  m/s; c -  $V = 0.4$  m/s

When studying the profiles (fig. 3) of the distribution of elements on the friction surface of hydrogenated steel 60C2, it should be noted that the oxygen content on the surface and in the near-surface region increases, as well as the carbon content decreases. In addition, iron was found on the friction surface, the amount of which

changes with depth (fig. 3 a, b, c). The presence of these elements indicates the predominant possible formation of iron carbides and oxides, whereas Fe is absent when tested in air.

It was found that the increase in the friction speed of hydrogenated samples leads to depletion of the surface in carbon and its amount is significantly less than in air. The oxygen content on the surface is almost the same, does not depend on the research modes, and its concentration increases monotonously with depth. The amount of oxygen on the friction surface of hydrogenated steel 60C2 is significantly greater than in air, which can be explained by the presence of hydrogen in the contact zone.

In all cases, silicon was found on the friction surface of hydrogenated 60C2 steel, the amount of which increases with depth for low friction speeds (up to 0.2 m/s) (fig. 3 a), with increasing speed - its amount on the surface and in the near-surface zone is the same (fig. 3 b, c).

The presence of silicon in the contact zone makes it possible to form chemical compounds of silicon with elements of the environment, especially oxygen. At the same time, no depletion of the inner layers of silicon is observed due to saturation of the surface of hydrogenated samples with it, in contrast to the results obtained in air. The amount of silicon registered on the hydrogenated friction surface is less than in air. That is, it can be stated that during friction of hydrogenated samples, silicon diffusion into the contact zone from the inner layers does not occur.

When considering the formAuger spectrum of carbon obtained from friction surfaces of hydrogenated steel 60C2, it can be noted that it corresponds to the carbide phase. In our opinion, this is due to the fact that iron and manganese form compounds with carbon, while other elements that can lead to carbide formation have not been registered.

The presented results of the study allow us to conclude that as a result of friction of hydrogenated steel 60C2, a change in the chemical composition of the surface and the near-surface region occurs in comparison with the volume of the sample, which is associated with the activation of the surface layer and the formation of secondary structures on them, which, as is known, affect the process of friction and wear. In addition, the qualitative and quantitative nature of the secondary structures formed in the presence of hydrogen differs from those formed in air, which confirms the influence of hydrogen.

The use of the SIMS method made it possible to analyze changes in the microstructure in thin surface friction layers of hydrogenated steel 60C2 with different structural states, and to establish the nature of the phases, their crystalline structure, and the parameters of the unit cell necessary for identifying the phases and composition within the region of their homogeneity.

The study of friction surfaces of hydrogenated 60C2 steel in the transmission microdiffraction mode allowed us to record diffuse halos (fig. 4a), the number of which reflects the qualitative picture of the surface layer activated by friction after elastic-plastic deformation [6, 7, 10]. The electron diffraction pattern indicates that the microstructure of the friction surface in the presence of hydrogen of 60C2 steel samples has a finely dispersed structure and consists of a mixture of phases of material components, contacting pairs and products of interaction with atmospheric oxygen.

It should be noted that the order of dispersion of the friction surfaces studied in air and after hydrogenation is practically the same; however, a slight increase in the dispersion of the friction surface studied in the presence of hydrogen is noticeable, which is apparently due to the fact that hydrogen promotes greater oxidation of the structure.

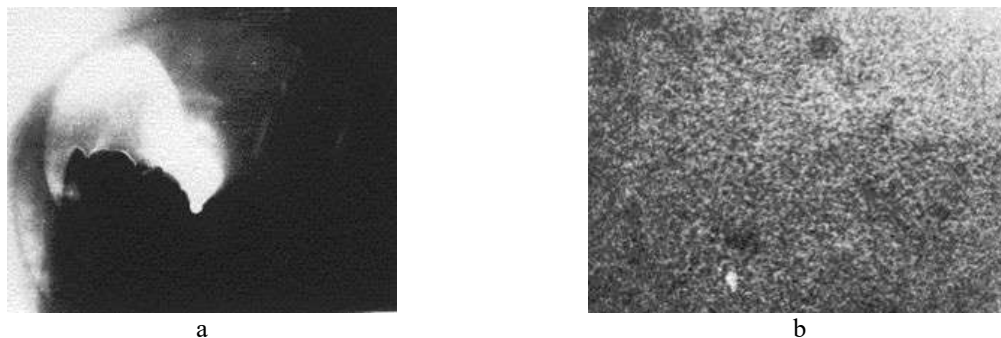


**Fig. 4. Electron diffraction pattern of surface friction layers (a) and distribution of elements on the friction surface (b) of hydrogenated steel 60C2 with a tempering structure of 300°C**

According to the stoichiometric composition, the microstructure of the friction surface after hydrogenation, as in air, is a complex, difficult to activate complex in the form of a finely dispersed mixture of oxides of Fe, Mn, Si and complex spinel phases of the  $\text{FeMn}_2\text{O}_4$  type, which are formed on the surfaces of the material during the friction process.

On the friction surfaces of hydrogenated steel 60C2, with different tempering structure, the appearance of new structural components was noted, representing a practically uniform distribution of ellipsoid fragments over the friction surface (fig. 4 b), distinguished by additional dissolution of carbide phases in the matrix. On the friction surfaces of hydrogenated steel 60C2, the presence of uniformly distributed ultra-dispersed new formations similar to those found on the friction surfaces in air was not detected.

X-ray phase analysis hydrogenated friction surfaces, carried out on a DRON-UM1 diffractometer, showed that the structure of the samples is a solid solution based on iron and a finely dispersed mixture of strengthening phases, mainly in the form of Fe, Si carbides and intermetallic compounds. The presence of a solid solution of  $\text{Fe}_2\text{O}_3$  in the surface layers was noted. When determining the physical broadening of the lines, caused by the dispersion of crystals and distortion of the crystal lattice, on friction surfaces in the presence of hydrogen of samples with a tempered martensite structure ( $300^\circ\text{C}$ ), the absence of FeO was established, apparently due to its thermodynamic instability and oxidation to  $\text{Fe}_3\text{O}_4$ . Thus, a decrease in the oxidation rate and the intensity of wear product formation leads to an increase in the wear resistance of the material with such a structural state.

Results of physical-chemical and the results of the microphase analysis of friction surfaces of hydrogenated 60C2 steel using an electron microscope are shown in fig. 5. It follows from them that the friction surfaces differ qualitatively and quantitatively (fig. 5a) from the surfaces obtained during similar tests in air. Several types of secondary structures can be distinguished on the surfaces obtained in the presence of hydrogen, differing in chemical composition and in different ability to reflect light (T1, T2, T3, T4). Let us recall that other types of secondary structures were obtained in air: T5, T6, T7, T8. Supersaturated solid solutions of iron with dissolved oxides of Si, Mn have a light shade, which can be attributed, in our opinion, to secondary structures of the second kind, according to the classification proposed by V.I. Kostetsky [6-9]. The following should be noted: the amount of dissolved oxides of Si, Mn on the friction surfaces in the presence of hydrogen is less than in air. And, as is known, silicon dioxide found on the friction surface promotes the formation of glass-forming oxide, which has unique physical and chemical properties - sufficiently high hardness without brittleness, and on friction surfaces examined in air, the amount of silicon oxide is significantly greater than after hydrogenation. Obviously, hydrogen affects the process of SiO formation, namely, the presence of hydrogen reduces the amount of silicon oxide formed. This, in turn, can also explain the increase in intensity wear resistance of hydrogenated steel 60C2 with a low-temperature tempering structure (up to  $400^\circ\text{C}$ ).

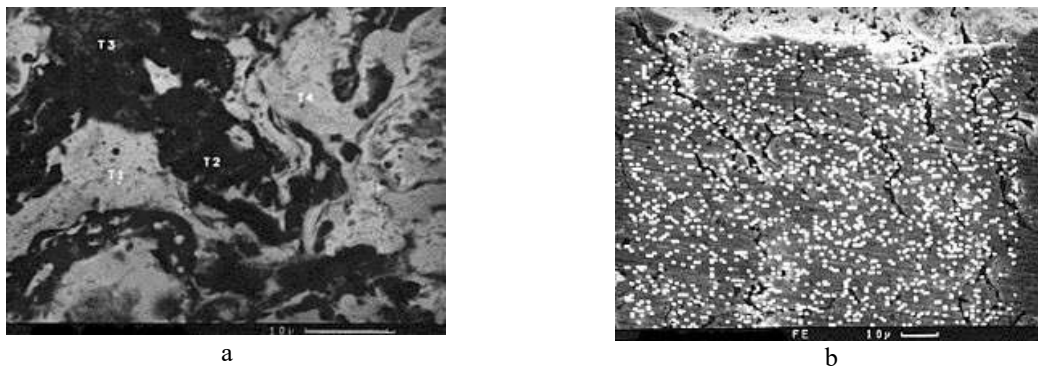


**Fig. 5. Formation of secondary structures on friction surfaces (a) and distribution of iron on friction surfaces of hydrogenated steel 60C2 with a tempering structure of  $300^\circ\text{C}$**

Fig. 5 b shows the distribution of iron on the friction surface of hydrogenated steel 60C2, from which it is evident that the amount of iron on the friction surface obtained during the study in air is significantly less than in the presence of hydrogen (fig. 5 b). This confirms the result we obtained earlier. In addition, the iron is distributed uniformly over the surface of the material. A large number of micro cracks are observed on the hydrogenated friction surface, which can obviously explain the increase in the wear rate of the material saturated with hydrogen.

## Conclusions

The conducted qualitative and quantitative analysis of friction surfaces of samples made of hydrogenated steel 60C2, with different structural states, allows us to draw the following conclusion:

- the chemical composition of the friction surface of hydrogenated steel 60C2 differs from the chemical composition of the volume, the friction surface and the near-surface region contain iron and are enriched with carbon, the concentration of which decreases with increasing friction-sliding speed. This promotes the formation of secondary structures consisting mainly of iron oxides and reduces the amount of silicon oxide formed, which in turn reduces the wear resistance of the material in the presence of hydrogen;

- the iron content on the surface increases with increasing load (speed); with increasing speed, a new phase, iron carbide, is formed in the near-surface region;

- hydrogen significantly affects the composition of the friction surface and the near-surface region, which is manifested in its greater oxidation through the predominant formation of iron oxide and lesser silicon oxide, the formation of more brittle secondary structures that do not contribute to the wear resistance of friction pairs.

Comparing the tribological characteristics of hydrogenated steel 60C2, with different structural states, with the obtained results of studies of friction surfaces by physicochemical methods, it is possible to draw a conclusion about the relationship between the friction and wear indicators with the processes occurring on the surface of the material during friction, and the significant influence of hydrogen present in the contact zone on them. It has been

proven that during friction on the contact surface of hydrogenated steel 60C2, regardless of its structural state, the process of formation of secondary structures occurs, which determine the process of friction and wear of the material. Reduction of the wear intensity of steel 60C2 with a tempered martensite structure (300°C) is accompanied by the formation of secondary structures on the surface, which have a higher resistance and shield the base material from direct contact and destruction. In addition, the saturation of the material with hydrogen changes the nature and mechanism of formation of secondary structures, which in turn leads to a change in the mechanism of friction and wear of the material.

### References

1. Закалов О. В., Закалов І. О. Основи тертя і зношування в машинах : навчальний посібник. Тернопіль : Видавництво ТНТУ ім. І. Пулюя, 2011. 322 с.
2. Ya.M. Gladkii, S.S. Bys, V.V. Mylko. Hydrodiodiffusion machining of structural materials. Materials Science. Mai 2020, Volume 18, pp. 345–453.
3. Триботехніка і надійність машин : навчальний посібник / Ю. О. Харламов та ін. Сєверодонецьк : Вид-во СХУ ім. В. Даля, 2021. 184 с.
4. Tribology composite stringer, Heidelberg, 2016. ISBN: 978-3-642-3381-6.
5. Tribology for engineers. Wood head Elsevier. Cambridge. 2017. ISBN: 843346159.
6. Tribology for engineers. Wood head Elsevier. Cambridge. 2017. ISBN: 843346159.
7. LI Bershadsky. Structural thermodynamics of tribosystems. К.: Knowledge, 1990.-30 p.
8. Дискретне зміцнення та зносостійкість циліндричних трибосистем ковзання: [монографія] / Диха О. В. [та ін.]. — Хмельницький: ХНУ, 2016. — 197 с. : рис., табл. — Бібліогр.: с. 173—194. — 300 прим. — [ISBN 978-966-330-260-7](https://doi.org/10.26907/2542-0419.2016.197)
9. Савуляк В. І. Методи та засоби дослідження складу, структури та властивостей матеріалів : навчальний посібник. Вінниця : ВНТУ, 2021. 76 с.
10. «Триботехніка». Курс лекцій / Д. П. Журавель та ін. Мелітополь : Видавничо-поліграфічний центр «Люкс», 2019. 280 с.

**В.В. Щепетов, С.С. Бись, М.Р. Бялик, В.Ю. Медведчук, Я.С. Бись.** Вплив наводнювання на механізм зношування сталі.

У статті проаналізовано трибологічні характеристики наводненої сталі 60C2, з різним структурним станом, з отриманими результатами досліджень поверхонь тертя фізико-хімічними методами. Це дозволило зробити висновок про взаємозв'язок показників тертя і зношування з процесами, що протікають на поверхні матеріалу при терті, і значного впливу на них водню в зоні контакту. Доведено, що в процесі тертя на поверхні контакту наводненої сталі 60C2, незалежно від її структурного стану, відбувається процес утворення вторинних структур, які визначають процес тертя та зношування матеріалу. Зниження інтенсивності зношування сталі 60C2 зі структурою мартенситу відпуску (300°C) супроводжується утворенням на поверхні вторинних структур, що мають більш високу стійкість і екранують основний матеріал від безпосереднього контакту та руйнування. Крім того, насичення матеріалу воднем змінює характер та механізм утворення вторинних структур, що у свою чергу призводить до зміни механізму тертя та зношування матеріалу.

**Ключові слова:** тертя, знос, водень, поверхневі структури



## Texture of materials of elements of tribological systems of machines and mechanisms in non-equilibrium processing and functioning conditions

V.V. Aulin<sup>1\*</sup>[0000-0003-2737-120X](https://orcid.org/0000-0003-2737-120X), Ye.V. Manko<sup>1</sup>[10009-0005-6355-2413](https://orcid.org/10009-0005-6355-2413), V.M. Chumak<sup>1</sup>[10009-0002-1913-9371](https://orcid.org/10009-0002-1913-9371),  
S.V. Lysenko<sup>1</sup>[10000-0003-0845-7817](https://orcid.org/10000-0003-0845-7817), O.D. Derkach<sup>2</sup>[20000-0002-5537-8022](https://orcid.org/20000-0002-5537-8022), D.O. Makarenko<sup>2</sup>[20000-0002-3166-6249](https://orcid.org/20000-0002-3166-6249)

<sup>1</sup>Central Ukrainian National Technical University, Ukraine

<sup>2</sup>Dnipro State Agrarian And Economic University, Ukraine

\*E-mail: [AulinVV@gmail.com](mailto:AulinVV@gmail.com)

Received: 19 May 2025; Revised 02 June 2025; Accepted: 18 June 2025

### Abstract

The article is devoted to microtexturing of metal and polymer materials of tribological system elements, its influence on the characteristics and properties of working surfaces of samples and parts. Various types of microtexture of steel and composite materials based on zirconium oxide are considered. The mechanism of their formation is clarified. Mainly, the mechanisms of microtexturing are associated with the field of tension created during friction and laser processing. It is determined that laser processing of steel samples leads to combined microtexturing and a texture gradient along the depth of the surface layer of the sample. Texture in composites is revealed both during laser processing and during friction testing. It is shown that the revealed texture positively affects the operational characteristics of parts, increasing the level of reliability and wear resistance, as well as the tribological efficiency of tribocouplings of parts of assemblies, systems, units of machines and mechanisms.

**Key words:** steel, composite, tribological system, microtexturing, X-ray radiation, laser processing, texture perfection, friction testing, reliability, wear resistance.

### Introduction

Increasing the durability of mating parts, assemblies, systems and units of machines and mechanisms in general is one of the important and priority tasks of modern mechanical engineering. This problem can be solved only on the basis of an integrated approach, which includes the creation of new materials from which parts are made, the development of effective innovative technologies, manufacturing, strengthening and manufacturing and modification of working surfaces of parts. At the same time, during strengthening, restoration and modification, it is necessary to take into account the influence of technological parameters on the initial, intermediate and final state of the material of the part as a whole. This means that first of all it is necessary to determine the microstructure, to find out its texture, to identify the distribution of alloying elements and phase composition, stress-strain state, that is, to find out the evolutionary development of the material of the part during processing by various technologies and during operation [1].

The main task of texturing is to reproduce the roughness and surface finish of materials of tribological system (TrS) elements, which, thanks to microtexture, are constantly used to reduce friction and wear and increase the tribological efficiency of the system.

The microtexture of the working surfaces of mating parts of machines and equipment has a synergistic triple effect: reserve for liquid and solid lubricants; collection of wear particles; limitation of abrasion and formation of a hydrodynamic film.

The microstructuring of the friction surface can be optimized using mathematical methods, finite element methods, and computational hydrodynamics based on the Navier-Stokes and Reynolds equations for the hydrodynamic mode of operation of the TrS.

The latter method simulates the flow of the lubricating medium and makes it possible to predict the bearing capacity, velocity and pressure field in the TrS, and also takes into account inertial effects. Artificial intelligence



(AI) methods are used to model the evolutionary behavior of the TrS with optimized microtexture, primarily the genetic algorithm method.

The shear effect, which is characteristic of hydrodynamic lubrication in the TrS, the film thickness, the friction coefficient and energy consumption are associated with the artificially formed texture of the working surfaces of triboelements (parts). The texture has a positive effect both in conditions of dry friction of mating parts, and for friction with solid and liquid lubrication in the presence of a layer of oil, grease, ceramic composite or solid lubricant.

Texturing the friction surface and controlling its properties, such as roughness, is one of the methods for increasing the efficiency of the friction surface. Texturing methods are definitely relevant methods for improving the characteristics and properties of the working surfaces of tribo-coupling parts made of metal and composite materials, since they effectively reduce friction and wear processes. Changing the roughness and surface relief guarantees an improvement in the tribological properties of the mating surfaces by the components and measures involved, which significantly increase the TrS.

### Literature review

It is known that the surface of the material of parts is considered textured if there is a preferential orientation of crystallites in polycrystalline materials and high-molecular compounds in composites relative to the external coordinate system [2].

Texture is formed under the influence of various types of anisotropies, forces, during material production, part formation, and external influences of various physical and chemical nature.

The practical interest in the textures of materials is due to the fact that they determine the anisotropy of the characteristics and properties of the working surfaces of tribocoupled parts. If all the crystallites of the polycrystal of metals and high-molecular compounds in composites have one predominant orientation, then such a texture is single-component [3]. If there are several groups of crystallites and high-molecular compounds, each of which is characterized by its own orientation, then such a structure is multicomponent.

In real conditions, there is a certain deviation of the orientation of some crystallites or high-molecular compounds in the textured material from the "ideal" location relative to the direction of the influence that causes texture formation by a certain angle  $\delta$ . This phenomenon is due to the scattering of the texture. The degree of scattering of the texture is generally greater, the stronger the external influences acting on the material of the parts. This may be the degree of plastic deformation.

The formation of the surface texture of a triboelement (TrE) changes the contact area between them, reduces friction and increases the tribological efficiency and service life of the TrS. Non-equilibrium strengthening, restoration and modification technologies are widely used to create the texture of the working surfaces of parts, including laser processing [4]. They allow you to create a microtexture that can perform different functions depending on the operating conditions: accumulate and direct the lubricant, and then release it at the stage of use. Depending on the geometry of the texture, friction decreases, hydrodynamic pressure increases.

The effects of surface texturing strongly depend on the operating conditions of the TrS, which can enhance or weaken them.

To improve the tribotechnical characteristics, it is possible to apply a coating to the textured surface, i.e. to treat the textured surface. In this case, the shear resistance is reduced, the substrate is protected by a soft coating, the contact area between mechanical parts and friction is reduced, and solid lubrication is implemented. The key parameters when using solid lubricants are the contact area between moving TrE, the load, its effect on microstructural changes in the contact areas and the formation of a film between the mating surfaces [5].

The texture of the working surfaces of parts can change heat transfer, implement better heat removal from the contact zone, which increases the wear resistance of parts. The distribution of the stress field in the surface layers of the material of the mating parts and the wettability of their surfaces can also change.

There are various texturing methods: micromilling, microcasting, electrochemical processing, etc., but laser texturing of the working surfaces of parts has the most advanced texture, since it is created under non-equilibrium conditions [2,3,21].

By adjusting the parameters of the texturing process, it is possible to control the shape and optimize the geometric factors of the surface structure of the part itself. However, the method is difficult to apply on a large scale due to high energy consumption.

It is known that the stress-induced martensitic transformation in zirconium oxide ceramic  $ZrO_2$  from the metastable tetragonal (T) to the stable monoclinic (M) phase, on the one hand, and twinning, on the other hand, are two competing mechanisms of deformation of composite materials [4,6,22]. This occurs at a temperature at which the stress-induced TM transformation is more likely to be observed in the material. With increasing temperature, when the thermodynamic stimulation of the transformation decreases, another strengthening mechanism begins to operate, based on the reorientation of coherent mechanical twins in the field of applied stresses. In the literature, this is defined as ferroelasticity [6,23]. The action of the ferroelasticity mechanism in ceramic materials during laser processing and under friction conditions is practically indistinguishable. Ferroelasticity is observed under conditions of high temperatures and high sliding speeds or under high-temperature friction [15-17].

Usually, the reorientation of crystal lattices by the mechanism of ferroelasticity is accompanied by the appearance of a texture, which is detected by the X-ray method [8,9,22,23]. This is manifested in a change in the relative intensity of X-ray lines in the doublets (002)-(200), (202)-(220), (113)-(311), (004)-(400) and others of the T-phase [8,9,22,23]. Unfortunately, ferroelasticity for the T-phase of zirconium dioxide cannot be considered the only reason for the appearance of such a texture. In work [9] it was determined that the effect of the appearance of a texture during grinding of samples of ceramic materials is explained by the reorientation of the crystal lattice due to the reversible martensitic transformation, which occurred as a result of surface heating. According to [10,11], it is possible to separate these two named deformation mechanisms by simultaneously observing the behavior of the monoclinic phase content on the friction surface and in wear particles. It should be noted that the structural state of the friction surface at the time of its destruction (wear) is observed in the wear particles [12-14].

Thus, the analysis of literary sources and operational data shows that the cause of failure of about 80% of machine and mechanism parts is the wear of their working surfaces. This indicates that it is the working surfaces with a whole complex of tribological properties created during the hardening process that limit the service life of the mating parts [18-20].

At present, a sufficiently substantiated scientific approach has not been developed that would allow adequately describing and explaining the influence of a complex of technological measures, including laser processing and alloying and evolutionary factors on tribological properties. Thus, the scientific literature indicates that a positive effect on the tribological properties of working surfaces is their texture [24,25]. At the same time, there is practically no data on the influence of the microtexture of the working surface and the surface layer on the operating conditions of mating parts and their durability and tribological efficiency.

### Purpose

The purpose of the work is to clarify the possibilities of implementing microtexturing of materials (metals and polymers) of elements of tribological systems using laser processing, the type of formed textures and improving the characteristics and properties of surface layers of materials, as well as the tribological efficiency of conjugated parts of machines and mechanisms.

To achieve the set goal, the following tasks were solved:

- refinement of the methodology for X-ray microtexture studies of steel and composite materials;
- identification of types of microtextures of metallic materials after laser processing and study of their influence on the characteristics and properties of surface layers and increasing the efficiency of tribological systems;
- identification of microtexture types of ceramic materials after laser processing and friction testing and study of their influence on the characteristics and properties of surface layers and increasing the efficiency of tribological systems.

### Results

In practice, two types of texture are most commonly encountered: axial and bounded.

Axial (axisymmetric) texture is a texture in which all crystallites or macromolecular compounds are established in a predominant crystallographic direction  $\langle uvw \rangle$  along a certain direction on the surface and surface layer of the material of the sample (part). The direction  $\langle uvw \rangle$  is the texture axis, and  $uvw$  are the direction indices. The latter determine the orientation of crystallites or macromolecular compounds along the direction of influence of any nature, which caused the formation of the texture. The greater the angle of deviation from the direction of the ideal texture axis, the greater the degree of texture scattering. In the case of a multicomponent axial texture, a composition of textures is formed in metal or polymer materials:

$$\langle u_1 v_1 w_1 \rangle + \langle u_2 v_2 w_2 \rangle + \langle u_3 v_3 w_3 \rangle + \dots + \langle u_n v_n w_n \rangle. \quad (1)$$

Axial texture is formed under the influence of forces acting predominantly in one direction: drawing; extrusion; compression; deposition from a gaseous medium; crystallization, etc.

There is also a limited texture, in which crystallites or high-molecular compounds are fixed in a certain position: there is a certain plane  $\{hkl\}$  and direction  $\langle uvw \rangle$ , lying in this plane. A limited texture is formed when the sample (part) is subjected to forces in several directions. A typical example of such a texture is the texture that occurs during rolling. It is formed as a result of the action of compressive forces  $Q$  in the direction perpendicular to the rolling plane and tensile forces along the rolling direction. After deformation, certain planes  $\{hkl\}$  in the grains of a polycrystal or high-molecular compounds become parallel to  $Q$ , in the direction  $\langle uvw \rangle$  parallel to rolling. If a strong single-component rolling texture is observed, the crystallites practically lose their degree of freedom and the polycrystalline material becomes similar to an oriented block single crystal.

The rolling texture in general form is denoted by:  $\{hkl\}, \langle uvw \rangle$ . The indices  $hkl$  and  $uvw$  are related by

the zoning condition, which for the cubic system is written as follows:

$$hu + kv + lw = 0. \quad (2)$$

The observed scattering of the texture during rolling means that the planes  $\{hkl\}$  in some of the crystallites are slightly deviated from the plane of the working surface Q, and the directions  $\langle uvw \rangle$  are not strictly parallel to the rolling direction. The multicomponent rolling texture is denoted as follows:

$$\{h_1 k_1 l_1\} \langle u_1 v_1 w_1 \rangle + \{h_2 k_2 l_2\} \langle u_2 v_2 w_2 \rangle + \{h_3 k_3 l_3\} \langle u_3 v_3 w_3 \rangle + \dots + \{h_n k_n l_n\} \langle u_n v_n w_n \rangle. \quad (3)$$

Determination of the nature of the texture in polycrystalline materials and high-molecular compounds in polymers and assessment of their scattering can be carried out by analyzing direct and reverse pole figures constructed according to X-ray structural analysis data on diffractometers of various models using computer equipment and information technologies.

Direct pole figure (DPF) is a homostereographic projection (HSP) defined by the set of crystallographic planes  $\{hkl\}$  (stereographic projections of normals  $N_{hkl}$  to these planes  $\{hkl\}$ ) for all crystallites (grains) of a given polycrystal. The position of the points of the pole figure is defined by two angles  $\alpha$  and  $\beta$ , where  $\alpha$  is the radial coordinate, varying from 0 to 90 °;  $\beta$  is the azimuthal coordinate, varying from 0 to 360 °.

In the case of an axial texture, the projection plane is usually chosen parallel or perpendicular to the texture axis. In the case of a limited texture, the projection plane is chosen parallel to the rolling plane, and on the pole figure, the directions of force or field effects and the directions of normal (DN) projections perpendicular to them are fixed.

The inverse pole figure (IPF) is the distribution of pole densities  $P_{hkl}$  for a given direction in a sample (part) on a standard triangle of the stereographic projection of the directions of a single crystal of a given system. The pole density on the IPF shows the fraction of crystallites  $\{hkl\}$  whose plane poles coincide with the specified direction in the sample (part). Therefore,  $P_{hkl}$  it represents the probability of the coincidence of a given direction in the sample with the specified crystallographic directions. As a rule, the IPF is used to analyze the orientation of the normal to the studied plane of the sample (part).

The IPF is constructed in the region of a standard triangle, which is understood as a triangle highlighted in the standard projection of a single crystal, the vertices of which connect the three main directions. At the same time, near the different poles of the region of the standard triangle, the corresponding values of the pole densities are marked, which are determined using experimental data on the dependence of the intensity of diffracted X-ray radiation on the position of the sample relative to the incident beam of rays.

The advantages of texture analysis using IPF compared to DPF are as follows:

1. Larger distances of regions from each other, corresponding to different poles on the IPF than on the DPF. This is especially important in the case of scattered and multicomponent structures, when there is an overlap of different orientations on the pole figure.

2. More accurate quantitative determination of orientations describing the texture. In the case of DPF, there is a need to analyze several DPF for different normals, which is associated with an increased duration of the experiment and processing of the obtained data.

3. Ability to quantify texture components and their dispersion.

4. The method of constructing the IPF using the integral intensities of X-ray interference does not require the use of a special prefix, which is necessary for constructing the DPF using the tilt method.

The main disadvantages of studying texture from IPF are as follows:

1. When working with flat samples with a small working surface, it is necessary to analyze a whole set of wires or sections of a set of strips placed next to each other, which can lead to large errors;

2. With a multicomponent texture, the correctness of the choice of the combination of plane and direction indices for the rolling texture should be confirmed by DPF analysis, if necessary.

Let us consider the method of diffractometric analysis of the texture of sample materials.

Using DPF, the analysis is based on measuring the intensity of certain X-ray interferences (HKL) for different positions of the sample. Different positions of the sample are created by its rotation. For an untextured sample, crystallites and high-molecular compounds are arranged statistically randomly and changing the position of the sample in space should not affect the magnitude of the X-ray intensity and  $I_{HKL}$ .

For a textured sample in which the crystallites have a predominant orientation, changing the position of the sample changes the intensity of the X-ray radiation  $I_{HKL}$ , which, under certain conditions, reaches maximum values. In this case, texture maxima appear on the diffraction curve. Their angular position and magnitude are determined by the nature of the texture.

Two main methods of taking textures on a diffractometer are used: "reflection" taking, which is used for massive samples, and "transmission" taking on "thin" samples.

The type and method of constructing the DPF, and therefore the method of recording diffractometric curves, depend on the mutual location of the texture axis B and the sample plane q.

When they are parallel, the projection plane is parallel to the direction B and the projections of the normals  $N_{hkl}$  on the DPF are located on the parallels that are from the exit of the axis B on the projection circle at an angle  $\alpha$ . In this case, it makes sense to analyze only the dependences  $I(\alpha)$ . When the plane and the texture axis are perpendicular, the center of the DPF coincides with the projection of the axis B and the projections of the normals on the DPF are located on a circle of radius  $\rho$  with the center at point O.

If the sample plane is parallel to the texture axis, then the measurement is performed without rotation at an angle  $\beta$  ( $\beta = 0$ ). If the sample plane is perpendicular to the B axis, then the measurement is performed with rapid rotation of the sample at an angle  $\beta$  (60 rpm). Typically, the tilt method is used. The angle  $\alpha$  is changed by rotating the sample around the horizontal axis of the goniometer discretely through  $5^\circ$  in the range from 0 to  $75^\circ$ .

The axial texture axis ( $uvw$ ) is found from the analysis of the  $I(\alpha)$  curves. To find it, the angles  $\langle uvw \rangle$  corresponding to the peaks of the diffraction curve  $\beta$  are determined, which are related to the angle  $\alpha_{\max}$  between the normal and the texture axis by the relations:

$$\alpha_{\max} = 90^\circ - \beta, \text{ at } q \parallel B; \alpha_{\max} = \beta, \text{ at } q \perp B. \quad (4)$$

Analysis of axial texture using diffractometric curves of X-ray structural analysis is a fairly fast method. In the presence of several components of the axial texture and their scattering, it is convenient to use DPF. On the curves  $I(\alpha)$ , 5...7 levels of identical intensity values are selected, which are plotted on the vertical diameter ( $\beta = 0$ ) on the PC monitor at points corresponding to certain angles  $\alpha$ . Parallels are drawn through the points using a Wolf grid or circles using a Boldyrev grid. Using a table of angles, based on the  $I(\alpha)$  dependencies, the axis of the axial texture is determined. After that, the texture scattering is found and the DPF is constructed.

To record diffraction curves, the sample surface area is set perpendicular to the goniometer plane ( $\alpha=0$ ). The diffraction curves  $I_{HKL}(\theta)$  are recorded in the same way as in phase analysis on a diffractometer. In this case, the sample and the counter are rotated around the goniometer axis, changing their position by angles  $\theta$  and  $2\theta$ , respectively.

During the measurement, all diffraction maxima (HKL) that can be obtained on a given X-ray radiation are recorded. As a rule, when studying the texture of metals with a cubic lattice, hard radiation from a molybdenum anode is used. In this case, secondary characteristic radiation is possible. It is attenuated by a thin aluminum foil, which is installed in front of the counter. For metals with non-cubic grids, softer radiation is used. In a structureless reference sample, the crystallites are arranged randomly with respect to the q plane, so the integral intensity of X-ray radiation is determined only by the radiation intensity multipliers and the measurement geometry.

For a textured sample, the intensity of the X-ray lines also depends on the type of texture. The value of the pole density is determined by the formula:

$$P_{hkl} = \frac{\left( \frac{I_{P\text{ЛД}}}{I_{HKLeK}} \right) \sum_N P_{hkl}}{\sum_N P_{hkl} \left( \frac{I_{P\text{ЛД}}}{I_{HKLeK}} \right)}, \quad (5)$$

where  $I_{HKL}$  – the integrated intensity of X-ray interference of the analyzed planes ( $hkl$ ) of the studied textured sample;  $I_{HKLeK}$  – the same for the reference sample;  $I_{P\text{ЛД}}$  – the intensity of X-ray lines of the diffraction spectrum;  $p_{hkl}$  – the repeatability factor for the planes ( $hkl$ );  $N$  – the number of analyzed poles.

The accuracy of determining the pole density corresponds to 10...20%. The untextured sample is made of the same material as the textured one in order to perform the normalization operation. The normalization condition is introduced into the formula in order to take into account the possible unevenness in the spatial distribution of normals due to the texture. The normalization value is performed in such a way that the average value of the pole density in any direction for the untextured sample would be the same:

$$P_{hklek} = \bar{P} = \frac{\sum_N (P_{hkl} p_{hkl})}{\sum_N P_{hkl}} = 1. \quad (6)$$

For a textured sample  $P_{hklek} \neq \bar{P}$ .

IPF makes it possible to quantitatively determine the proportion of components that determine texture:

$$f_{hkl} = \frac{\left( \frac{I_{HKL}}{I_{HKLeK}} \right) p_{hkl}}{\sum_N P_{hkl} \left( \frac{I_{P\text{ЛД}}}{I_{HKLeK}} \right)}. \quad (7)$$

If the operating conditions of the part, the shape and location of the surfaces of maximum tangential stresses are known, then it is possible to theoretically calculate or experimentally determine which orientation of the crystals in the part provides the greatest strength and durability. The predominant orientation of crystallites in polycrystalline materials and high-molecular compounds occurs under directed external influence or the orienting action of the external environment.

In real conditions, there is often not one, but several preferred orientations of crystallites or high-molecular compounds, that is, a multicomponent texture of triboconjugates of machines and mechanisms arises.

When manufacturing and operating parts and their tribo-coupling parts, it is necessary to take into account both the texture of the source material and the methods that allow creating and controlling a certain texture.

The authors of the work believe that one of the effective ways to create and control texture can be laser processing of the working surfaces of parts and their mating surfaces.

The research was carried out on cylindrical samples ( $d=22$  mm;  $h=12$  mm) with the initial texture  $\langle 110 \rangle$  and grain size  $30..40$   $\mu\text{m}$ . Laser processing was carried out on laser installations "Kvant-16" ( $\lambda=1.06$   $\mu\text{m}$ ;  $\tau=5 \cdot 10^{-3}$  s), LGN-702 ( $\lambda=10.6$   $\mu\text{m}$ ;  $P=780 \pm 20$  W). The surface after laser irradiation is a set of tracks both without overlap and with overlap of  $15..30\%$ .

The conditions for the formation of the texture of the surfaces of parts made of metal materials during their hardening by laser technologies, as well as the influence of technological parameters on the quality of the texture, were revealed. The research was carried out on samples that were subjected to the following laser hardening technologies: thermocyclic, thermomechanical laser technology of thermal treatment and complex laser alloying. Laser treatment was carried out in continuous and pulsed radiation modes with and without surface melting. The materials under study were: samples of steel 3, 45, IX-15, 40X, 65Г; aluminum alloys АЛ-5, АЛ-9, АК-7. The model materials were carbonyl iron and pure aluminum and copper.

The texture analysis was carried out using direct and reverse pole figures, which are built on the basis of the diffractometric method. The texture was determined using the dependences of intensity on the angle of inclination using a PC. The samples were examined on X-ray installations YPC-60, ДРОН-3М using  $K \alpha \text{CO}$  - X-ray radiation. When a texture gradient was detected, the samples were subjected to sequential etching from the surface in a helium atmosphere or by an electrolytic method.

The metal samples were studied after laser heat treatment, chemical-thermal boriding, and laser boron doping.

The tilt method was used to remove the lines  $\langle 001 \rangle$ ,  $\langle 110 \rangle$ ,  $\langle 112 \rangle$ ,  $\langle 123 \rangle$ ,  $\langle 200 \rangle$ ,  $\langle 002 \rangle$ ,  $\langle 211 \rangle$ ,  $\langle 202 \rangle$  both from the surface and from different depths of the laser exposure zone, etching the layers in steps  $0,1$  mm.

The initial texture on the samples of steel 3 was  $\langle 110 \rangle$ , and on steel 45 –  $\langle 001 \rangle$ .

As a result of laser processing, it was found that laser irradiation, depending on the power density, can form different types of textures, the degree of perfection of which is not uniform in the depth of the laser impact zone. This was found both in the case of laser heat treatment and in the case of laser alloying. It is characteristic that during laser processing a whole series of textures appears, which is not observed during mechanical impact, when there is one type of texture. For example, during laser heat treatment of steel 3, textures  $\langle 210 \rangle + \langle 211 \rangle + \langle 321 \rangle$  were recorded, with the initial axial texture  $\langle 110 \rangle$ . Note that the power density of laser radiation did not exceed the critical one, at which melting was observed.

It has been determined that during the crystallization of the material after laser melting, a texture appears: the dendrites have a directional direction in the laser exposure zone.

It was found that the degree of perfection of the axial crystallographic texture along the depth of the boride layer varies exponentially. For steel 45 with the initial texture of the  $\text{Fe}_2\text{B}$   $\langle 001 \rangle$  phase:

$$P = 6,60 + 8,82(1 - \exp(-0,0026h)),$$

where  $h$  is the depth of the boride layer.

After laser irradiation, the strengthened layer was also textured in depth, and the degree of perfection of the texture of the  $\text{Fe}_2\text{B}$  phase varies according to a linear law:

$$P = 5,87 + 0,26h.$$

Correlation analysis was performed using the usual method:  $r = 0,861$ .

Studies have shown that there is a relationship between the texture of the working surface of metal parts strengthened by a laser beam and their wear resistance: the higher the degree of perfection of the texture, the greater the wear resistance.

The work also established a correlation between the degree of texture perfection and wear resistance of samples boronized by laser doping: the greater the thickness of the doped layer and its texture, the higher the wear resistance.

The authors explain the detected effects both by the redistribution of carbon and boron in the studied steels, and by the orienting action of the laser beam, its various effects on the structure of the material.

We also note that the study of textured structural materials has not only practical but also great theoretical importance, because textured polycrystalline materials are closer to single crystals the more perfect their texture is, even though they have crystallite (grain) boundaries.

Studies have shown that in the field of laser radiation, a whole spectrum of textures can be obtained on the surface of a structural material. In addition, during sequential etching of samples, texture was detected even at a

certain depth to 0,5 mm. It is characteristic that at different levels of the surface layer a different texture is observed, that is, we have a gradient of textures during laser processing of the surface of samples of metallic materials.

The latter indicates the specifics of the effect of laser radiation on structural metal materials.

Gradient texture allows for targeted production of functional, reinforced surface layers on parts, which will ensure their high performance. This is especially true for parts of tribological systems.

Comparative analysis of textures obtained during thermocyclic, thermomechanical and laser treatments showed that the degree of perfection of textures on the same materials is different. Laser treatment has a higher degree of perfection. These results can be explained by the different intensity of laser radiation energy directed at the material and the different duration of its absorption by the material surface.

As ceramic materials for the study, ceramics with a composition of 98 wt.%  $ZrO_2$  (zirconium oxide) + 2 wt.%  $Y_2O_3$  (yttrium oxide) were selected. Ceramic material of this composition was prepared by sintering in vacuum at a temperature of 1879 K with different holding times. The technology for preparing this ceramic provided different grain sizes, and accordingly, different contributions of the transformation strengthening mechanism. In the initial state, all ceramic samples consisted of tetragonal and cubic phases. Friction and wear tests of ceramics based on zirconium oxide were carried out on a YMT-1 friction machine using the "disk-finger" scheme. The speed increase was provided stepwise, under conditions of friction without lubricant. The main sample made of ceramics was a finger. The conjugate specimen was a disk rotating in a vertical plane, made of cast high-speed steel, the hardness of which was HRC 60.

X-ray examination of wear particles and friction surfaces of ceramics in the initial state and after friction was carried out on a ДРОН-УМ1 X-ray diffractometer with  $Cu-K\alpha$  radiation. The shooting was carried out at points in the angle interval  $2\theta$ : 20...48°. The accelerating voltage was 40 kV, the tube current was 22  $\mu A$ . Using special computer software, the relative intensities  $I$  of the X-ray lines (002) and (200) of the tetragonal modification of zirconium oxide were analyzed. For each friction mode, the ratio  $I_{(002)}/I_{(200)}$  was determined. The content of the monoclinic phase on the friction surface was determined by the ratio of the integral intensities of the lines of the {111} type of tetragonal and monoclinic modifications.

An X-ray study of the surface of samples of ceramic materials based on zirconium oxide  $ZrO_2$  after laser processing without melting and dry sliding of the samples in a wide range of speeds was carried out. The surface structure was analyzed and it was shown that the textural state of the friction surface is similar to the textural state observed previously on the surface of samples of similar materials after rough grinding. The main trends in the change in the ratio of the intensities of the X-ray lines  $I(002)/I(200)$  of the tetragonal phase  $ZrO_2$  depending on the sliding velocity and grain size of the ceramic were identified. The mechanisms of lattice reorientation operating at different sliding speeds are substantiated. It is determined that high-strength ceramics are a promising material for tribotechnical use. The implementation of the wear mechanism of ceramic materials can be associated with the processes of deformation of surface layers in the material both under laser processing and friction conditions. This is especially important for ceramic materials that are prone to structural changes under the influence of created or applied stresses.

Studies conducted on samples that were not subjected to laser processing without surface melting showed that in all friction modes, a microtexture is formed on the working surface of the ceramic. The samples that were subjected to laser processing also had a microtexture (table 1).

Table 1

**Dependence of the ratio of X-ray intensities  $I_{(002)}/I_{(200)}$  on the speed of movement of the sample during friction. Ceramic grain size 1.6  $\mu m$**

Surface type	Sample movement speed during friction						
	0	0.2	0.4	0.6	0.8	1.0	1.2
Textured under friction conditions	0.5	0.8	0.9	1.0	1.2	1.4	1.5
Polished	0.5	0.5	0.5	0.5	0.5	0.5	0.5
Laser processing	2.2	2.2	2.0	2.0	2.0	2.1	2.1

After friction, the ratio  $I_{(002)}/I_{(200)}$  increases in such a way that it always exceeds the value characteristic of a random orientation of crystal lattices, which is approximately 0.5. Note that in the initial state, a pre-polished surface was considered.

It is determined that after a speed of movement of 0.2 m/s the ratio  $I_{(002)}/I_{(200)}$  reaches a value of the order of 0.2, and after laser treatment 2.2. Further increase in the friction velocity causes a smooth increase in the ratio of the intensity of X-ray lines  $I_{(002)}/I_{(200)}$  on the untreated laser radiation to a value of about 1.5. After laser processing of ceramic samples, a more perfect texture  $I_{(002)}/I_{(200)} = 2.2$  was found. This behavior was observed on all studied samples of composite materials regardless of grain size. In addition, it was found that the ratio of the intensity of the lines  $I_{(002)}/I_{(200)}$  increases with increasing ceramic grain size (table 2).

Table 2

**Dependence of the ratio of the intensities of the X-ray lines  $I_{(002)}/I_{(200)}$  on the size of the ceramic grain and the speed of movement of the sample subjected to laser processing**

$v$ , m/s	Ceramic grain size $\bar{d}$ , $\mu\text{m}$											
	0.80	1.00	1.20	1.40	1.60	1.80	2.00	2.20	2.40	2.60	2.80	3.00
1.1	1.30	1.32	1.36	1.38	1.40	1.43	1.48	1.50	1.54	1.59	1.60	1.62
0.4	0.80	0.85	0.90	0.95	1.00	1.10	1.20	1.40	1.16	1.18	1.20	1.23
0.1	0.80	0.83	0.85	0.88	0.90	0.91	0.93	0.96	0.98	0.99	1.00	1.15

The ratio of the intensity of the X-ray lines  $I_{(002)}/I_{(200)}$  under the specified conditions varied in the range (0.8...2.2).

Analysis of the obtained data on the ratio of line intensities in the (002)-(200) doublets of the tetragonal phase shows that most of the grains of the composite material are oriented relative to the friction direction so that the applicate axis  $c$  perpendicular to the friction surface. Taking X-ray diffraction patterns without rotating the sample under conditions of beam diffraction along and across the sliding direction did not reveal differences in the intensity of the lines in the doublets. This indicates that the abscissa  $a$  and ordinate  $b$  axes tetragonal cells are oriented arbitrarily in the plane of the friction surface.

The amount of monoclinic phase in wear particles, as well as on the friction surface, decreases with increasing sliding speed. Already at speeds above 1.1 m/s, there are no traces of martensitic transformation (monoclinic phase) either on the friction surface or in wear particles. In those cases where the monoclinic phase is present after friction, it was found that its content in wear particles is always higher than on the friction surface.

At the lowest speed in the tribocontact zone, the temperatures are low, and therefore reorientation of the composite lattice through the martensitic phase is possible. Obviously, this process takes place at speeds of 0.2 m/s, which is indirectly confirmed by the data of the X-ray structural analysis of the surface of samples of composites based on zirconium oxide, where lines of the monoclinic phase and the strongest inversion of the peaks (002)-(200) of the tetragonal phase are observed. In this, the irreversible oriented tetragonal-monoclinic transformation under the influence of contact stresses prevails. The obtained data indicate that at a speed of 0.9 m/s, a significant proportion of the reversibility of the martensitic transformation appears. This led to a decrease in the content of the monoclinic phase in the wear particles and its almost absence on the friction surface. Reorientation in this case can be carried out according to the scheme: tetragonal-monoclinic transformation under the influence of contact stress and monoclinic-tetragonal transformation under the influence of heating.

The flash temperature estimates [13] showed that with increasing velocity, the contact temperatures initially reach the temperature range ( $>1273$  K) of the stability of the tetragonal phase, and then increase within (1773...2273 K) of the two-phase tetragonal-cubic region of the phase diagram of the oxide system ( $\text{ZrO}_2\text{-Y}_2\text{O}_3$ ). In this case, the reorientation of the lattice of the composite material through the martensitic phase in this speed range becomes impossible. The texture observed in the composite material of both irradiated and non-irradiated samples during friction can be formed by the ferroelasticity mechanism. In addition, the resistance force for ferroelastic domain switching in ferroelastic materials, similarly to the coercive force for ferromagnetic materials, decreases with increasing temperature. If the test temperature is below the critical (analogous to the Curie temperature) and is about 2373 K, then this corresponds to the transition temperature to the single-phase cubic region. An increase in the ratio of the intensities of the X-ray lines  $I_{(002)}/I_{(200)}$  is observed with increasing friction test speed. With increasing temperatures in the tribocontact zone, the increase in the ratio of X-ray line intensities can be due to by increasing the number of reoriented domains in the ferroelastic materials of the composite due to a decrease in the resistance force during domain switching. Similar dependences of the ratio of the intensities of the X-ray lines  $I_{(002)}/I_{(200)}$  on the test temperature were obtained after grinding the sample surface.

Increasing the ratio of X-ray line intensities  $I_{(002)}/I_{(200)}$  with increasing grain size of the ceramic material, which is observed at different test speeds, it is possible to understand on the basis of the mechanisms of texture formation. This is a direct analogy to the well-known Hall-Petch effect for the deformation of polycrystalline materials, when the grain size of the material determines the mobility of dislocations. At the same time, the larger the grain size, the higher the mobility of dislocations in the material. In the case of a ceramic material based on zirconium oxide, the grain size determines the mobility of martensitic and twin boundaries. Plastic deformation both by the martensitic mechanism, due to the movement of martensitic plates, and by the mechanism of reorientation of twins, is easier to carry out in coarse-grained ceramics. At the same time, in the case of martensitic transformation, the strengthening of the surface texture with increasing grain size is also influenced by an increase in the thermodynamic factor of the tetragonal-monoclinic transformation.

The issue of ensuring the required level of tribological properties and characteristics by texturing the working surfaces of part materials requires the creation of physical and technological foundations and a comprehensive approach to solving the problem.

In our opinion, the problem of forming a perfect texture of the working surfaces of tribocoupling parts and methods for obtaining them requires solving a number of tasks:

- search for optimal technologies for creating textured work surfaces;
- evaluation of surface texture characteristics;

- the influence of the degree of texture perfection on the tribotechnical characteristics of the working surfaces of parts;
- obtaining surface layers with texture gradients in the case of laser processing;
- dynamics of changes in texture during the hardening process and under operating conditions;
- physical foundations of the creation and evolution of the surface texture of structural materials of a part under the influence of concentrated energy flows (laser radiation);
- the influence of hardening technologies on the quality of the surface texture of parts;
- further development of the methodology for research and optimization of texture parameters;
- use of computer technologies to assess the texture of the surfaces of parts and their mating surfaces;
- the influence of the degree of texture of the working surfaces of parts on their wear resistance and operational reliability.

### Conclusions

1. The essence and types of structuring of materials of samples and parts are clarified using the example of steel and ceramic materials. It is shown that the texture of the working surfaces of samples and parts can be formed in the process of various methods and processing methods during strengthening, restoration and modification. Attention is focused on the formation of microtexture in non-equilibrium conditions of laser processing and during friction testing.

2. X-ray methods for detecting the texture of working surfaces of samples and parts made of steel and ceramic materials on diffractometers of various types are considered. The methodology for X-ray studies of texture and the degree of its improvement are specified. The technological parameters of laser processing of samples made of steel and composite materials are determined, both in conditions without melting and with melting of the surface.

3. On steel samples, X-ray lines  $\langle 001 \rangle$ ,  $\langle 110 \rangle$ ,  $\langle 112 \rangle$ ,  $\langle 123 \rangle$ ,  $\langle 200 \rangle$ ,  $\langle 002 \rangle$ ,  $\langle 202 \rangle$  were recorded by tilting, both from the surface and from different depths in the friction zone and the laser exposure zone. Combined textures were detected, for example, for steel 3:  $\langle 210 \rangle + \langle 211 \rangle + \langle 321 \rangle$ , with the initial axial crystallographic structure  $\langle 110 \rangle$ . A gradient of textures with depth was observed. A linear law of change in the degree of texture perfection during laser heat treatment and an exponential law – during laser doping with boron were determined.

4. The study of texture on samples of ceramic materials was carried out using the example of ceramics with the composition: 98 wt.% zirconium oxide + 2 wt.% yttrium oxide. The composite was obtained by sintering in vacuum at a temperature of 1873 K with different holding times. The samples were also subjected to laser processing in the mode of non-fusing the surface. The degree of texture was studied by the ratio of X-ray lines  $I_{(002)}/I_{(200)}$ . The fact of the formation of texture of samples of the studied composite was established both during laser processing and during friction testing.

5. It is shown that the texture of the surfaces of the mating parts makes it possible to provide the tribosystem with the necessary level of tribological properties and characteristics. At the same time, there is a need to create physical and technological foundations and a comprehensive approach to solving the problems of increasing the tribological efficiency of assemblies, systems, units, machines and mechanisms by texturing the mating surfaces of parts. For this purpose, a number of tasks have been formulated that need to be solved.

### References

1. Aulin, V. V., Kuzyk, O. V., & Kropivnyi, V. M. (2016). Z'iasuvannia pryrody protsesiv strukturnykh ta fazovykh peretvoren' v zalizovuhletsevykh splavakh na osnovi utvorennia molekuliarnoï formy vuhletsu [Clarification of the nature of structural and phase transformations in iron-carbon alloys based on the formation of a molecular form of carbon]. Zbirnyk naukovykh prats Kirovohrads'koho natsional'noho tekhnichnoho universytetu. Tekhnika v sil's'kohospodars'komu vyrobnytstvi, haluzeve mashynobuduvannia, avtomatyzatsiia, (29), 94–104. (In Ukrainian).
2. Aulin, V. V., Kropivnyi, V. M., & Kuzyk, O. V. (2017). Formuvannia struktury vysokomitsnykh chavuniv pry vyhotovlenni ta lazernii mofikatsii detalei mashyn [Formation of the structure of high-strength cast irons during manufacturing and laser modification of machine parts]. In Modern methods, innovations, and experience of practical application in the field of technical sciences: International research and practice conference (Radom, Poland, December 27–28, 2017) (pp. 103–106). Radom: Radom Academy of Economics. (In Ukrainian).
3. Aulin, V., Lysenko, S., Hrynkiv, A., Tykhyi, A., Kuzyk, O., & Livitskyi, O. (2023). The regularity of the change in the coefficient of friction of the coupling of “shaft-sleeve” parts using polymeric materials. Problems of Tribology, 28(1/107), 81–91. [in English].
4. Aulin, V., Lysenko, S., Hrynkiv, A., & Holub, D. (2022). Thermodynamic substantiation of the direction of nonequilibrium processes in triadconjugations of machine parts based on the principles of maximum and minimum entropy. Problems of Tribology, 27(2/104), 55–63. [in English].
5. Marchuk, V. Ye., Kindrachuk, M. V., et al. (2019). Napruzhenno-deformovanyi stan teksturovanykh poverkhon' trybolohichnykh system [Stress-strain state of textured surfaces of tribological systems]. Eastern-European Journal of Enterprise Technologies, 3(12), 44–49. (In Ukrainian).

6. Marchuk, V. Ye., Kindrachuk, M. V., et al. (2019). Stress-strained state of textured surfaces with selectively indented regions. *Functional Materials*, 26(4), 773–778. [in English].
7. Lesyk, D. A., Dzhemelinskyi, V. V., Danyleiko, O. O., & Khyzhevskiy, V. V. (2016). Doslidzhennia mikrorelefiu ta struktury poverkhnevoho sharu pry lazernii ta ultrazvukovii termodeformatsiiniy obrobtsti instrumentalnoi stali [Investigation of surface layer microrelief and structure during laser and ultrasonic thermodeformational treatment of tool steel]. *Visnyk NTUU "KPI". Seriiia Mashynobuduvannia*, (3) [78], 58–64. (In Ukrainian).
8. Mohyliak, I. A. (2021). *Lazerne mikro-nanostrukturovannia ta lehuвання pry poverkhnevyykh shariv napivprovidnykiv* [Laser micro/nanostructuring and doping of semiconductor surface layers] (PhD thesis). Ivan Franko National University of Lviv. (In Ukrainian).
9. Dzhemelinskyi, V. V., & Lesyk, D. A. (2013). Vplyv impul'snykh lazerno-ul'trazvukovykh dzherel enerhii na formuvannia poverkhnevoho sharu detalei [Influence of pulsed laser-ultrasonic energy sources on the formation of the surface layer of parts]. *Skhidnoevropeyskyi zhurnal peredovykh tekhnolohii – Eastern-European Journal of Enterprise Technologies*, 2/5(62), 26–30. (In Ukrainian).
10. Dzhemelinskyi, V. V., & Lesyk, D. A. (2014). Kombinovane lazerno-ul'trazvukove poverkhneve zmitsnennia detalei i mozhlyvosti yoho vykorystannia pry vyrobnytstvi ta remontu obladnannia [Combined laser-ultrasonic surface hardening of parts and its application possibilities in equipment manufacturing and repair]. *Zbirnyk naukovykh prats (Haluzeve mashynobuduvannia, budivnytstvo)*. PoltNTU, 3(42), 61–69. (In Ukrainian)
11. Bernatskyi, A. V. (2013). Pidvyshchennia fizyko-mekhanichnykh vlastyvostei poverkhnevyykh shariv stali lazernym ta kombinovanyim lehuванняm [Improvement of physical and mechanical properties of steel surface layers by laser and combined alloying]. *Skhidnoevropeyskyi zhurnal peredovykh tekhnolohii – Eastern-European Journal of Enterprise Technologies*, 6/1(66), 25–31. (In Ukrainian).
12. Mil'man, Yu. V., Hrinkevych, K. E., Mordel', L. V., Kozyriev, D. V., Tkachenko, I. V., & Kuprin, V. V. (2013). Osoblyvosti mekhanichnykh ta trybolohichnykh vlastyvostei intermetalidiv na osnovi aliuminiu, nikeliu ta tytanu za umov lokalnoho navantazhennia [Peculiarities of mechanical and tribological properties of aluminum-, nickel- and titanium-based intermetallics under local loading]. *Elektronna mikroskopiia i mitsnist materialiv: Zbirnyk naukovykh prats IPM NANU*, 19, 86–95. (In Ukrainian).
13. Stupnytskyi, V. V., & Makhorkin, Ye. M. (2013). Trybotekhnichniy kriterii formuvannia funktsional'no-orientovanoi tekhnolohii vyhotovlennia detalei v mashynobuduvanni [Tribotechnical criterion for formation of functionally oriented technology of manufacturing parts in mechanical engineering]. *Mizhvuzivskyi zbirnyk "Naukovi notatky"*, 42, 305–313. (In Ukrainian).
14. Mao, B., Siddaiah, A., Liao, Y., & Menezes, P. L. (2020). Laser surface texturing and related techniques for enhancing tribological performance of engineering materials: A review. *Journal of Manufacturing Processes*, 53, 153–173. [in English].
15. Shamsul Baharin, A. F., Ghazali, M. J., & A Wahab, J. (2016). Laser surface texturing and its contribution to friction and wear reduction: A brief review. *Industrial Lubrication and Tribology*, 68(1), 57–66. [in English].
16. Wang, S., Yan, F., & Chen, A. (2018). Tribological effects of laser surface texturing and residual stress. *Industrial Lubrication and Tribology*, 70(1), 126–132. [in English]
17. Wu, C., Ma, T., et al. (2015). Tribological behavior of femtosecond laser textured surfaces of 20CrNiMo/beryllium bronze tribo-pairs. *Industrial Lubrication and Tribology*, 67(2), 75–82. [in English].
18. Effect of laser surface texturing on the tribological properties and scuffing mechanism of CKS piston ring against cast iron cylinder liner under high intensifying. (2022). *Tribology Transactions*, 65(6), 213–226. [in English].
19. Zhang, Y., Yang, J., Liu, W., Li, D., & Ren, S. (2022). Effect of laser surface texturing on the tribological properties and scuffing mechanism of CKS piston ring against cast iron cylinder liner under high intensifying. *Tribology Transactions*, 65(6), 213–226. [in English].
20. Etsion, I., & Sher, E. (2005). Experimental investigation of partial laser surface texturing for piston-ring friction reduction. *Tribology Transactions*, 48(4), 583–588. [in English].
21. Jin, Y., Yan, X., Sun, X., Wang, F., & Fan, K. (2021). Tribological analysis of laser-textured WC-Co against Ti6Al4V under dry and lubricated conditions. *Lubricants*, 13(1), Article 36, 1–12. [in English].
22. Waseda, Y. (2010). *X-ray diffraction crystallography: Introduction, examples and solved problems*. Berlin: Springer. [in English].
23. Cullity, B. D., & Stock, S. R. (2001). *Elements of X-ray diffraction* (3rd ed.). Upper Saddle River, NJ: Prentice Hall. [in English].
24. Aulin, V. V., Derkach, O. D., Makarenko, D. O., & Hryn'kiv, A. V. (2018). Vplyv rezhymiv ekspluatatsii na znoshchuvannia detaley, vyhotovlenykh z polimerno-kompzytnoho materialu [Influence of operating modes on wear of parts made of polymer-composite material]. *Problemy trybolohii*, 4, 65–69. (In Ukrainian).
25. Kniazieva, H. O., Kniaziev, S. A., Tkachuk, M. M., & Pinchuk, N. V. (2021). Perevahy ta nedoliky riznykh metodiv doslidzen' fazovo-strukturnykh staniv materialiv (ohliadova stattia) [Advantages and disadvantages of various methods for studying phase-structural states of materials (review article)]. *Visnyk NTUU "KhPI". Seriiia: Mashynoznavstvo ta SAPR*, 2, 51–55. (In Ukrainian).

**Аулін В.В., Манько Є.В., Чумак В.М., Лисенко С.В., Деркач О.Д., Макаренко Д.О.**  
Текстурованість матеріалів елементів трибологічних систем машин і механізмів в нерівноважних умовах обробки та функціонування.

Стаття присвячена мікротекстуруванню металевих і полімерних матеріалів елементів трибологічних систем, впливу його на характеристики і властивості робочих поверхонь зразків і деталей. Розглянуто різні типи мікротекстури сталевих та композитних матеріалів на основі оксиду цирконію. З'ясовано механізм їх утворення. Переважно механізми мікротекстурування зв'язують з полем напруженості, створених в процесі тертя та лазерної обробки. Визначено, що лазерна обробка сталевих зразків призводить до комбінованого мікротекстурування і градієнту текстури за глибиною поверхневого шару зразка. Виявлена текстурованість у композитах як при лазерній обробці, так і при випробуванні тертям. Показано, що виявлена текстурованість позитивно впливає на експлуатаційні характеристики деталей, підвищуючи рівень надійності і зносостійкості, а також трибологічну ефективність трибоспряджень деталей вузлів, систем, агрегатів машин і механізмів.

**Keywords:** сталь, композит, трибологічна система, мікротекстурування, рентгенівське випромінювання, лазерна обробка, досконалість текстури, випробування тертям, надійність, зносостійкість.